Design and Modeling of an Energy Storage System Based on Solid Oxide Reversible Cells with Syngas as Fuel and Co-Electrolysis of CO_2 and H_2O

MSc. Sustainable Energy Technology

Sebastian Diaz Rodriguez

TU Delft Delft University of Technology

Challenge the future

Design and Modeling of an Energy Storage System Based on Solid Oxide Reversible Cells with Syngas as Fuel and Co-Electrolysis of CO_2 and H_2O

MASTER OF SCIENCE THESIS

MSc. Sustainable Energy Technology

Sebastian Diaz Rodriguez

Faculty of Electrical Engineering, Mathematics and Computer Science

Faculty of Mechanical, Maritime and Materials Engineering

Delft University of Technology

August 2018

Report by:

Sebastian Diaz Rodriguez

(4600886)

in partial fulfilment of the requirements for the degree of

Master of Science

in Sustainable Energy Technology

at the Delft University of Technology

Thesis supervisors:

Dr. P.V. Aravind
Dr. Vikrant Venkataraman

Graduation Committee Members:

Dr. PV Aravind
Dr. Ir. Milinko Godjevac
Dr. Ir. Jose Rueda Torres
Dr. Vikrant Venkataraman
Theo Woudstra

Abstract

The intermittent nature of renewable energy sources makes it difficult for electric utility companies to effectively implement these technologies in the power grid due to mismatches between supply and demand. Solid oxide cells are electrochemical devices that are receiving a lot attention as an effective power grid balancing technology, given their ability to operate as Solid Oxide Fuel Cells (SOFC) for electric power generation, and as Solid Oxide Electrolysis Cells (SOEC) for chemical fuel production. Solid Oxide Reversible Cells (SORC) are capable of working alternately in these two modes, thus can be used to store electricity in the form of fuel when energy supply in the grid exceeds the energy demand and can release this energy when demand exceeds the supply from generation systems.

The purpose of this project was to design an energy storage system that uses solid oxide reversible cells and syngas as fuel, consuming it to produce electricity during operation as a fuel cell and producing it back to store electric power through the co-electrolysis of water and CO_2 when working as an electrolysis cell. The design and steady-state simulation of the system was performed using the process simulation software Aspen Plus, where a base configuration of the plant was constructed and improved using as main criteria the roundtrip efficiency and exergy efficiency achieved. This approach allowed to locate the main sources of energy and exergy losses, therefore strategies could be implemented to reduce them, finally achieving a more advanced and efficient system. Overall, it was possible to attain improvements in system roundtrip efficiency from 29% to 44%; in SOFC exergy efficiency from 44% to 64%; and in SOEC exergy efficiency from 66% to 68%.

Acknowledgements

This project has been a learning experience that I have enjoyed very much and the perfect closure of my masters in Sustainable Energy Technology. Special thanks to Prof. Aravind for the opportunity to work in a topic at the forefront of the renewable energy revolution which I am sure will bring many opportunities to our common future; and to Vikrant Venkataraman for his invaluable guidance through the entire duration of this project.

I would also like to thank Theo Woudstra for his help and teachings in the area of power plants and exergy analysis that were the core of this project. His course with Prof. Aravind and Prof. Tighe on Advanced Applied Thermodynamics gave me the knowledge I lacked to fulfill my objectives. Special thanks also to Yashar Hajimolana, Sotiris Giannoulidis, Enrique Gutierrez, Pratik Basarkar, Jonah Poort, Ali Saadabadi, Bart Numan, Jelle Stam and Mayra Recalde Moreno del Rocio for their help teaching me how to use Aspen Plus, helping me with my final report and/or my final presentation and for teaching me things that I could use for my project.

Finally, I would like to thank my mom, my dad and my sister for being always there for me, advising me and supporting me throughout all these years in the Netherlands. I love you three with all my heart.

Thank you all.

Table of Contents

List of Figures

List of Tables

List of Symbols

A_{cell}	Active area of one cell	m^2
$D_{eff,k}$	Effective diffusion coefficient of component k	m^2/sec
D_{k-l}	Binary diffusion coefficient between components k and l	m^2/sec
$D_{Kn,k}$	Knudsen diffusion coefficient of component k	m^2/sec
$E_{act,k}$	Activation energy of cell component k	J/mol
Ex_{chem}	Chemical exergy of a flow of matter	W
$ex^{o}_{chem,k}$	Molar chemical exergy at standard conditions of component k	J/mol
Ex_{stream}	Exergy of a flow of matter	W
Ex_{TM}	Thermo-mechanical exergy of a flow of matter	W
F	Faraday's constant	C/mol
Δg	Change in Gibbs free energy	J/mol
Δg^0	Change in Gibbs free energy at standard conditions	J/mol
$\Delta g^{o}_{f,k}$	Standard Gibbs free energy of formation of component k	J/mol
h^o	Enthalpy at standard conditions	J/mol
Δh	Change in enthalpy of reaction	J/mol
Δh^0	Change in enthalpy of reaction at standard conditions	J/mol
$\dot{H}$	Enthalpy rate	W
i	Operating current/DC current	A
j	Operating current density	A/m^2
$j_{0,k}$	Exchange current density of electrode k	A/m^2
M_k	Molar mass of component k	g/mol
n	Number of electrons transferred in an electrochemical reaction	
$\dot{N}$	Molar flow rate	mol/sec
N_{cells}	Total number of cells in a stack	
p	Pressure of operation	bar

p_o	Standard pressure/pressure of dead state	bar
p_k	Partial pressure of component k	bar
$p_{k,env}$	Environmental partial pressure of component k according to Baehr composition	bar
P_e	Electric power/electric work	W
$\dot{Q}$	Rate of heat transferred to/from the environment	W
R	Universal gas constant	$(J \cdot K)/mol$
r_{ohmic}	Specific ohmic resistance	$\Omega \cdot m^2$
r_p	Average radius of the pores in the electrode	m
s^o	Entropy at standard conditions	$J/(mol \cdot K)$
Δs	Change in entropy	$J/(mol \cdot K)$
t	Operation time	sec
T	Temperature of operation	K
T_o	Standard temperature/temperature of dead state	K
U_f	Fuel utilization	
U_{rev}	Reversible voltage/Nernst voltage	V
U_{tn}	Thermoneutral voltage	V
$V_{act,k}$	Activation overpotential of electrode k	V
V_{cell}	Operating voltage of a cell	V
$V_{conc,k}$	Concentration overpotential of electrode k	V
V_{ohm}	Ohmic overpotential	V
V_{stack}	Operating voltage of a stack of cells	V
$V_{d,k}$	Diffusion volume of component k	
$\alpha_{a,k}$	Anodic transfer coefficient of electrode k	
$\alpha_{c,k}$	Cathodic transfer coefficient of electrode k	
$\gamma_{0,k}$	Activation overpotential pre-exponential factor for electrode k	A/m^2
δ_k	Thickness of cell component k	m

ε	Porosity of the electrodes	
$\eta_{Ex,Univ}$	Universal exergy efficiency	
η_{ExFun}	Functional exergy efficiency/Second Law efficiency	
$\eta_{RT,stack}$	Stack roundtrip efficiency	
$\eta_{RT,system}$	System roundtrip efficiency	
σ	Conductivity	$(\Omega \cdot m)^{-1}$
$\sigma_{0,el}$	Conductivity pre-exponential factor for the electrolyte	$(\Omega \cdot m)^{-1}$
τ	Tortuosity of the electrodes	

List of Acronyms

AC	Alternating current
ASR	Area-specific resistance
BOP	Balance-of-plant
DC	Direct current
FE	Fuel electrode
H/C	Hydrogen-to-carbon ratio
OE	Oxygen electrode
PCM	Phase-change material
PEM	Polymer electrolyte membrane
RWGS	Reverse water-gas shift
SOC	Solid oxide cell
SOEC	Solid oxide electrolysis cell
SOFC	Solid oxide fuel cell
SORC	Solid oxide reversible cell
TM	Thermo-mechanical
TPB	Triple-phase boundary
WGS	Water-gas shift
YSZ	Yttrium-stabilized zirconia

1. INTRODUCTION

In the last few years, the share of renewable energy in electric power generation has increased drastically as countries around the world work toward the decarbonization of the energy industry in order to fend off climate change. Solar photovoltaic and wind energy are the main contributors to this transition, while many other technologies based on biomass, thermal, hydraulic, and tidal sources are under constant development and investigation. Nevertheless, the intermittent and varying nature of these energy sources still poses a challenge for their implementation due to intrinsic daily and seasonal variations in their nature. Besides this intermittency, the integration of this technology is usually difficulted by a recurrent mismatch between the times of higher energy production from renewables and the times of highest demand from consumers i.e. the peaks of generation do not commonly correspond to those of demand, thus energy storage technologies are needed in order to balance energy grids that rely heavily on renewable sources.

Solid Oxide Cells (SOC) are electrochemical devices that have received a lot of attention as a possible energy storage technology since they can convert the chemical energy found in bonds of “fuel” molecules directly into electrical energy, and vice versa. More commonly, SOCs are used to oxidize fuels like hydrogen or methane into water and/or carbon dioxide to produce electric power, in which case the cell is called a Solid Oxide Fuel Cell, or SOFC. Unlike traditional power plants that suffer from many energy losses as they convert chemical energy into electric power through several steps, SOFCs achieve this conversion directly, considerably reducing the losses in the system. For their potential as an effective and clean energy production system, extensive research has been done on this technology.

More recent is the use of SOCs in the reverse mode of operation, i.e. using electric power to generate chemical fuels through the electrolysis of water and carbon dioxide to produce hydrogen and carbon monoxide. In this type of operation, the cell is referred as a Solid Oxide Electrolysis Cell, or SOEC. The production of hydrogen or synthesis gas (the mixture of hydrogen and carbon monoxide) out of electricity opens a whole new world of possibilities to decarbonize industries beyond the energy sector,

as these substances can be used as building blocks for the production of many chemicals and fuels for transportation, provided that the electric energy comes from sustainable sources, as well as the water and carbon dioxide [1]. Focusing on the energy industry, SOECs can convert electricity into chemicals that can be stored for any period of time; a practice known as power-to-gas or power-to-X. In combination with SOFCs, a system can be envisioned where in periods or excess supply of electricity from renewable technologies SOECs can convert this excess energy into fuels that can be stored and used later in SOFCs to produce power when the demand is above the instantaneous generation.

In practice, the same SOC device can be used alternately as an SOFC and as an SOEC, however, this technology is much less developed, since usually the cells are made with properties that optimize one mode of operation, and that do not necessarily benefit the other. Therefore, intensive research is being carried out to manufacture cells that are capable of working in both modes. Many names are used today for this new type of reversible SOCs; following the conventions already shown, in this work these are referred as a Solid Oxide Reversible Cells, or SORC. Working with SORCs has many advantages over working with separate SOFCs and SOECs, like having only a single unit to achieve electric power production and electrolysis, which translates into a simpler system and a smaller area footprint. Moreover, reversible operation makes it possible to operate the system for longer periods of time since it can be used whenever there is an excess or a lack of electric energy in the grid, thus enhancing the economics of the plant.

Although individual SORCs are very efficient devices, many of these must be assembled into a stack to generate the required electric currents and voltages, which at the same time must be coupled with many other components to create a complete energy storage system. These components beyond the stack are known as the Balance-of-Plant (BOP) and can include items such as heat exchangers, storage tanks, mixers, compressors or turbines that add losses to the system above those intrinsic to the electrochemical device [2]. The BOP is needed, however, in order to control the characteristics of the material and energy streams in the system. An especially challenging task of the BOP is the management of heat, as reactions in SOCs can be exothermic or endothermic, depending on the mode of operation, while these cells

must be kept at a constant temperature above $700°C$ at all times to conduct an electric current. SORCs systems can be studied with process simulation software, which are powerful tools to determine the best configuration of the BOP, as well as the operation strategies to maximize efficiency for a specific purpose.

This project focused on the characteristics and performance of an energy storage system based on solid oxide reversible cells that works exclusively with synthesis gas (or syngas), consuming it as fuel to produce electric power during operation as solid oxide fuel cells and producing it back to store electric power through the simultaneous co-electrolysis of a mixture of water and CO_2 when working as solid oxide electrolysis cells. It was assumed that in SOFC mode, only H_2 reacts electrochemically while CO is consumed through the water-gas shift reaction; and that in SOEC mode, only H_2O reacts electrochemically while CO_2 is consumed through the reverse water-gas shift reaction. The design and steady-state simulation of the system was performed with the process simulation software Aspen Plus, where a base configuration of the plant was constructed and improved using as main evaluation criteria the roundtrip efficiency and exergy efficiency achieved in every iteration of the system.

Process chains that include co-electrolysis often include the conversion of the syngas produced into methane either by using low temperatures in the SOC stack [2], or by adding methanation reactors in the system [2] [3]. This practice attempts to use the net exothermic nature of methanation to manage more effectively all heat requirements during operation as an SOFC or as an SOEC, and to increase the energy density of the stored fuel. However, this adds complexity to the system and increases its capital cost. As a result, this project focused on designing a plant working exclusively with syngas since studies of SORC systems without methanation are important to understand the limits and feasibility of SORCs for energy storage applications. The use of syngas as fuel and co-electrolysis for fuel production in the same stack of cells produces the simplest configuration for a SORC system that works with carbon-containing gases, therefore the models designed in this project can be used as benchmarks for more complex configuration and increase the available options when deciding what systems can be used for storage applications.

The goal of this project can be achieved by answering the following questions:

- What are the operating parameters of the SORC stack that promote high efficiency while only functioning with syngas?

- What are the largest sources of energy and exergy losses and how can they be reduced or avoided?

- What are the system configurations and operation strategies that influence the most the energy and exergy efficiencies?

This report is structured in the following way: Chapter 2 introduces the underlying principles behind solid oxide cells, including their construction, chemical reactions and their thermodynamics. Chapter 3 presents a literature review of previous studies regarding SOC systems that are relevant for this project. Chapter 4 describes the computer model developed starting with the electrochemical model used, followed by the implementation of SORC stacks models in Aspen Plus. The base model for simulations is also introduced, as well as the energy and exergy metrics used as performance criteria. Chapter 5 shows the results of several studies carried out to progressively improve the base system into a final advanced configuration. Finally, conclusions and recommendations are given in Chapter 6 and 7.

This research project was part of a joint effort known as the BALANCE Project[1], which aims among other things to implement SORCs in power-to-gas applications for balancing power grids supplied by intermittent renewable sources. The partners in this group include the Technical Research Centre of Finland (VTT); the Technical University of Denmark (DTU); the French Alternative Energies and Atomic Energy Commission (CEA); the Italian National Agency for New Technologies, Energy and Sustainable Economic Development (ENEA); the University of Birmingham; the École Polytechnique Fédérale de Lausanne (EPFL), the Institute of Power Engineering (IEn), and the Delft University of Technology (TU Delft). The BALANCE Project is recognized and funded by the European Union's Horizon 2020 research and innovation program under grant agreement No. 731224. TU Delft is in charge of the design and preliminary energy and exergy analysis of different process chains for SORC systems.

[1] https://www.balance-project.org/

2. BACKGROUND INFORMATION

This chapter aims to introduce the underlying principles behind solid oxide cells. First, the construction of standard planar cells is explained. This is further developed with an explanation of the different materials used and the way they carry out equilibrium and electrochemical reactions. The most relevant reactions for this work are then examined, as well as the thermodynamic concepts used to describe SOCs. This chapter also aims at introducing the terminology used throughout this work.

2.1. Basic Construction and Operation of Solid Oxide Cells

As stated in the introduction, Solid Oxide Cells (SOC) are solid-state electrochemical devices that are capable of converting the chemical energy in the bonds of certain compounds directly into electric energy, as well as performing the reverse operation converting electrical energy into chemical energy. An SOC that works in the first mode of operation is known as a Solid Oxide Fuel Cell (SOFC), while an SOC that works in the reverse mode is known as a Solid Oxide Electrolysis Cell (SOEC). In principle, a solid oxide cell can work interchangeably as an SOFC and as an SOEC, but in practice the cell is optimized to work in just one way. However, new Solid Oxide Reversible Cell (SORC) technologies are being developed that are optimized to operate efficiently in both modes.

All three types of SOCs possess the same physical configuration and are constructed with four basic components: the electrolyte membrane, the fuel electrode, the oxygen (or air) electrode, and the current collectors. Figure 2.1 shows each of these components and the way they are put together to construct a single cell. Many geometries are possible with solid oxide cells, however, the planar geometry shown in Figure 2.1 is the most commonly used and is the one utilized in this work.

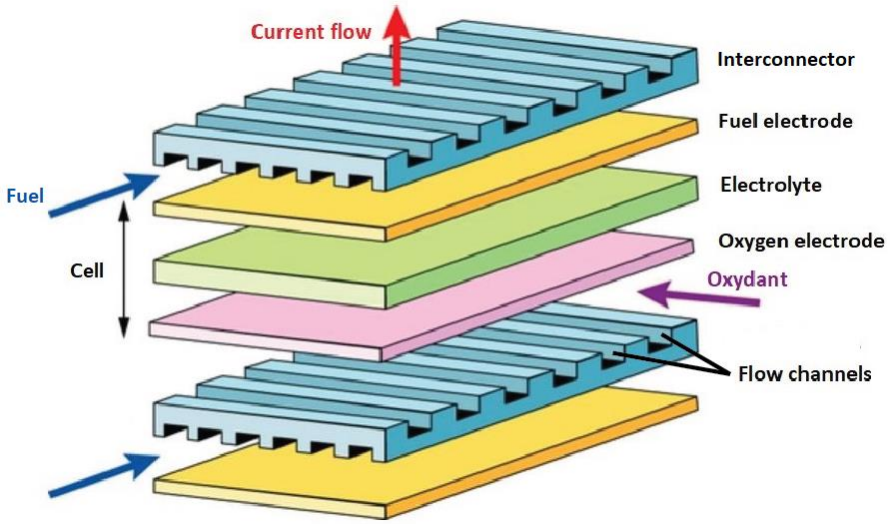

Figure 2.1. Basic configuration of a solid oxide cell. Figure taken and modified from University of Cambridge [4].

The electrolyte membrane is placed between the fuel and oxygen electrode in order to physically separate these two and the gases that are fed into each of them: fuel into the fuel electrode, and oxygen or air into the oxygen electrode. The current collectors, or interconnectors, are then placed in contact with the electrodes to allow the flow of an electric current out of the cells. Grooves in the interconnectors known as flow channels leave a free space between them and the electrodes through which the gases used are taken in and out of the cells. The interconnectors make it possible to connect individual cells in series and form a stack (Figure 2.2).

Figure 2.2. Solid oxide cells stack.

The composition of the electrodes and the high temperatures of operation make it possible for electrochemical reduction-oxidation reactions of components to occur in SOCs. These reactions involve the transfer of electrons between reducing and oxidizing species due to their difference in chemical potential at their respective electrodes, which creates an electric potential and current responsible for the production of power in SOFC mode and the electrolysis of compounds in SOEC mode. The most common fuel with any type of fuel cell technology is hydrogen gas, which reacts with oxygen to produced water, according to Reactions 2.1-2.3:

Fuel electrode: $2H_2 + 2O^{2-} \leftrightarrow 2H_2O + 4e^-$ 2.1

Oxygen electrode: $O_2 + 4e^- \leftrightarrow 2O^{2-}$ 2.2

Overall: $2H_2 + O_2 \leftrightarrow 2H_2O \quad \Delta h^0_{298K} = -286\ [kJ/mol]$ 2.3

From left to right, Reactions 2.1-2.3 represent fuel cell operation, while in the opposite direction they show electrolysis operation. It should be noted that in reality these reactions are not equilibrium reactions as the symbol "↔" might suggest, since the reactions go in only one direction according to the mode of operation, and no real equilibrium can exist since the oxygen is separated from the hydrogen by the electrolyte [5]. In this case, however, the symbol "↔" is used in to imply the ability of SOCs to drive the reactions in both directions.

Figure 2.3 shows the flow of charge as Reactions 2.1-2.3 progress along an SOFC and an SOEC. Unlike the electrodes, the material of the electrolyte membrane is non-porous, therefore the oxygen and the fuel are never in direct contact. The electrolyte, however, allows the flow of oxide ions between electrodes (O^{2-}) while remaining impervious to the flow of electric current. In SOFC mode the electrons needed to complete Reactions 2.1-2.3 must therefore travel from the fuel electrode to the oxygen electrode through an external circuit as an electric current that produces an electric work on any load connected to it. In SOEC mode the flow of oxide ions and electric current is reversed by changing the polarity of the electrodes. When the electrolyte is hot and conductive, the oxidation process occurring in SOFC mode is a spontaneous

and exothermic process that doesn't require more energy inputs, while the reduction process (electrolysis) in SOEC mode does require a voltage source to drive Reactions 2.1-2.3 from right to left, as well as a heat source since the reactions are endothermic.

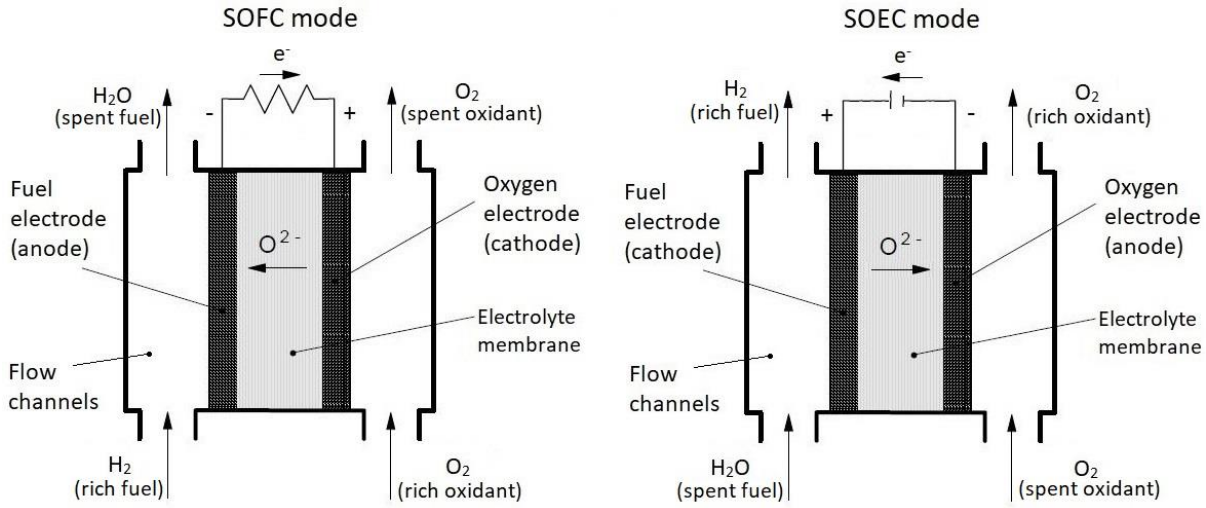

Figure 2.3. Basic flow of matter and change during SOFC and SOEC operation.

It can be observed in Figure 2.3 that switching between SOFC and SOEC operation changes the polarity of the electrodes, thus in SOFC mode the fuel electrode is the anode, while in SOEC mode it is the cathode. This applies as well to the oxygen electrode. To avoid confusion throughout this text, the use of the terms cathode and anode for the electrodes is avoided, referring to the them only as the **fuel electrode** or the **oxygen electrode**, according to the gases that enter and exit each of them.

In Figure 2.3 can be seen that the **rich fuel** is defined as the gas mixture that enters the fuel electrodes of the stack in SOFC mode and that leaves these electrodes in SOEC mode, while the **spent fuel** is the gas mixture that enters the fuel electrodes of the stack in SOEC mode and that leaves these electrodes in SOFC mode. This definitions extent to the more complex mixtures of gases beyond pure hydrogen and water that can be used in SORCs that are introduced in Section 2.2. The **oxidant** is the term used to refer to the oxygen-containing gas fed to the oxygen electrodes, whether it is air, pure oxygen or special mixtures.

2.2. Materials Used in Solid Oxide Cells

The electrolyte membrane is the main component that distinguishes SOCs from other types of fuel cell technologies, and in fact gives solid oxide cells their name. The solid oxide membrane is typically composed of yttrium-stabilized zirconia (YSZ), a nonporous material that has the ability to be highly conductive to oxide ions (O^{2-}) while being impervious to the flow of electric current. In order to achieve high enough conductivity, YSZ must be heated to temperatures above $700°C$ and up to $1000°C$ while remaining stable. Typical operating temperatures are between $700°C - 800°C$ [2] [6]. The non-porous membrane separates the rich/spent fuel from the oxidant and force their electrochemical reaction to occur, as the oxygen can only cross the electrolyte as a charged ionic species, creating a flow of current.

The fuel electrode of SOFCs and SOECs is commonly composed of a porous nickel yttrium-stabilized zirconia (Ni-YSZ) cermet. A cermet is a composite material made out of ceramic and metallic components that aim to take advantage of the properties of both for a specific application. In the case of Ni-YSZ, the metal used is nickel, which is a good and low cost electronic conductor that also acts as a catalyst for equilibrium reactions when using carbonaceous mixtures as reacting components. The YSZ matrix of the cermet serves the purpose of connecting the bulk of the fuel electrode to the electrolyte to allow the conduction of O^{2-}into the electrode. Additionally, the YSZ matrix prevents the sintering of the nickel inside the porous matrix, which reduces the available surface area, and helps match the thermal expansion coefficient of the fuel electrode to the electrolyte [6].

The oxygen electrode is also usually composed of a cermet, but in this case lanthanum-based perovskite materials are preferred. Currently strontium-doped $LaMnO_3$ (LSM) is the most used material, thus forming LSM-YSZ composite electrodes. The YSZ serves the same purpose as in the fuel electrode. In the case of the LSM, it is chosen mainly for its electronic conductivity, and because it matches the thermal expansion coefficient of YSZ and has a relatively high electro-catalytic activity for the reactions involving oxygen [6] [7].

Electrochemical reactions in SOCs only occur in specific sites within the electrode known as Triple-Phase Boundaries (TPBs), where the electrolyte material, the electronic conducting material and the gases come into contact at the same time [8] [2] [9]. Figure 2.4 schematizes this for the fuel electrode (anode) of an SOFC. The reactivity of the electrodes is therefore proportional to the number and availability of these reaction sites. Both the fuel and oxygen electrodes are made porous in order to allow the diffusion of gases from the flow channels to the interior of the electrodes and to the electrolyte surface thus using more of the bulk volume of the electrodes. However, increasing the porosity also decreases the quantity of active material, thus it cannot be too high. Given the tradeoff between these two characteristics, a lot of research on SOCs is done in the optimization of the TPBs and the production techniques of the electrodes.

Figure 2.4. Triple-Phase Boundaries (TPB) of an SOC.

The high temperature of operation required to work with YSZ-based SOCs gives these devices some advantages over other types of lower temperature fuel cell/electrolyzer technologies, specially over polymer electrolyte membrane (PEM) cells, which represent the main competing technology in the market. One of the main advantages is a larger tolerance to contaminants and the ability to work with carbon-containing gases. PEM cells must work exclusively with pure hydrogen, otherwise their electrodes are irreversibly damaged due to the poisoning of the expensive platinum catalysts they use. These catalysts are utilized to accelerate the rate of reaction at the low temperature of operation (below $90°C$). SOCs don't need platinum catalysts for this purpose as the elevated temperatures and the presence of nickel increase the

kinetics of the chemical reactions taking place so much that they can be assumed to instantly achieve near-equilibrium within the cell [2] [10] [11].

Nevertheless, SOCs have disadvantages of their own. One of them is that the ceramic constituents of the cells must be heated slowly and evenly in order to not generate temperature gradients that can break them. This problem is exacerbated by the difference in thermal expansion coefficient of the different components of the cells that could separate them, breaking the electric circuit. This increases their startup time and prevents their use in applications that require fast response [6]. Moreover, it is difficult to design a stack with materials that are resistant to these temperatures and the redox environments inside, while keeping their cost low [8]. Because of these issues, a lot of research is done into finding electrolyte materials that allow high ionic conductivity at lower operation temperatures. One of the most researched is Strontium and Magnesium doped Lanthanum Gallate (LSGM) electrolytes which can work efficiently at temperatures as low as $650°C$ [2] [12] [13].

2.3. Carbonaceous Mixtures in SORCs

Historically, SOFCs have operated with hydrogen as fuel while SOECs have operated with steam as reacting gas, due to the high efficiency, low toxicity and availability of these feedstocks. Additionally, hydrogen has a much higher specific energy content compared to conventional fuels, and the by-product of its oxidation with oxygen is water. Nevertheless, hydrogen has a very low density, therefore SOFC systems operating with hydrogen must pressurize it to achieve attractive volumetric energy densities and reduce the land footprint of the system [2] [14]. But hydrogen gas is difficult to compress; and given the small size of this molecule, it is even capable of escaping many of the conventional containers available in the market [6] [15].

The combination of carbon-containing compounds like methane, syngas or methanol with hydrogen gas increases the volumetric energy density of the system [2] [16], while the production of the gas itself from excess electric energy of a power grid opens the opportunity to produce high-value chemicals and fuels through Fischer-Tropsch synthesis, methanation or methanol formation [16].

At the high operating temperatures of SOCs, carbon-containing gases like methane or carbon monoxide can be added as fuel for SOFC operation, since reforming and shift reactions are favored enough to convert these gases into hydrogen. Furthermore, carbon dioxide can be added as a reactant for SOEC operation since between $700 - 900°C$ the change in Gibbs free energy of H_2O is close to that of CO_2 [16], thus the applied voltage is capable of reducing both components at the same time. This fuel flexibility give SORCs a large advantage over low temperature cells, since the carbonaceous mixtures produced have higher energy densities than pure hydrogen, and some compositions can be stored in already available infrastructure.

The simultaneous electrolysis of water and carbon dioxide is known as **co-electrolysis** and is being investigated around the world for its potential to create high-value chemicals from the resulting mixture of hydrogen and carbon monoxide known as synthesis gas, or **syngas**. Although this gas is by definition a mixture of H_2 and CO, for simplicity reasons in this work the term is extended to also account for mixtures of hydrogen and carbon monoxide that contain some levels of water vapor and carbon dioxide, as well as traces of methane. The electrochemical reactions involving carbon dioxide are given by Reactions 2.4-2.6 [16], which from left to right represent fuel cell operation, while in the opposite direction they show electrolysis operation:

Fuel electrode	$2CO + 2O^{2-} \leftrightarrow 2CO_2 + 4e^-$	2.4
Oxygen electrode:	$O_2 + 4e^- \leftrightarrow 2O^{2-}$	2.5
Overall:	$2CO + O_2 \leftrightarrow 2CO_2 \quad \Delta h^0_{298K} = -283\ [kJ/mol]$	2.6

Reactions 2.4-2.6 are all electrochemical reactions that occur at the TPBs of the SOCs. However, when working with carbonaceous gas compositions like syngas or methane, many equilibrium reactions become possible within the porous volume of SOCs due to the elevated temperatures of operation and the presence of nickel in the fuel electrode material which acts as a catalyst [2] [10] [16]. The most important equilibrium chemistries involved include:

- Water-Gas Shift (→) / Reverse Water-Gas Shift (←)

$$CO + H_2O \leftrightarrow CO_2 + H_2 \qquad \Delta h^0_{298K} = -41\ [kJ/mol] \qquad 2.7$$

- Methane Reforming (→) / Methanation (←)

$$CH_4 + H_2O \leftrightarrow CO + 3H_2 \qquad \Delta h^0_{298K} = 206\ [kJ/mol] \qquad 2.8$$

$$CH_4 + 2H_2O \leftrightarrow CO_2 + 4H_2 \qquad \Delta h^0_{298K} = 165\ [kJ/mol] \qquad 2.9$$

$$CH_4 + CO_2 \leftrightarrow 2CO + 2H_2 \qquad \Delta h^0_{298K} = 247\ [kJ/mol] \qquad 2.10$$

Reaction 2.7 shows the **Water-Gas Shift** (WGS) and **Reverse Water-Gas Shift** (RWGS) reactions. As can be observed from their enthalpy of reaction at standard condition (Δh^0), the WGS is moderately exothermic, therefore increasing the temperature of the system increases the reaction rate but shifts the equilibrium towards the reactants, and vice versa. The WGS dominates over the RWGS at temperatures up to around $827°C$; at higher temperatures the equilibrium shifts to the reactants and the RWGS becomes much more predominant [17] [18]. The presence of nickel also catalyzes Reactions 2.8-2.10 known as the reforming and methanation reactions. From left to right, Reaction 2.8-2.10 are known as **steam methane reforming** and Reaction 2.10 as **dry methane reforming**. In the reverse direction, all of these chemical equations are known as **methanation reactions**. Reforming reactions are all strongly endothermic, therefore they are promoted by higher operating temperatures [5].

SOCs operating with carbon-containing mixtures can suffer from carbon deposition, which deactivates the catalytic activity of the whole cell, as the carbon covers the surface of the nickel and prevents gases from reaching it [2] [19]. Carbon deposition occurs mainly through Reactions 2.11-2.13. Reaction 2.11 mostly occurs during SOEC mode when the concentration of carbon monoxide and the voltages are high enough that it reduces carbon dioxide beyond carbon monoxide. The Boudouard Reactions 2.12-2.13 occur under pressurized conditions and low temperatures [16]:

$$CO_{(g)} \rightarrow C_{(s)} + \frac{1}{2} O_2 \qquad 2.11$$

$$CO_{(g)} + H_{2(g)} \rightarrow C_{(s)} + H_2O_{(g)} \qquad 2.12$$

$$2CO \rightarrow C_{(s)} + CO_{2(g)} \qquad 2.13$$

Enough steam or carbon dioxide must be added to the mixture to prevent carbon deposition, as these react with solid carbon oxidizing it back to carbon monoxide. Carbon deposition boundaries are a function of temperature, pressure and feed composition. This means that a safe composition of the gases used must be determined for an SORC system. This can be done through a thermodynamic equilibrium analysis of carbon-hydrogen-oxygen systems [2].

2.3.1. Carbon Deposition Boundaries

Carbon deposition boundaries are mostly a function of temperature, pressure and the elemental composition of the system. The final gas composition is normally determined from thermodynamic studies of systems containing the main reacting elements: oxygen, hydrogen and carbon, thus resulting in an optimum **hydrogen-to-carbon ratio** (H/C ratio) [2]. An increasing H/C ratio implies that the system will tend towards more hydrogen and water content. An H/C ratio that tends to infinity corresponds to a pure $H_2 - H_2O$ system. Figure 2.5 shows a C-H-O ternary diagram based on the work of Wendel [2] on SORC systems. It depicts several gas compositions whose H/C ratio lies below the carbon deposition boundaries at typical temperatures and pressures of operation of solid oxide cells.

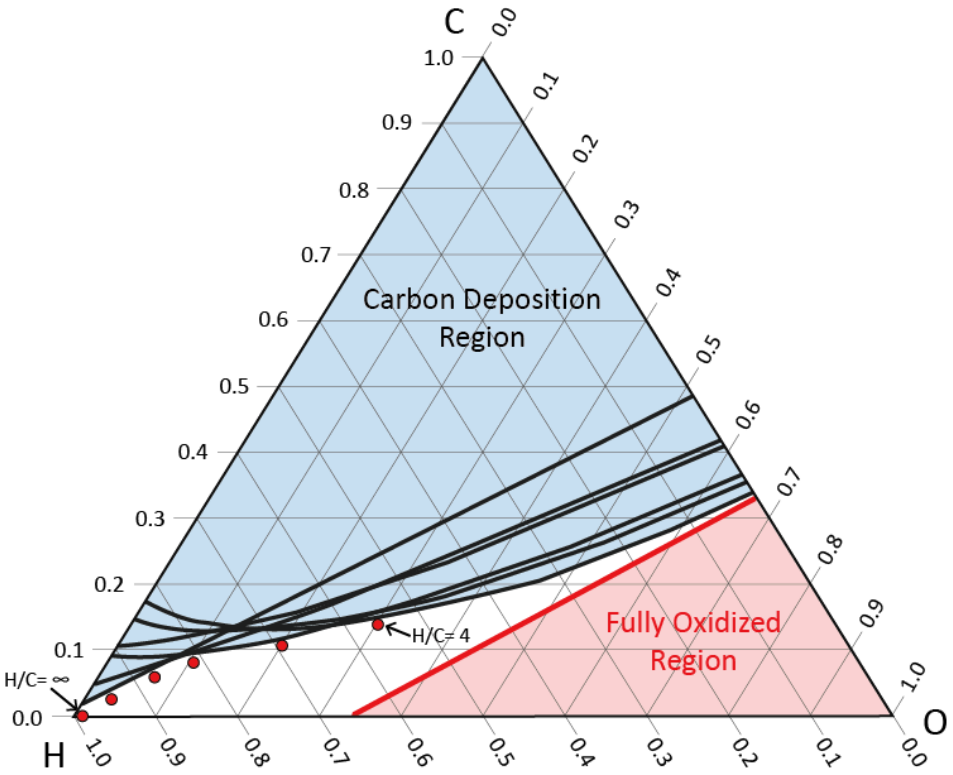

Figure 2.5. Ternary diagram for a C-H-O system, showing carbon deposition boundaries at different temperatures and pressures, and safe H/C ratios (red dots) for an SORC system. Figure based on the work of Wendel [2].

The formation of methane inside the system through the methanation Reactions 2.8-2.10 was limited in this project, since its aim was to evaluate the performance of an SORC system that does not include methanation steps in order to simplify its construction and be able to use readily available technologies based on YSZ cells. Since methane reforming is mostly promoted at temperatures above $700°C$, this study focused on the temperatures between $700 - 800°C$. As a rule, conditions in the SORC system that promoted a CH_4 content above a 1% dry mole basis were not considered.

It must be noted that a higher methane content is not necessarily detrimental to the process chain, however preventing methanation makes it possible to develop the most basic system configuration for SORCs working with carbon-containing species, which can then be used as a reference to compare whether or not it makes sense to go for energy storage systems with more complex process chains. It can also be used as a reference when deciding to include or not fuel synthesis processes like Fischer-Tropsch or methanol reactors to take advantage of the syngas production.

2.4. Thermodynamics of Solid Oxide Cells

The thermodynamic properties that describe the behavior of solid oxide cells are important to understand what the theoretical limits of the technology are. This knowledge serves as the starting point to determine the components that are required to build a high efficiency system based on SORCs that work with a specific rich/spent syngas composition.

2.4.1. Reversible Voltage

For a chemical reaction at a constant pressure and temperature $T\ [K]$, the enthalpy change of reaction, $\Delta h\ [J/mol]$, of the system is related to the change in Gibbs free energy, $\Delta g\ [J/mol]$, and the change in entropy, $\Delta s\ [J/(mol \cdot K)]$, by the thermodynamic relation [20]:

$$\Delta h = \Delta g + T\Delta s \qquad 2.14$$

Δg represents the reversible work that the system can perform at a fixed temperature $T\ [K]$, which for an SORC translates into to the maximum electric potential that can be produced in SOFC mode, or the minimum electric potential required for electrolysis in SOEC mode. The term $T\Delta s$ therefore represents the remaining energy that is released or must be supplied in the form of heat for SOFC or SOEC operation, respectively. The change in Gibbs free energy is related to the electric potential in the cell by the relation [16]:

$$U_{rev} = \frac{-\Delta g}{nF} \qquad 2.15$$

where $U_{rev}\ [V]$ corresponds to the **reversible voltage** of the cell, also known as Nernst voltage; $n\ [-]$ is the number of electrons transferred in the electrochemical reaction taking place, and $F = 96{,}485\ [C/mol]$ is Faraday's constant.

The enthalpy of reaction for a specific reaction has a fixed value at a specific temperature and pressure (since it depends on state variables), and in most systems this value changes very little as a function of temperature. Therefore, Equation 2.14 implies that as the temperature increases, the term $T\Delta s$ increases with it, and the value of Δg must decrease to keep Δh constant. As a result, the reversible voltage of the cell decreases (Equation 2.15). Figure 2.6 plots this behavior for Reaction 2.3. All of this means that the performance of SOFC operation decreases at higher temperatures since the cells produce a lower voltage, while on the other hand the performance of SOEC operation increases as less voltage is needed for electrolysis.

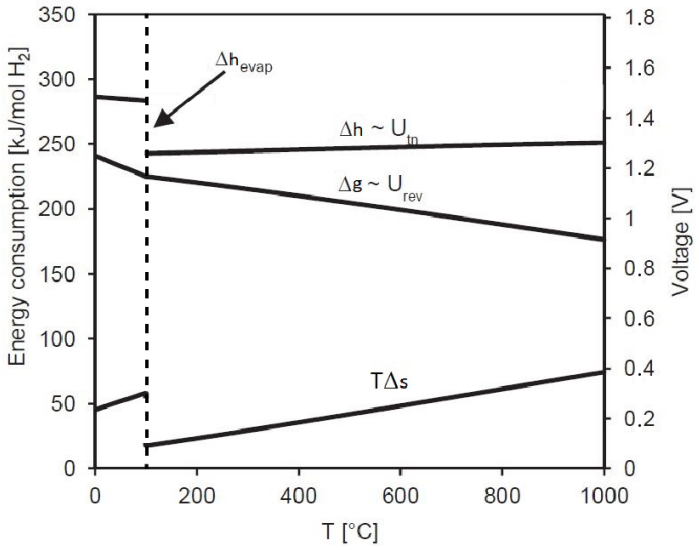

Figure 2.6. Change in enthalpy of reaction (and thermoneutral voltage), Gibbs free energy (and reversible voltage) and entropy as a function of temperature for Reaction 2.3.

2.4.2. Nernst Voltage

It is possible to calculate the reversible voltage for a cell at conditions different to standard conditions. For Reaction 2.3, it can be shown that the change in Gibbs free energy can be written in the form of Equation 2.16 [21]:

$$-\Delta g = -\Delta g^0(T) + RT \cdot \ln\left(\frac{p_{H_2} \cdot {p_{O_2}}^{1/2}}{p_{H_2O}}\right) \qquad 2.16$$

where $\Delta g^0(T)\ [J/mol]$ is the change in Gibbs free energy at a standard pressure $p_0 = 1.01325\ [bar]$ and temperature $T\ [K]$. The constant $R = 8.314\ [(J \cdot K)/mol]$ is the universal gas constant; and $p_k\ [Pa]$ is the partial pressure of component k. Combining Equation 2.15 and Equation 2.16 we get Equation 2.17, known as the Nernst equation:

$$U_{rev} = \frac{-\Delta g^0(T)}{2F} + \frac{RT}{2F} \cdot \ln\left(\frac{p_{H_2} \cdot {p_{O_2}}^{1/2}}{p_{H_2O}}\right) \qquad 2.17$$

For Equation 2.17 the number of electrons transferred is given per mole of hydrogen in Reaction 2.3, therefore $n = 2$. The Nernst equation is only valid for non-reacting gas mixtures under chemical equilibrium. This implies that it can only be applied if the gas species have attained chemical equilibrium or quasi-equilibrium at their specific temperature [11] [21]. This is not a problem for solid oxide cells, since their high temperatures of operation allow them to have very fast kinetics where species can be assumed to instantly achieve near-chemical equilibrium [2] [10]. Therefore, it is possible to use Equation 2.17 for modeling purposes.

2.4.3. Thermoneutral Voltage

The **thermoneutral voltage**, $U_{tn}\ [V]$, is generally defined as the change in enthalpy of reaction divided by the units of charge transferred [16]:

$$U_{tn} = \frac{\Delta h}{nF} \qquad 2.18$$

Therefore, Equation 2.18 is the theoretical voltage that should be applied to an electrochemical cell so that the heat taken by the endothermic electrolysis reactions would equal the total heat produced by internal losses in the cell. As a result, a cell operating at U_{tn} would be at isothermal and adiabatic conditions.

The thermoneutral voltage is a concept that is easier to understand for SOEC operation of a solid oxide reversible cell, given the endothermic nature of the electrolysis reactions taking place; it is difficult to apply to SOFC operation if only electrochemical reactions are considered since an SORC in this mode of operation is in most cases exothermic [2] [22], therefore always produces excess heat beyond isothermal and adiabatic conditions even if operated at its reversible voltage.

Nevertheless, the concept of the thermoneutral voltage can be more easily applied to SOFC operation if reactions other than the electrochemical reactions are considered. As it was explained in Section 2.3, an SORC operating with carbonaceous gas mixtures will experience some endothermic equilibrium reactions like the reforming reactions and the RWGS reaction; these can take some of the heat generated by the electrochemical reactions as well as that generated by other exothermic reactions like the WGS and methanation reactions. Therefore, the net enthalpy change in Equation 2.18 for the whole SOFC operation has to take into account the enthalpy changes of all the electrochemical and equilibrium reactions at the same time. Wendel [2] developed a general definition for the thermoneutral voltage considering the steady-state energy balance of a solid oxide cell shown in Equation 2.19:

$$\dot{Q} - P_e = \left(\dot{H}_{fuel/reactant,out} + \dot{H}_{oxidant,out}\right) - \left(\dot{H}_{fuel/reactant,in} + \dot{H}_{oxidant,in}\right) \quad 2.19$$

where $\dot{Q}$ $[W]$ is the rate of heat transferred to/from the environment, P_e $[W]$ is the net electric power generated or consumed by the SOC, and $\dot{H}$ $[W]$ is the enthalpy rate of each of the inlet and outlet gas streams of the fuel and oxygen electrodes. The net electric power of the single cell is by definition given by Equation 2.20:

$$P_e = i \cdot V_{cell} \quad 2.20$$

where V_{cell} $[V]$ is the operating voltage of the cell, and i $[A]$ is the direct current passing through it in either SOFC or SOEC mode. During thermoneutral operation, the term $\dot{Q}$ is equal to zero (adiabatic and isothermal), thus Wendel finally defined the thermoneutral voltage in the form of Equation 2.21, which is applicable to SOFC and SOEC operation [2]:

$$U_{tn} = -\frac{\left(\Delta\dot{H}_{fuel/reactant} + \Delta\dot{H}_{oxidant}\right)}{i} \quad 2.21$$

The thermoneutral voltage of the co-electrolysis of CO_2 and H_2O will be between the thermoneutral voltage of pure water and the thermoneutral voltage of pure carbon dioxide. At a temperature of $800°C$ these respectively correspond to $U_{tn,H_2O} = 1.29$ $[V]$ and $U_{tn,CO_2} = 1.46$ $[V]$ [11]. The degree to which the thermoneutral voltage will tend to that of water or to that of carbon dioxide will depend on how prevalent the electrolysis of each component is.

3. LITERATURE REVIEW

This chapter summarizes the previous works in the field of SOC-based systems relevant to this project. Although it was not possible to explore all the literature available, the works presented here and throughout this report provided important parameters and enough theoretical and experimental information to design the SORC systems studied and justify the assumptions made to build the computer model.

Given the innate ability of solid oxide cells to work interchangeably as fuel cells and as electrolyzers, modeling studies of reversible operation are usually achieved by creating separate models of an SOFC and an SOEC where the results of each of them are then processed together; or by combining such two models in the same simulation environment, therefore allowing to process the results simultaneously. In this sense, any literature about the simulation of SOFC systems, SOEC systems and SORC systems can be utilized as long as the properties of the cells and their operation is similar.

3.1. Cell and Stack Level Studies

The point of departure in the study of SOCs is at the cell and stack levels. The difference between these two is mostly that stack modeling incorporates the series connection of multiple cells and accounts for energy losses due to the interconnectors used. Modelling at this level can be done in many dimensions: in 0D models, the cells or stack are taken as a black box where dimensions have no effects in any direction and the behavior of the whole system is represented by general algebraic equations of thermodynamics, electrochemistry and transport phenomena. 1D models hold two dimensions constant and changes are analyzed along the third, which is usually the direction of flow of the gases through the electrodes. 2D models hold only one dimension constant, and 3D models analyze the full volume of the system, allowing to achieve much more detailed studies. These last two, however, are also much more computationally-demanding [23]. 0D models give the overall input-output behavior of the SORC stack for properties like power production/consumption, temperature,

pressure or gas composition, which are usually enough for the analysis of systems that contain more components than the stack. Since this work is focused on the design of such systems, the computer model developed was zero-dimensional.

Stoots et al. [11] developed a 0D mathematical model for SOEC co-electrolysis in order to predict and compare thermodynamic voltages and gas compositions with those obtained from button-cell stacks using scandium-stabilized zirconia electrolytes. Results of the model showed great similarity with experiments for variations in inlet gas composition, electrical current, and stack operating temperatures. The electrochemical model used lumped together all the loss mechanisms inside the cells in a parameter known as the Area-Specific Resistance (ASR), usually defined in units of Ω/cm^2. Stoots et al. showed that the ASRs between electrolysis of pure water and co-electrolysis showed no considerable differences, therefore implying that CO_2 is likely not consumed through electrochemical reactions (Reactions 2.4-2.6) but through the RWGS reaction. It was also concluded that coelectrolysis increases the yield of syngas over the RWGS reaction equilibrium compositions.

ASRs are derived experimentally from the cells studied therefore they have good accuracy. However, ASRs only work within narrow operating conditions and are commonly defined as a function of temperature, since this parameter has the largest effect on cell losses [3] [5] [11] [19] [24] [25]. Since the systems designed in this process take into consideration variations in the pressure, a more detailed model for each overpotential was used. Polarization overpotentials are discussed in more detail in Section 4.1.2.

Ni et al. [26] developed a cell-level 0D mathematical model for steam electrolysis in solid oxide cells that accounts for the main sources of losses inside the device, namely activation, Ohmic and concentration overpotentials. With this model they were able to conclude that fuel electrode-supported YSZ cells would provide a better efficiency than electrolyte-supported cells due to a more positive trade-off between concentration and ohmic overpotentials. Their model also made it possible to conclude that these cells should operate at the highest possible temperature in order to decrease their resistance and increase reaction speeds. Similarly, Hernandez-Pacheco et al. [27] developed similar 0D model for a solid oxide fuel cell using hydrogen as fuel, that allowed them to also conclude that fuel electrode-supported

YSZ cells would provide a better efficiency for the same reasons as Ni et al. [26]. Both of these works were used to derive the algebraic expression in Chapter 4 for the polarization overpotentials that affect the SORC stack in both modes of operation, primarily for the concentration overpotentials. Common equations and parameter values for activation and Ohmic losses were found throughout literature, including the works of Li et al. [9], Hauck et al. [10], Buttler et al. [28], Ni et al. [26], Hernandez-Pacheco et al. [27], Ebbesen et al. [29], and Doherty et al. [22].

Hauck et al. [10] created a 0D model for an SORC stack in Aspen Plus, capable of using carbonaceous mixtures in both modes of operation, and validated the results of the model with the data obtained from the experimental work of Kazempoor and Braun [30] on the use of solid oxide cells for energy storage, proving that in SOEC operation the CO_2 in the inlet mixture was consumed primarily by the RWGS reaction, and that chemical equilibrium was most likely reached within the stack. In order to build the SORC stack, Hauck et al. combined separate SOFC and SOEC Aspen models in the same Aspen flowsheet, each of them based on the works of Tjaden et al. [31] and Redissi and Bouallou [5], respectively. This same strategy was reproduced in this project, however the stack model for SOFC operation was based instead on the works of Sebastiani [24] and Mor [25] on solid oxide reversible cells.

Modelling of co-electrolysis in SOCs is a topic under current investigation, given the complex reaction mechanisms that H_2O and CO_2 can follow during the electrolysis process, including the WGS and RWGS reactions and direct electrochemical conversion. Studies like the ones from Hauck et al. [10], Doherty et al. [22], Graves et al. [17] and Li et al. [9] argued that in many cases CO_2 is not reduced electrochemically but reacts only through the RWGS reaction. However, deeper cell-level studies on the mechanisms of reaction during co-electrolysis show that CO_2 is indeed reduced [11] [19]. Wendel [2] argued that unless the cells are operated under electrolysis conditions where diffusion losses (concentration overpotential) affect performance, it is reasonable to assume that CO_2 is not reduced electrochemically but reacts only through the RWGS reaction, however, more detailed studies focusing on cell materials, cell structures and chemical reaction mechanisms should consider the direct reduction CO_2.

3.2. System Level Studies

A system level study requires considering many different unit operations other than the SORC stack, like compressors, expanders and heat exchangers that increase the difficulty to implement mathematical models. Because of this, it is common to do such studies in process simulation software like Aspen Plus[2] or gPROMS[3] that contain extensive libraries of chemicals, predetermined unit operation models and work environments that simplify the design process. It is possible to make 3D models of solid oxide cells in these computer programs [32]; however, these tend to be less rigorous than studies made with finite-element analysis software like COMSOL[4] or ANSYS[5]. As a result, most stack models in studies at system level are zero-dimensional. Nevertheless, this is usually enough since the input-output behavior of the stack is all that is needed at this level of analysis [23].

Barelli et al. [33] developed an Aspen Plus model of an SOEC stack coupled with a methanation process in order to explore the feasibility of creating mixtures of hydrogen gas and methane (referred as hydromethane) for automotive applications. The design of the stack used a predetermined ASR to calculate polarization losses and varied the amount of carbon dioxide that was allowed to react electrochemically in order to determine the effect of CO_2 electrolysis in the performance of the system, finding that complete consumption of this component through the electrochemical pathway provides the best plant efficiency (60.2%) and highest fuel energy density (21.9 $[MJ/Sm^3]$).

Buttler et al. [28] designed a system model of an SOEC used for steam electrolysis with a 1D numerical model of the stack, utilizing the commercial software Engineering Equation Solver[6] (EES), and analyzed the effect of heat integration on the

[2] https://www.aspentech.com/products/engineering/aspen-plus

[3] https://www.psenterprise.com/products/gproms

[4] https://www.comsol.com/

[5] https://www.ansys.com/

[6] http://www.fchart.com/ees/

stack current density, hydrogen production and required cell area, revealing a tradeoff between lower current densities, which increase efficiency and reduce stack degradation, and higher cell areas that increase investment costs. A techno-economic analysis for a specific cell area cost of 1,500 €/m^2 showed that the system must operate in the endothermic region of electrolysis, therefore if the additional heat needed was provided by electricity, heat integration will have a strong dependency on future electricity prices.

Zhang et al. [34] created a 0D Aspen Plus model for a natural gas-fed SOFC system based on the tubular cell technology developed by Siemens-Westinghouse. The model considers the cell as internally reforming, meaning that all the methane supplied is transformed inside the stack into hydrogen before its electrochemical consumption. This is a reasonable assumption when modeling SOFC operation with carbonaceous mixtures due to the high temperature of SOCs and the presence of nickel in the fuel electrode [2] [22] [31] [34]. However, reforming of carbonaceous mixtures rich in methane is not always fully a task of the cell, and instead external reforming reactors are added to avoid high temperature gradients across the cells due to the endothermic nature of the reforming reactions. Tjaden et al. [31] developed a 0D Aspen Plus model that included such a reactor to reform biogas before its use as fuel inside an SOFC stack. The model analyzed the impact of the type of reforming (steam, partial oxidation or autothermal) on the overall efficiency of the plant, finding steam reforming as the most efficient option. Barelli and Ottaviano [19] developed as well a 0D Aspen Plus model with a reformer prior to the SOFC stack, however their analysis compared steam methane reforming versus dry methane reforming, proving that the latter increases the electric output of the system while at the same time reduces CO_2 emissions.

Doherty et al. [22] made a study of the combined use of biomass gasification and tubular SOFCs by creating a 0D model in Aspen Plus. Results from the model showed that the SOFC system should be allowed to have high fuel utilizations (Section 4.2) for higher efficiency. Additionally, the system showed the ability of SOFCs to increase the performance of traditional biomass systems by making an analysis on the Güssing

CHP plant in Austria where it was concluded that replacing the gas engine of the plant with an SOFC could increase the overall efficiency by up to 8%.

System studies on SORC systems working with carbonaceous mixtures tend to include strategies that promote the formation of methane inside the system (methanation). This is done in order to avoid working with hydrogen gas, whose low volumetric energy density and difficulty to compress decrease energy density. Additionally, the heat generated by methanation can help with the heat management of the system. These strategies include using methanation reactors or the utilization of intermediate temperature SOCs ($< 650°C$) that use materials different to YSZ [2] [3] [12] [13].

An exhaustive work in the field of SORCs working with carbonaceous mixtures was performed by Wendel [2], where he explored the use of intermediate temperature SOCs to design and optimize an SORC system using the software programs EES and gPROMS. He was able to develop system configurations using a stack made out of strontium- and magnesium-doped lanthanum gallate (LSGM) electrolytes operating at less than $650°C$ that could work at roundtrip efficiencies (Section 4.5) higher than 70%, proving the advantage of methanation for energy storage application with solid oxide cells. However, this involved a system also containing a methanation reactor and several compression and expansion units, giving the it a lot of complexity. Additionally, intermediate reversible cells are still not commercially available, limiting the implementation of such system. Nevertheless, reference [2] was a main source of information that heavily influenced this project, given the depth of the analysis at the cell and system levels, and the design methodology used.

Mottaghizadeh et al. [3] developed an SORC system working with carbonaceous mixtures in Aspen Plus using commercially available SOCs. The structure of their system was similar to the one proposed by Wendel [2] [13] also using a methanation reactor inside the system. However, the heat management was improved by using thermal energy storage systems composed of phase-change materials (PCM). The end result was a system capable of delivering a roundtrip efficiency of up to 54.3%, with full heat integration.

Sebastiani [24] and Mor [25] extended their analysis of SORC systems beyond energetic performance by also considering an exergy analysis of the system. This

additional approach helped not only to identify within the plant how energy was transferred between processes, but also how effectively this energy was used. Sebastiani modeled an SORC system in Aspen Plus that works with hydrogen as fuel for SOFC mode and steam as reactant for SOEC mode. His conclusion was that such an SORC system can achieve roundtrip efficiencies as high as 53% if the system was pressurized to up to 10 [bar] and a gas turbine was used in SOFC mode. Major sources of exergy destruction included heat exchangers, compression and combustion. Mor built upon the work of Sebastiani and changed the fuel composition in SOFC mode from hydrogen to syngas, while keeping steam electrolysis in SOEC mode. Her results showed a roundtrip efficiency of her best design as high as 49% for pressurized operation to up to 4 [bar] and the use of a gas turbine in SOFC mode. Major exergy losses occurred in the outlet gases. Both of these studies, however, considered the inlet gases to enter the system at (storage) pressures close to atmospheric, which would not be practical for energy storage systems that try to increase energy density by storing the working gases at high pressure.

Based on the literature consulted, this project contributed to new knowledge in the field of SORC systems and energy storage technologies by using energy and exergy analyses as performance criteria. Additionally, the system was designed to work with carbonaceous mixtures in both modes of operation, with SOEC mode using co-electrolysis and SOFC mode consuming syngas directly. The gases that entered and left the fuel electrodes of the stack were kept in a closed system and were stored in high pressure containers, while the oxidant was taken from the air through an open air cycle. The configuration of the balance-of-plant was inspired on the works of Wendel [2] and Mottaghizadeh et al. However, the formation of methane was kept intentionally low in order to explore the characteristic of a system that works exclusively with syngas. This approach would make it possible to use commercially available high-temperature SOCs based on YSZ technology, while simplifying the system configuration by removing methanation reactors.

4. COMPUTER MODEL

Chapter 2 introduced the different chemical reactions that take place in an SORC that works with carbonaceous mixtures, as well as the basic thermodynamic equations that describe solid oxide cells. This chapter builds on these definitions to describe the computer model developed in this study. It starts by describing the assumptions regarding electrochemical reactions and co-electrolysis that shape the modeling strategy of the cells. Based on these assumptions, the equations describing the overpotentials affecting solid oxide cells are introduced, followed by the definition of concepts like the fuel utilization, power production and the Equal Charge Constraint.

The computer model in Aspen Plus is explained for the SORC stack and the Balance-of-Plant components. This section also explains the requirements of the gas mixtures used to avoid carbon deposition, and the solution strategy utilized to quickly determine their equilibrium compositions in Aspen. Finally, roundtrip and exergy efficiency performance metrics are derived, and the general solution methodology and base scenario are presented.

4.1. Electrochemical Model

The thermodynamic relations explained in Section 2.4 are all expressed in terms related to the electrochemical Reaction 2.3. However, the presence of carbon monoxide in SOFC operation and carbon dioxide in SOEC operation imply that the electrochemical Reaction 2.6 could also play a role. Additionally, the reversible voltage is just the theoretical voltage that the cell delivers or requires, but not the one that is actually obtained. In this section, the electrochemical model for the SORC working with syngas and co-electrolysis is explained, introducing the assumption of $H_2 - H_2O$ only electrochemistry and the polarization overpotentials resulting from it.

4.1.1. Electrochemical Reaction Pathways for Syngas

The system studied in this work consists of an SORC that directly uses syngas (H_2 and CO) as fuel during SOFC operation and performs the co-electrolysis of CO_2 and H_2O during SOEC operation. The presence of a carbonaceous mixture of gases for both modes of operation implies that all the electrochemical and equilibrium reactions introduced in Chapter 2 take place at the same time in the stack and must be accounted for. It is then of special interest to define to what degree the H_2 and CO, and the H_2O and CO_2 are consumed electrochemically and by equilibrium reactions during SOFC and SOEC operation, respectively.

SOFC reaction pathways

As it was explained before in Section 2.2, because of the high operating temperatures of SORCs and the presence of nickel in the electrodes the kinetics of equilibrium reactions are very fast, and reactions can be assumed to reach near-equilibrium. In the case of SOFC operation, this means that the reforming reactions and the WGS reaction that govern at the usual operating temperatures ($700°C - 800°C$) are very quick to convert almost all the methane and carbon monoxide that enter the cells into hydrogen gas before these have a chance of reaching the TPBs. In this case, the solid oxide cells are referred as internally reforming.

The conversion of CH_4 and CO to hydrogen gas is also promoted by the larger size of these molecules compared to hydrogen, that make them diffuse with more difficulty inside the porous matrix of the electrode all the way to the TPBs. This gives enough time for them to be converted into hydrogen gas [9]. Given that it is mostly hydrogen that arrives at the TPBs, it can be assumed that only H_2 reacts electrochemically with the O^{2-} ions coming from the oxygen electrode, while the CO and CH_4 in the syngas are consumed exclusively through the WGS reaction and the steam reforming reactions [31].

SOEC reaction pathways

In SOEC mode, conditions in the fuel electrode can be such that it is possible to have either co-electrolysis of carbon dioxide and water or only electrolysis of H_2O. In this work it was assumed that only H_2O electrolysis takes place at the TPBs, while the CO_2 in the syngas was consumed exclusively through the RWGS reaction. Although this definition of co-electrolysis implies no direct electrochemical reaction of carbon dioxide, this assumption is backed by several works that showed that this phenomenon might be the dominant reactions pathway for CO_2, and is the result of electrode conditions where CO_2 is not capable of diffusing fast enough to reach the TPBs before it is consumed by the RWGS reaction [9] [10] [11] [17] [22] or because of a situation where even if the CO_2 molecules reach the TPBs, these don't have the catalytic capacity to directly electrolyze CO_2 so instead it is again consumed by the RWGS reaction [35].

In conclusion, for the reaction pathways considered in this study:

- In SOFC mode, only H_2 reacts electrochemically while CO is consumed through the WGS reaction.

- In SOEC mode, only H_2O reacts electrochemically while CO_2 is consumed through the RWGS reaction.

The main implication of these assumptions was that the thermodynamic equations presented in Section 2.4 were the only ones needed to describe the electrochemistry of the SORC; and all polarization overpotentials were given by the $H_2 - H_2O$ system, while CO and CO_2 had no influence on any of them. This simplified the model without removing too much accuracy.

4.1.2. Polarization Overpotentials

The reversible voltage described in Section 2.4 is the maximum theoretical voltage that an SORC can deliver in SOFC mode. It is as well the minimum voltage needed to achieve electrolysis in SOEC mode. In reality, however, lower voltages than the reversible voltage are needed in SOFC mode and higher voltages are needed in SOEC mode because of different phenomena that kinetically limit the charge transfer processes inside the cells, adding barriers to the flow of current that create energy losses in the system. These phenomena are known as polarization overpotentials or polarization resistances and are divided into three main categories:

- Activation overpotentials (V_{act}).
- Ohmic overpotentials (V_{ohm}).
- Concentration overpotentials (V_{conc}).

After accounting for overpotentials, the final operating voltages of an SORC in SOFC mode and SOEC mode are respectively defined by Equations 4.1 and Equations 4.2:

$$V_{cell,SOFC} = U_{rev} - (V_{act} + V_{ohm} + V_{conc}) \quad 4.1$$

$$V_{cell,SOEC} = U_{rev} + (V_{act} + V_{ohm} + V_{conc}) \quad 4.2$$

During SOFC operation the overpotentials reduce the output of the SORC, while during SOEC operation the polarity of the overpotentials is inversed, adding up to the power required for electrolysis. A single solid oxide cell typically ends up operating between 0.5 and 2.0 $[V]$ [2].

Activation overpotentials

The activation overpotentials account for the energy barriers that must be overcome by the electrochemical reactions at the TPBs of each electrode during the charge transfer processes between charged and non-charged species. The general description of this phenomena is given by the well-known Butler-Volmer equation:

$$j = j_{0,k}\left[e^{\frac{nF\cdot\alpha_{a,k}}{RT}\cdot\eta_{act,k}} - e^{\frac{nF\cdot\alpha_{c,k}}{RT}\cdot\eta_{act,k}}\right] \quad 4.3$$

$$j = \frac{i}{A_{cell}} \quad 4.4$$

where $j\ [A/m^2]$ is the current density running through one cell; $i\ [A]$ is the direct current running through the stack (and every individual cell), and $A_{cell}\ [m^2]$ is the active area of one cell. The subscript k refers to the fuel electrode or the oxygen electrode; $\alpha_{a,k}\ [-]$ and $\alpha_{c,k}\ [-]$ are the anodic and cathodic transfer coefficients, respectively, and $j_{0,k}\ [A/m^2]$ is the exchange current density of electrode k.

The exchange current density is the net current that exists at the electrode-electrolyte interface when the cell is at the open-circuit voltage (equilibrium). It is a property of the electrode itself that depends on temperature, the materials used, and the fabrication techniques utilized. It is very hard to obtain explicit values for the exchange current density, thus empirical Arrhenius-type formulations like the one of Equation 4.5 are normally used [10] [31] [28] [32] [22] [26] [27]:

$$j_{0,k} = \gamma_{0,k}\cdot e^{\frac{-E_{act,k}}{RT}} \quad 4.5$$

where the pre-exponential factor $\gamma_{0,k}\ [A/m^2]$ and the activation energy $E_{act,k}\ [J/mol]$ of the electrode k are empirical values.

The Butler-Volmer equation can be simplified by assuming that the transfer coefficients for both electrodes are equal to 0.5. In this case the inverse hyperbolic sine approximation shown in Equation 4.6 can be used, making it possible to determine the activation overpotential for each electrode as an explicit function of the current density [10] [31] [28] [36].

$$V_{act,k} = \frac{2RT}{nF}\cdot sinh^{-1}\left(\frac{j}{2\cdot j_{0,k}}\right) \quad 4.6$$

Since only H_2 and H_2O are assumed to react electrochemically, according to Reactions 2.1 and 2.2 the coefficient n is equal to 2 for the fuel electrode, and 4 for the oxygen electrode.

Ohmic overpotentials

Ohmic overpotentials are caused by the natural resistance of the electrodes, connections and interconnector to the flow of electrons, and the resistance of the electrolyte membrane to the flow of ions from the cathode to the anode. The electronic resistivities of the connections and current collectors are usually very small, and it is normal to model them to be independent of temperature. On the other hand, the ohmic losses in the system are largely dominated by the resistivity of the electrolyte, which is a strong function of temperature [10] [28] [26] [27]. Hauck et al. [10] described the overall ohmic overpotential in a solid oxide cell in the form of Equation 4.7:

$$V_{ohm} = j\left(r_{ohmic,el} + r_{ohmic,conn}\right) = j\left(\frac{\delta_{el}}{\sigma_{el}} + r_{ohmic,conn}\right) \qquad 4.7$$

where $r_{ohmic,conn}\ [\Omega \cdot m^2]$ is the specific ohmic resistance of electron-conducting elements in the cell and $r_{ohmic,el}\ [ohm \cdot m^2]$ is the specific ohmic resistance of the electrolyte, which is defined as the inverse of the conductivity $\sigma_{el}\ [(\Omega \cdot m)^{-1}]$ of the electrolyte times its thickness $\delta_{el}\ [m]$. The conductivity of the electrolyte can be represented with an Arrhenius-type equation of the form of Equation 4.8:

$$\sigma_{el} = \sigma_{0,el} \cdot e^{\frac{-E_{act,el}}{RT}} \qquad 4.8$$

where the pre-exponential factor $\sigma_{0,el}\ [(\Omega \cdot m)^{-1}]$ and the activation energy $E_{act,el}\ [J/mol]$ of the electrolyte are empirical values taken from the literature. From Equation 4.7 and Equation 4.8 it can be observed that the Ohmic overpotentials are a linear function of the current density and the thickness of the electrolyte, however they have an inversely exponential relationship with temperature.

Decreasing the temperature of an SORC stack makes it possible to use cheaper materials for its construction; however, the conductivity of the electrolyte decreases exponentially and much faster than other overpotentials, thus the cell must be kept at high temperatures. At high temperatures, activation and ohmic overpotentials of YSZ-based cells tend to be very small because of the strong exponential dependency on the temperature of the cells.

Overall, ohmic overpotentials tend to be larger than activation overpotentials, and it is because of this that they are the main source of polarization losses in solid oxide cells [10]. These losses are converted directly into heat that heats up the cell in a process known as Joule heating or Ohmic heating. During SOEC operation, the solid oxide cells will usually work at the thermoneutral voltage when these Ohmic losses equal the heat requirements of all the endothermic reactions taking place inside it.

Concentration overpotentials

Concentration overpotentials are the manifestation of the mass transport limitations of the components involved in the electrochemical reactions taking place in an SORC as they diffuse from the flow channels to the active sites in each electrode and vice versa. In a working cell, the concentration of the reacting species near the active sites decreases as the current density of the cell goes up since the rate of electrochemical reactions is given by the current density. These reactants can only be replenished by the diffusion of gas from the flow channel through the pores of the electrode. Therefore, if the rate of diffusion struggles to keep up with the rate of reaction, the partial pressures of reactants at the TPBs drops and the local Nernst potential lowers with respect to the ideal Nernst potential that would be obtained from their partial pressures at the bulk and this is translated into a voltage drop i.e. an overpotential.

Assuming that only H_2 and H_2O electrochemical reactions take place, the concentration overpotential in the fuel electrode during SOFC operation is given by Equation 4.9 [27]:

$$V_{conc,FE,SOFC} = \frac{RT}{2F} \cdot \ln\left(\frac{p_{H_2,bulk} \cdot p_{H_2O,TPB}}{p_{H_2,TPB} \cdot p_{H_2O,bulk}}\right) \qquad 4.9$$

while the concentration overpotential in the fuel electrode during SOEC operation is given by Equation 4.10 [26]:

$$V_{conc,FE,SOEC} = \frac{RT}{2F} \cdot \ln\left(\frac{p_{H_2,TPB} \cdot p_{H_2O,bulk}}{p_{H_2,bulk} \cdot p_{H_2O,TPB}}\right) \qquad 4.10$$

According to Reactions 2.3, in the oxygen electrode only oxygen gas participates in the electrochemical reactions. Therefore, the concentration overpotential in the oxygen electrode during SOFC operation is given by the Equations 4.11 [27]:

$$V_{conc,OE,SOFC} = \frac{RT}{4F} \cdot \ln\left(\frac{p_{O_2,bulk}}{p_{O_2,TPB}}\right) \tag{4.11}$$

while the concentration overpotential in the oxygen electrode during SOEC operation is given by the Equations 4.12 [26]:

$$V_{conc,OE,SOEC} = \frac{RT}{4F} \cdot \ln\left(\frac{p_{O_2,TPB}}{p_{O_2,bulk}}\right) \tag{4.12}$$

where the terms $p_{k,bulk}$ $[Pa]$ and $p_{k,TPB}$ $[Pa]$ are the partial pressures of $k = H_2$, H_2O or O_2 at the flow channels and at the TPBs, respectively. The partial pressure of these gases at the TPBs can be determined by applying mass and charge conservation principles. The explicit methodology to do this is not discussed in this work, however, a comprehensive derivation is presented in the work of Ni et al. [26] and Hernandez-Pacheco et al. [27]. Applying Fick's Law for one-dimensional diffusion and the Dirichlet boundary condition, and assuming that the TPB sites are located only at the electrode-electrolyte interface, Equations 4.9 and Equations 4.11 for SOFC operation can be rewritten in the form of Equation 4.13 for the fuel electrode and Equation 4.14 for the oxygen electrode:

$$V_{conc,FE,SOFC} = \frac{RT}{2F} \cdot \ln\left(\frac{1 + j\left(\frac{RT}{2F}\frac{\delta_{FE}}{D_{eff,H_2} \cdot p_{H_2O,bulk}}\right)}{1 - j\left(\frac{RT}{2F}\frac{\delta_{FE}}{D_{eff,H_2} \cdot p_{H_2,bulk}}\right)}\right) \tag{4.13}$$

$$V_{conc,OE,SOFC} = \frac{RT}{4F} \cdot \ln\left(\frac{1}{1 - j\left(\frac{RT}{4F}\frac{\delta_{OE}}{D_{eff,O_2} \cdot p_{O_2,bulk}}\right)}\right) \tag{4.14}$$

while Equations 4.10 and 4.12 for SOEC operation are rewritten the form of Equation 4.15 for the fuel electrode and Equation 4.16 for the oxygen electrode:

$$V_{conc,FE,SOEC} = \frac{RT}{2F} \cdot \ln\left(\frac{1 + j\left(\frac{RT}{2F}\frac{\delta_{FE}}{D_{eff,H_2O} \cdot p_{H_2,bulk}}\right)}{1 - j\left(\frac{RT}{2F}\frac{\delta_{FE}}{D_{eff,H_2O} \cdot p_{H_2O,bulk}}\right)}\right) \qquad 4.15$$

$$V_{conc,OE,SOEC} = \frac{RT}{4F} \cdot \ln\left(1 + j\left(\frac{RT}{4F}\frac{\delta_{OE}}{D_{eff,O_2} \cdot p_{O_2,bulk}}\right)\right) \qquad 4.16$$

where δ_{FE} $[m]$ and δ_{OE} $[m]$ are respectively the thicknesses of the fuel and the oxygen electrodes. The effective diffusion coefficients, D_{eff} $[m^2/sec]$, must be determined from the gas composition and the geometry of the cell. These coefficients depend on the type of molecules in the system and the type of diffusion in the electrodes: molecular diffusion occurs when the size of the pores is larger than the mean free path of the molecules, therefore the interaction between molecules is dominant. If this is not the case, then the interactions between the molecules and the pore walls become more relevant and Knudsen diffusion dominates. Both types of diffusion occur in SOCs of planar geometry [22] [26] [27]; therefore, the effective diffusion coefficient of component k, $D_{eff,k}$ $[m^2/sec]$, is determined from Equation 4.17:

$$D_{eff,k} = \frac{\varepsilon}{\tau}\left(\frac{D_{k-l} \cdot D_{Kn,k}}{D_{k-l} + D_{Kn,k}}\right) \qquad 4.17$$

where ε and τ are the porosity and tortuosity of the electrode; D_{k-l} $[m^2/sec]$ is the binary diffusion coefficient between component k and component l; and $D_{Kn,k}$ $[m^2/sec]$ is the Knudsen diffusion coefficient of component k, which in the fuel electrode is H_2 or H_2O during SOFC or SOEC mode, respectively, and in the oxygen electrode is always O_2 for the $O_2 - N_2$ system if air is used. The binary diffusion coefficient results from the interaction between of molecules in the system, and it can be calculated with Equations 4.18 for both modes of operation [10]:

$$D_{k-l} = \frac{1.43 \cdot 10^{-7} \cdot T^{1.75}}{p \cdot \sqrt{\frac{2}{{M_k}^{-1} + {M_l}^{-1}}} \cdot \left({V_{d,k}}^{1/3} + {V_{d,l}}^{1/3}\right)^2} \qquad 4.18$$

where $p\,[bar]$ is the operating pressure of the SORC; $T\,[K]$ is the operating temperature; and $M\,[g/mol]$ and $V_d\,[-]$ are respectively the molar mass and diffusion volume of components k and l, with $V_{d,H_2O} = 13.1$, $V_{d,H_2} = 6.12$, $V_{d,O_2} = 16.3$ and $V_{d,N_2} = 18.5$. The Knudsen diffusion coefficient of component k was calculated using Equation 4.19 [10]:

$$D_{Kn,k} = \frac{2}{3} \cdot r_p \cdot \sqrt{\frac{8RT}{\pi M_k}} \qquad 4.19$$

where $r_p\,[m]$ is the average radius of the pores in the electrode. In Equation 4.19 the universal gas constant is equal to $R = 8{,}314\,[J/(kmol \cdot K)]$. In case that the nitrogen content of the oxidant is below 5%, pure O_2 content can be assumed, and Equation 4.17 reduces to Equation 4.20 [10]:

$$D_{eff,O_2} = \frac{\varepsilon}{\tau} D_{Kn,O_2} \qquad 4.20$$

The partial pressure of the reactants and products changes along the cell as the electrochemical conversion occurs from inlet to outlet. This means that the partial pressure of reacting species is lower at the outlet than at the inlet, and according to Equation 2.17 the reversible voltage will be lower here. This drop in voltage along the cell is sometimes referred as Nernst losses. In order to average the effects of Nernst losses in the computer model, the average between the inlet and outlet partial pressures of the bulk components in the flow channels ($p_{x,bulk}$) was used in Equations 4.13-4.16 [22].

All the expressions derived in this chapter for the polarization overpotentials are a function of the current density passing through a solid oxide cell at a given time. When plotting Equations 4.1 and 4.2 as a function of current density, a polarization curve (or jV-curve) of the form of Figure 4.1 is obtained. In this curve it is possible to observe the relative position of the reversible voltage and thermoneutral voltage of Reaction 2.3 to the operating voltage of the cell for a temperature of $800°C$.

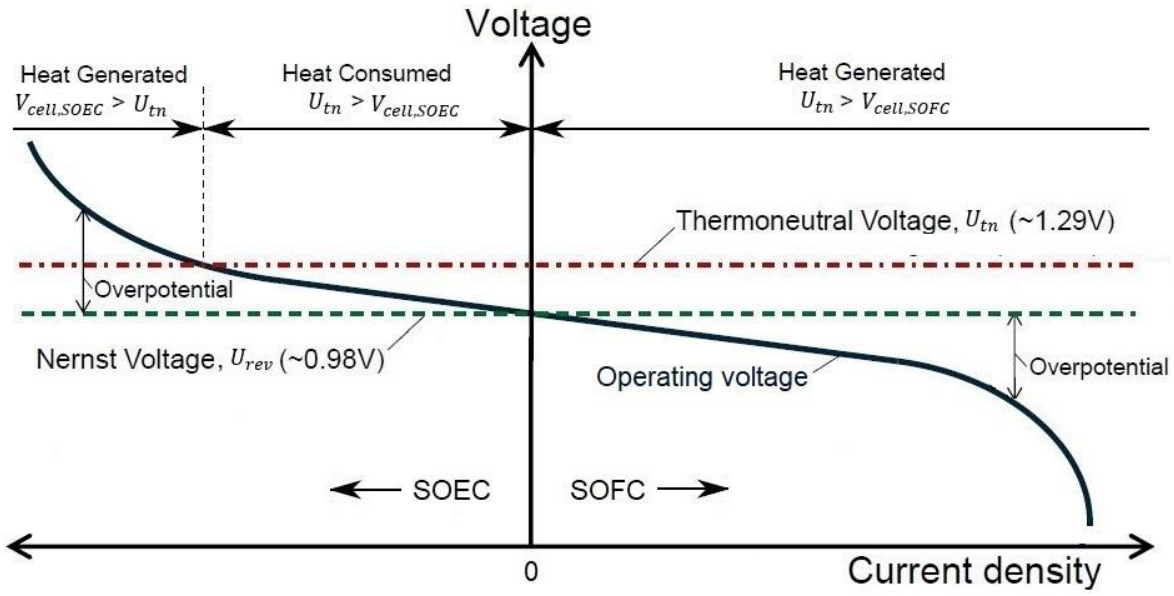

Figure 4.1. jV-curve of an SORC.

The polarization curve for the mathematical model developed can be observed in Appendix A where it is compared to the experimental results obtained by Kazempoor and Braun [30].

4.2. Fuel Utilization

In the operation of solid oxide cells, more specifically SOFCs, the concept of **fuel utilization** refers to the fraction of the inlet fuel mixture that is allowed to react compared to the total amount of fuel that enters the electrolytic cell. Since most SOFCs are operated using hydrogen as a fuel, defining the fuel utilization in terms of hydrogen consumption is almost a standard [2] [22]; a reasonable practice after considering that almost all the carbon containing components are transformed into H_2 inside the cell, as explained in Section 4.1.1. For an SORC in fuel cell mode operating with a carbon-containing gas mixture the fuel utilization, U_f, is given by Equation 4.21:

$$U_f = \frac{\dot{N}_{H_2,consumed}}{\dot{N}_{H_2,max,in}} = \frac{\dot{N}_{H_2,consumed}}{\dot{N}_{H_2,syngas} + \dot{N}_{CO,syngas} + 4 \cdot \left(\dot{N}_{CH_4,syngas}\right)} \qquad 4.21$$

In Equation 4.21, the numerator is the molar flow rate of hydrogen consumed electrochemically, while the denominator represents the theoretical maximum molar flow rate of hydrogen supplied as syngas to the cell, whether directly as hydrogen gas ($\dot{N}_{H_2,syngas}$ $[mol/sec]$), or in the form of carbon monoxide ($\dot{N}_{CO,syngas}$ $[mol/sec]$) or methane ($\dot{N}_{CH_4,syngas}$ $[mol/sec]$). The definition of the last two components is derived from Reaction 2.7 and 2.9, respectively, after assuming that enough steam is provided to the cell to allow the full conversion of these components into H_2.The fuel utilization is always kept below 100% since allowing the complete consumption of the fuel inside the cell would mean that at its outlet the concentration of reactants would drop to zero, therefore Nernst losses would make the reversible voltage in this region of the cell equal to zero (Equation 2.17) and no power would be produced here. The cell is said to be "starved" in this region, and this is an inefficient use of the whole active area available.

It is possible to develop an analogous definition to the fuel utilization for SOEC mode; a parameter known as the reactant utilization. However, this concept has been harder to standardize. As previously shown, the fuel utilization for carbonaceous mixtures is based on the H_2 consumed and the theoretical moles of H_2 available, which is acceptable considering that internally reforming capacity of the cells. However, the reactant utilization for carbonaceous mixtures must be based on co-electrolysis, which involves the simultaneous reduction of H_2O and CO_2 in proportions that vary with the characteristics of the cells. Both Wendel [2] and Mottaghizadeh et al. [3] attempted to define the reactant utilization on the basis of the theoretical oxygen available in the feedstock gas, however the resulting equations were different. Nevertheless, the need to include the reactant utilization in this project was by-passed after considering the concept of Equal Charge Constraint presented in Section 4.2.2.

4.2.1. Current and Power

The expressions derived in Section 4.1.2 for the polarization overpotentials are all a function of the current density passing through a solid oxide cell at a given time. In SOFC operation, the current and current density produced are related to the fuel consumed and total inlet fuel according to Equations 4.22 and 4.23 [22]:

$$i = 2F \cdot \dot{N}_{H_2,consumed} \quad 4.22$$

$$i = 2F \cdot U_f \cdot \dot{N}_{H_2,max,in} \quad 4.23$$

The electric power, $P_{e,stack}\,[W]$, produced by a stack of cells in SOFC mode or consumed in SOEC mode is given by Equations 4.24 and 4.25:

$$P_{e,stack} = i \cdot V_{stack} \quad 4.24$$

$$P_{e,stack} = i \cdot N_{cells} \cdot V_{cell} \quad 4.25$$

where $V_{stack}\,[V]$ is the total voltage produced from a series connection of individual solid oxide cell, and $N_{cells}\,[-]$ is the total number of cells. The cell voltage, $V_{cell}\,[V]$, is defined from Equation 4.1 or Equation 4.2 according to the mode of operation. Equation 4.24 can also be rewritten in the form of Equations 4.26 and 4.27:

$$P_{e,stack} = j \cdot A_{cell} \cdot N_{cells} \cdot V_{cell} \quad 4.26$$

$$P_{e,stack} = j \cdot A_{tot} \cdot V_{cell} \quad 4.27$$

where $A_{tot}\,[m^2]$ is the total active area of the stack: a parameter commonly used in industrial and research settings to characterize solid oxide cells [11] [22] [31] [34].

4.2.2. Equal Charge Constraint

When using an SORC system for energy storage applications, it is important to track the state of charge of the system after it is used in SOFC (discharge) and SOEC (recharge) modes, as this parameter informs about the required operation times and currents needed to maintain constant operating conditions in the system [2]. The charge that is removed (in SOFC mode) or added (in SOEC mode) is directly proportional to the oxygen that crosses the electrolyte membrane in either mode of operation. Equations 4.22 can be modified according to Reaction 2.3 to express this relationship in the form of Equation 4.28:

$$i = 4F \cdot \dot{N}_{O_2,consumed} \quad 4.28$$

Where the term $\dot{N}_{O_2,consumed}$ $[mol/sec]$ represents the moles of oxygen consumed in either mode of operation.

If the amount of oxygen added to the rich syngas in SOFC operation is not the same as the amount of oxygen removed from the spent syngas in SOEC mode, then the resulting composition of the outlet gases after they leave the stack will not be the same of the gases that are kept inside the respective storage units. Mixing these two different gases can dilute or concentrate certain species in the tanks, making it difficult to keep constant operating conditions in the system, and requiring constant tracking of the composition in the tanks. Therefore, in order to maintain constant compositions an **Equal Charge Constraint** [2] was imposed on the system modeled:

$$\left(4F \cdot \dot{N}_{O_2,consumed,SOFC}\right) \cdot t_{SOFC} = \left(4F \cdot \dot{N}_{O_2,consumed,SOEC}\right) \cdot t_{SOEC} \quad 4.29$$

Where the terms t_{SOFC} $[sec]$ and t_{SOEC} $[sec]$ represent the total time that the system is operated in SOFC and SOEC mode, respectively. It is possible to rearrange Equation 4.29 into Equation 4.30 to express the current required in SOEC mode, i_{SOEC}, as a function of the current used in SOFC mode, i_{SOFC}:

$$i_{SOEC} = \frac{t_{SOFC}}{t_{SOEC}} \cdot i_{SOFC} \quad 4.30$$

In this work, equal times of operation in both modes was assumed in order to allow more straightforward comparisons between SOFC and SOEC operation for a single stack. Therefore, $t_{SOFC} = t_{SOEC}$ and consequently $i_{SOEC} = i_{SOFC}$.

Through Equations 4.21-4.23, the Equal Charge Constraint and Equations 4.28-4.30, it became possible to define the current for the SORC system for both modes of operation by just fixing the fuel utilization in SOFC mode. This made it possible to avoid the need of defining a reactant utilization, as the total current is a function of the oxygen removed or added in each mode of operation, no matter what components are reduced in SOEC mode.

4.3. Stack Model

The simulation of the process chains involved in this study was carried out using the commercial software Aspen Plus V8.8 of the company AspenTech. Aspen Plus is a chemical process simulator used extensively in industry to model unit operations and chemical plants through complete mass balances, energy balances, mass transfer, heat transfer, separation and equilibrium calculations among other functionalities. The unit blocks of the software are its core feature. These represent several unitary operations that can be combined in a variety of ways to create full chemical plants and processes. However, Aspen Plus is not provided with unit blocks explicitly designed for electrochemical processes, like the ones taking place in SORCs. Nevertheless, several studies of SOCs have successfully recreated with great accuracy the electrochemistry of these devices using the available unit blocks and calculator blocks provided by the software. This study built upon these models to recreate an SORC stack working with syngas as fuel, and co-electrolysis of CO_2 and H_2O.

4.3.1. SOFC Stack

Figure 4.2 shows the 0D Aspen model for the SORC stack in SOFC operation, while Figure 4.3 is the respective 0D model for SOEC operation. In solid oxide cells, the inlet rich/spent syngas mixture usually enters the stack at a temperature 100°C below the outlet temperature of the cells; the inlet gases are then heated to the reaction temperature by convention in the electrodes [2]. The inlet gases are preheated close to the reaction temperature since temperatures that are too low can form temperature gradients in the cells that can cause their degradation or destruction, or the sintering of the nickel catalyst inside the electrodes.

In the SOFC stack (Figure 4.2), the rich syngas stream (FCFUEL) entered the fuel electrode at the block FC-YSZ, 100°C below the temperature of operation of the SORC where it mixed with the oxygen that is needed to achieve a predetermined current density and fuel utilization. This amount of oxygen was determined in a calculator block and was assigned to the stream FCO2ION. Besides acting as a mixer, FC-YSZ

heated up the mixture of fuel and oxygen to the operation temperature of the SORC, representing the internal heating of the gases by convection.

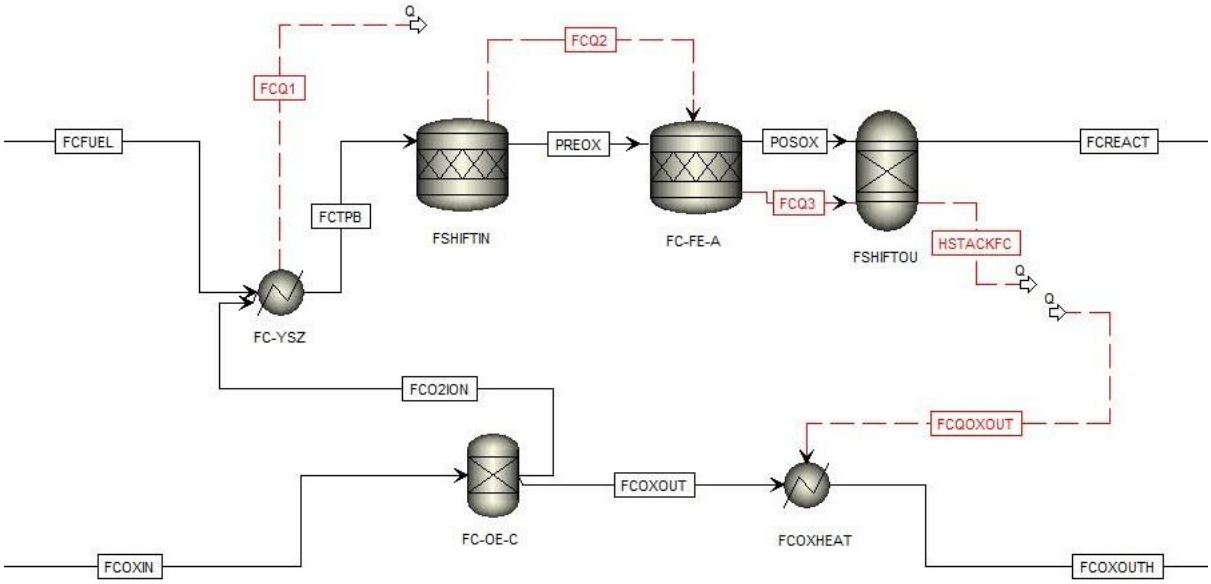

Figure 4.2. SOFC stack model in Aspen Plus.

The mixture of rich fuel and oxygen then entered the fuel electrode represented by the RStoic blocks FSHIFTIN and FC-FE-A and the RGibbs block FSHIFTOU, where it reacted and left the stack as the spent syngas stream FCREACT. In FSHIFTIN, the WGS Reaction 2.7 and steam reforming Reaction 2.9 were input in order to convert all the available CH_4 and CO into H_2. After that, in FC-FE-A all the oxygen transferred from the air reacted with the H_2 through Reactions 2.1-2.3, following the assumption that only H_2 reacts electrochemically with the oxygen ions transported through the electrolyte. In the following block, FSHIFTOU, the water produced by Reactions 2.1-2.3 reacted with the available CO_2 and H_2 until chemical equilibrium was achieved, reaching the final gas composition that left the SORC stack. Using an RGibbs reactor to obtain the final gas composition is a common practice when modeling SOFCs in Aspen with results corroborated by experiments [10] [19] [31] [22] [34].

The division of the fuel electrode with combined RStoic and RGibbs models had the purpose of dividing electrochemical reactions from equilibrium reactions. FSHIFTIN and FSHIFTOU represented the latter, while FC-FE-A represented the electrochemical reactions in the cells. It was possible to determine the reversible voltage of the cells

by using Equation 2.14 and Equation 2.15; Aspen-calculated inlet and outlet entropies and enthalpies were used to determine the changes of these quantities in the block FC-FE-A, then solving for the change in Gibbs free energy and reversible voltage. The overpotentials were also calculated with the equations presented in Section 4.1.2 and the cell parameters in Table 4.1, thus allowing to calculate the operating voltage of the cell, the stack voltage and the produced stack power.

The separator block FC-OE-C acted as the oxygen electrode. Its split fraction was obtained and assigned with a calculator block according to the oxygen flow assigned to the stream FCO2ION and the oxygen content in the inlet oxidant stream (FCOXIN). Since SOFC mode is net exothermic, excess heat was always produced in the stack, which was removed from the cells with the oxidant stream to keep the cell at a constant temperature. An energy balance was performed in a calculator block so that part of this heat was used in the block FC-YSZ to warm up the rich fuel and oxygen to the reaction temperature, while the remaining heat was sent to the block FCOXHEAT to warm up the outlet oxidant stream. A design specification was used to vary the inlet oxidant flow rate until the outlet oxidant stream (FCOXOUTH) left at the temperature of operation of the SORC.

4.3.2. SOEC Stack

For SOEC operation (Figure 4.3) the construction of the stack model is similar to that of SOFC mode. Its main difference is that instead of an RStoic reactor model at the inlet, an RGibbs reactor is used instead. This is because the inlet gas, which consists mostly of H_2O and CO_2, can't be assumed to be converted into one single component as in the case of the SOFC model, since at the temperatures of operation the nickel catalyst does not promote the RWGS or methanation reactions as strongly as it promotes the WGS and steam reforming reactions. Therefore, a different configuration to the one used for the SOFC stack model was needed.

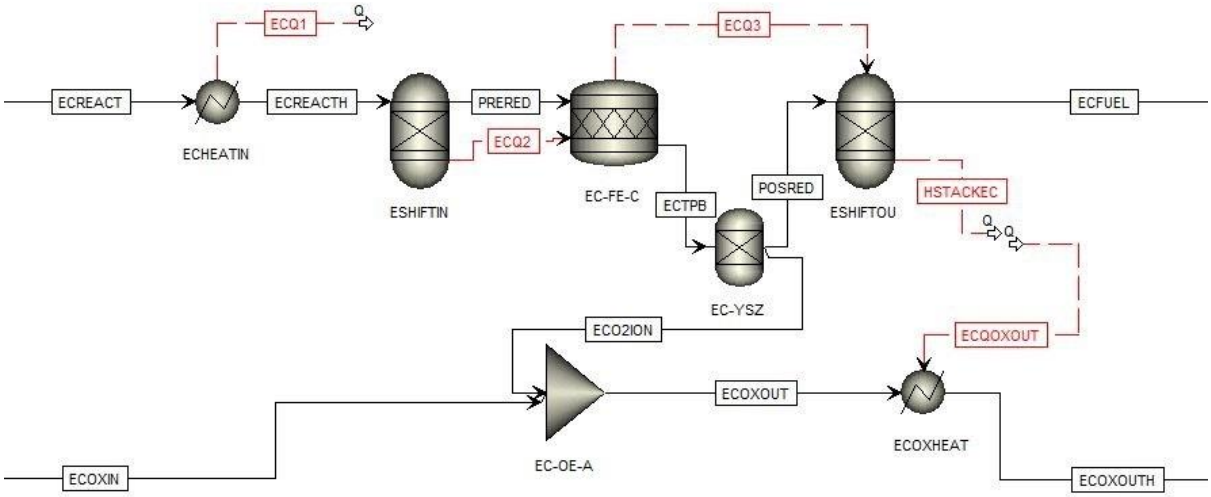

Figure 4.3. SOEC stack model in Aspen Plus.

In this new configuration two RGibbs reactors (ESHIFTIN and ESHIFTOU) were used to account for the equilibrium reactions taking place, while the RStoic reactor block EC-FE-C was used for the electrolysis reaction by introducing Reaction 2.3 (from left to right) and a certain fractional conversion. SHIFTIN was used to represent the equilibrium reaction at the inlet of the stack, while SHIFTOUT represented the reactions at the outlet as a result of changes in the composition of the gas due to the electrolysis in the block EC-FE-C. Following the Equal Charge Constraint, a calculator block was used to set the fractional conversion in EC-FE-C to a value where the oxygen produced in SOEC mode was equal to that consumed in SOFC mode. The separator block EC-YSZ acted as the electrolyte membrane, separating the oxygen produced from the gas mixture, and sending it to the oxygen electrode represented by the mixer block EC-OE-A.

The operating cell voltage, stack voltage and consumed stack power were calculated in the same way as in the SOFC arrangement. However, a significant difference between both calculations was that the SOEC stack could operate in endothermic or exothermic mode, while SOFC mode was only exothermic. Therefore, the calculator block in SOEC mode also determined the thermoneutral voltage of a cell using Equation 2.21 and compared it to the operating voltage where one of two situations could happen:

- **The operating voltage was lower than, or equal to the thermoneutral voltage ($V_{cell,SOEC} \leq U_{tn}$):** therefore, the cell operated endothermically and the excess heat required to keep the stack at a constant temperature had to be supplied from a source outside of the stack. This was done by heating the inlet air $100°C$ above the temperature of the stack, while the spent syngas still entered the fuel electrode at a temperature $100°C$ below the temperature of the stack.

- **The operating voltage was higher than the thermoneutral voltage ($V_{cell,SOEC} > U_{tn}$):** therefore, the cell operated exothermically and both the air and the spent syngas entered the stack at a temperature $100°C$ below the temperature of operation.

An energy balance was performed in a calculator block so that the internal heating of gases by convention in the cell was still performed in the Heater block ECHEATIN by using the heat provided by the inlet air and polarization losses. A design specification was used to vary the air flow rate until the outlet oxidant stream (ECOXOUTH) left at the temperature of operation of the SORC stack.

An important modelling consideration at the level of the stack was that the composition of the syngas only changed within the Aspen blocks that constitute the stack models i.e. the syngas was kinetically frozen outside of the stack and the total moles of each component remained always the same [2]. This assumption was made in order to simplify the computer model without having to consider composition changes outside of the SORC stack in components like turbines, compressors or storage tanks that operate at temperatures and pressures different from the stack, which can affect the chemical equilibrium of the syngas mixtures. This assumption was reasonable since these changes outside of the stack are very slow as they lack the presence of the nickel catalyst that is in the electrodes of the SOCs [2].

The characteristics of the solid oxide cells used in the SORC stack are given in Table 4.1 below. These are based on fuel electrode-supported yttrium-stabilized zirconia cells and were common for both SOFC and SOEC operation:

Table 4.1. Characteristics and properties of the SORC stack.

Symbol	Value	Units	Reference
A_{cell}	0.01	m^2	
N_{cells}	3,000	$-$	
$\gamma_{0,FE}$	$1.344 \cdot 10^{10}$	A/m^2	[10] [28] [26] [29]
$\gamma_{0,OE}$	$2.051 \cdot 10^{9}$	A/m^2	[10] [28] [26] [29]
$E_{act,FE}$	100,000	J/mol	[10] [28] [26] [29]
$E_{act,OE}$	85,634	J/mol	[10] [28] [26] [29]
$E_{act,el}$	120,000	J/mol	[9] [10] [28] [26] [29]
$r_{ohmic,conn}$	$5.7 \cdot 10^{-6}$	$\Omega \cdot m^2$	[10]
$\sigma_{0,el}$	33,330	$(\Omega \cdot m)^{-1}$	[9] [10] [28] [26] [29]
δ_{FE}	$3.2 \cdot 10^{-5}$	m	[10]
δ_{OE}	$1.75 \cdot 10^{-5}$	m	[10]
δ_{el}	$1.25 \cdot 10^{-5}$	m	[10]
r_p	$1 \cdot 10^{-6}$	m	[10]
ε	0.3	$-$	[10] [28] [29]
τ	5	$-$	[10] [28] [29]

4.4. Base System

Besides the SORC stack, other Balance-of-Plant (BOP) components like compressors, heat exchangers, valves and condensers are required in order to use syngas as an effective energy storage medium. The configuration and specifications of these components inside the system can have many different forms and characteristics that depend on the storage capacity needed, the nominal power required, the site specifications, and the economics and finances of the project, among many other constraints. Within the framework of the BALANCE Project, and for the purpose of using only syngas in the process chain, the SORC system was designed so that it worked under the following conditions:

- Closed storage system.
- Steady-state operation.
- Produced syngas containing less than 1% of CH_4 content in a dry mole basis.
- No methanation processes.
- Operation in SOFC mode and SOEC mode of equal duration.
- Constant composition in the storage tanks, and high-pressure storage.
- Oxygen and heat to the stack provided/removed by an open-air cycle.
- Operating temperature between $700 - 800°C$.
- Operating pressure between $1.2 - 10$ $[bar]$.
- Current density below 1.0 $[A/cm^2]$ to avoid excessive degradation of the electrodes and fixed fuel utilization.

This project didn’t include a detailed dimensioning of the BOP components utilized, and no techno-economic analysis was involved. However, some design choices were made taking into consideration practices that can prevent excessive capital, variable or operational costs.

Figure 4.4 shows the block diagram for the process chain used in this project as the base case, which is referred as the Base System. This is the simplest configuration that an SORC operating exclusively with syngas can have, and was constructed using as references the works of Wendel [2], Mottaghizadeh et al. [3], Sebastiani [24] and Mor [25], altered through engineering heuristics and educated assumptions. In this system it is possible to identify three main material streams: a rich/spent syngas stream, a water stream and an air stream. All heating requirements for these streams were satisfied by assuming the use of electric heaters that take energy from the power grid. The translation of the Base System in Figure 4.4 into Aspen Plus can be observed in Appendix B for SOFC operation and in Appendix C for SOEC operation.

The Base System in Figure 4.4 shows no extensive heat integration. Nowadays, it is very uncommon not to take advantage of internal heat sources to reduce energy inputs in systems working with solid oxide cells. However, this integration was deliberately left out in order to set the minimum performance that the system can provide. The aim of this project was to measure the impact of different advanced configurations on the syngas process chain in order to make improvements on the Base System on the basis of energy and exergy analyses. Therefore, within the scope of this project, the Base System was progressively transformed by adding new components and processes – including a preliminary heat integration – to measure the gains and losses that these different approaches cause on the SORC system.

Besides a base configuration of the BOP around the SORC stack, the base case for the input operational parameters of the whole system had to be established to be able make comparisons between the Base System and every subsequent change in its components, structure and operation strategy. The conditions for this base scenario are summarized in Table 4.2.

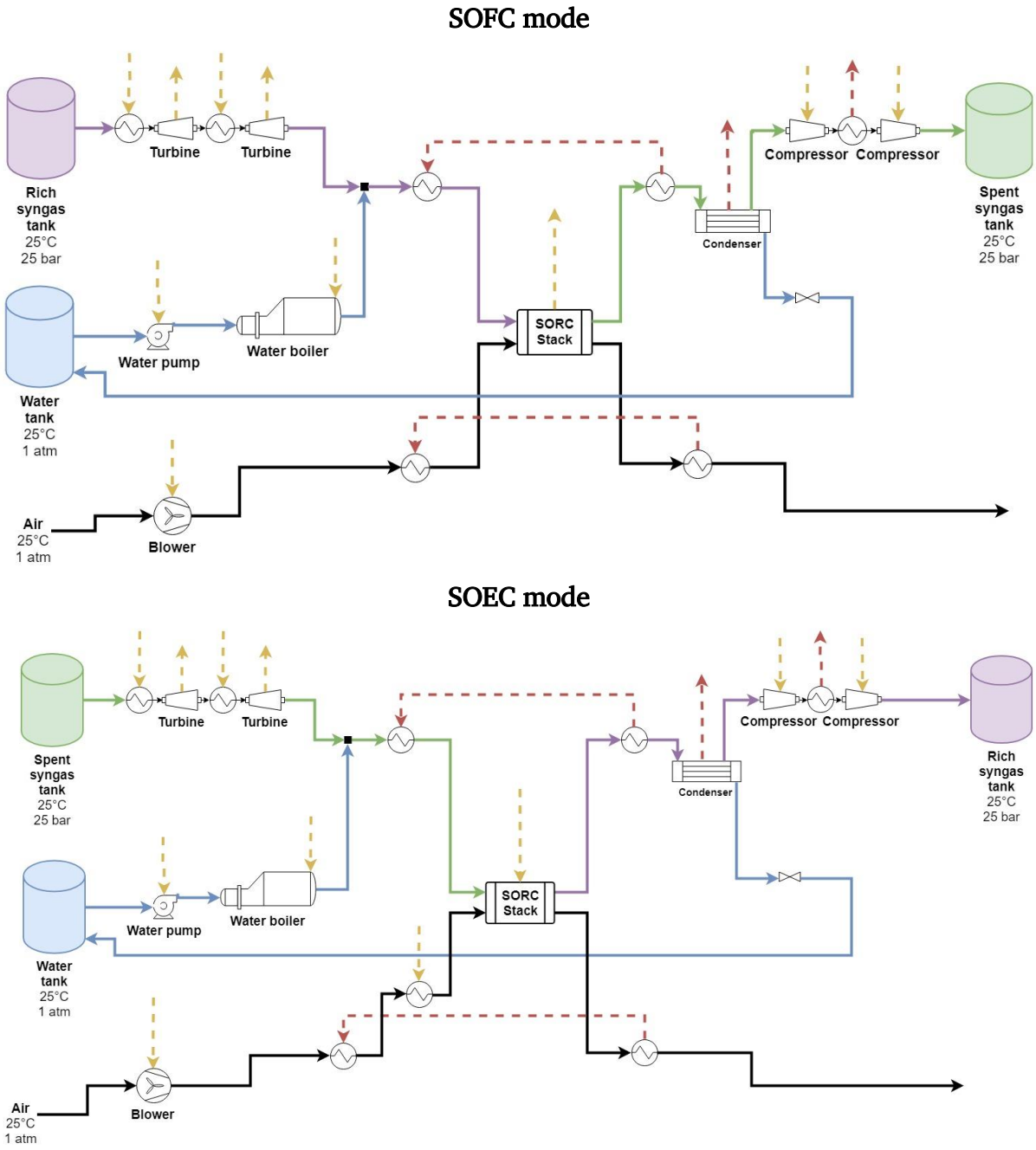

Figure 4.4. Block diagram of the SORC Base System. Solid lines represent material flows of rich syngas (purple), spent syngas (green), water (blue) and air (black). Dashed lines represent energy flows of heat (red) and electricity (yellow).

Table 4.2. Base input operational parameters.

Parameter	Value	Units
H/C ratio	4	–
Fuel utilization	80%	–
SOFC/SOEC operating temperature	800	$°C$
SOFC/SOEC operating pressure	1.2	bar
Current density	0.5	A/cm^2
Rich/spent syngas inlet temperature	25	$°C$
Rich/spent syngas storage pressure	25	bar
Water inlet temperature	25	$°C$
Water storage pressure	1.01325	bar
Air inlet temperature	25	$°C$
Air inlet pressure	1.01325	bar

Table 4.3 below summarizes the design parameters used for the BOP components selected for this study. These values were unchanged for every permutation of the Base System.

Table 4.3. Design parameters for BOP components.

Parameter	Value
Isentropic and mechanical efficiency of pumps, compressors and blowers	85%
Isentropic and mechanical efficiency of turbines	85%
Minimum pinch temperature of heat exchangers	$10°C$
Temperature of condenser	$50°C$
Efficiency of inverters, rectifiers and generators	92%

4.4.1. Storage Conditions

In order to reduce variable costs in the SORC system, it is desirable to be able to keep all the necessary syngas components within the system to avoid the need of external sources to resupply any component lost to the environment. Therefore, the SORC system was designed to be closed for the syngas components that are not found in abundance in the environment by storing them in high pressure vessels, as can be observed in Figure 4.4, namely carbon dioxide, carbon monoxide and hydrogen gas. Although water is relatively common in the environment, it was also kept in storage tanks since this makes it possible to put the plant in locations were natural water sources are not found. Since oxygen is abundant in the air, the environment was used as its storage medium, and was provided to the SORC stack through an open-air cycle.

One problem to always take into consideration when storing syngas is the possibility of hydrogen dissociation through the walls of the container that can cause their embrittlement and failure. Although special tanks for any syngas composition are available, these are often more expensive than more common steel tanks that are easier to manufacture. Nevertheless, hydrogen embrittlement can also be prevented by lowering the water content of the syngas below a 60% relative humidity and by keeping the temperature of storage below $220°C$ [15]. For this reason, water was always condensed and separated from the rest of the syngas components (CO_2, CO and H_2) and kept in its own container.

Carbon dioxide, carbon monoxide and hydrogen gas were compressed and kept together in pressurized storage vessels in order to increase the energy density of the SORC system and allow the use of smaller storage units. On the other hand, water was kept at atmospheric pressure since it could be easily compressed, thus saving in the cost of an additional pressurized unit.

In order to achieve the steady-state simulation constraint, it was assumed that the pressure in the storage tanks maintained itself constant as all the stored components were discharged into the system, thus their volumetric flow rates would also be constant, and the flow rate leaving the tanks is the same as the one entering the stack, and vice versa [2].

4.4.2. Pressure Changers

In the SORC system, many pressure-changing components were needed to in order to bring the reacting species from their storage pressure to the pressure of the stack and back. In this work the implementation of devices like turbines, compressors and blowers was made when specific criteria were met:

- Compressors were used to increase the pressure of gases only when the pressure ratio was equal or larger than 2. For pressure ratios below this value the density of the gas could be considered constant and blowers were used instead [37].

- Turbines were used to recover energy from high-pressure gases only when the pressure ratio was equal or larger than 2. For pressure ratios below this value the gases were expanded freely through a valve or vented directly to the environment [37].

- Intercooling was used for high compression ratios when the gas was needed as cold as possible after compression. On the other hand, when the gas was needed as hot as possible, the compression was done in one step without any intercooling [37].

These criteria can already be seen implemented in the Base System in Figure 4.4: the rich and spent syngas mixtures were stored at pressures much higher than the operating pressure of the stack, therefore compressors were needed when storing the syngas, while turbines could be used to expand this gas before its use in the stack. Because the volume of these gases increases with temperature, these were wanted as cold as possible before storage so that they could occupy less space in the tank, thus two steps of compression with intercooling were utilized. The expansion of the syngas from storage was made in two steps with preheating before each of them to ensure that the temperature of the gas would not fall too low that any remaining moisture in the syngas could condensate and damage the turbines.

Table 4.4 provides the pressure drops assumed through the different components of the SORC system. These were compiled by Tjaden et al. [31] from manufacturers in the framework of the SOFCOM European project. These pressure drops were used to calculate the overpressures needed to make it possible for fluids to flow inside the system and at the same time obtain the desired operating pressure in the stack.

Table 4.4. Pressure drops for different components.

Component	Pressure drop [bar]
Fuel electrodes in the stack	0.015
Oxygen electrodes in the stack	0.015
Heat exchanger (each side)	0.015

4.4.3. Heat Exchangers

One of the main challenges when working with SORCs is to have a good heat integration within the system. This is particularly difficult since the nature of the process changes when switching from one mode of operation to the other: while in SOFC mode the reaction is always net exothermic, in SOEC mode the reactions can be exothermic or endothermic, and this changes the required inlet temperature of the oxidant. Additionally, the composition of the syngas changes as it reacts within the stack and is used within the whole system, thus changing the mixtures' heat capacities and heating requirements.

In order to facilitate convergence, all the heat exchangers were simulated with pairs of Heater blocks instead of using built-in heat exchanger Aspen blocks (HeatX). The two heaters that represent a single exchanger were linked together with a heat flow (red dashed line) as can be observed in Figure 4.4 and in Appendix B-E. The outlet temperature was set for the heater that warms the primary stream of the exchanger, and the required heat for the specified temperature increase was taken from the second heater. The secondary stream was chosen if its temperature was always higher than that of the primary after removing the heat. Design specifications were used to ensure a pinch temperature of minimum $10°C$ for heat transfer. To ensure that this approach delivered correct results, shortcut HeatX block models were used in a

separate Aspen flowsheet to verify the inlet and outlet temperatures. The main properties of heat exchangers and heat flows in this work included:

- A minimum pinch temperature of $10°C$ for all heat transfer processes.
- Cooling processes achieved with water at the temperature of the environment.
- Countercurrent heat exchangers.
- No mixing of cold and hot streams.
- No heat losses to the environment.

Although it was said that all heating requirements in the Base System were provided by electricity, two preheating heat exchangers were already incorporated in SOFC and SOEC mode in Figure 4.4. This is because the temperature of the SORC stack is normally the highest in the whole system (if no burners are used), therefore the outlet flows from it are the only ones capable of preheating the inlet flows, thus the use of these preheaters is almost a standard practice [2] [19] [31] [22]. In the case of endothermic SOEC operation another electric heater is needed in the oxidant stream after the preheater to further warm up the air above the temperature of the stack.

4.5. Performance Metrics

The SORC system defined so far has the aim of working as an energy storage mechanism to stabilize power grids that are connected to intermittent renewable energy sources like wind or solar PV. The most relevant performance metrics for an energy storage system include its roundtrip efficiency, energy density, capital cost and levelized cost of energy [2]. Since this work did not include a techno-economic analysis, the last two metrics were not examined. An energy density measure was also not taken into consideration, as this parameter depends mostly on the storage pressure of the syngas mixtures, which can be changed by increasing the compression ratio

before storage. Therefore, the roundtrip efficiency was the only metric from this group that was examined in this work. This analysis was complemented with the calculation of exergy efficiencies that give information about the thermodynamic performance of the SORC system.

4.5.1. Roundtrip Efficiency

The **roundtrip efficiency** of an energy storage system is defined as the ratio of the energy released during discharge for a certain period of time, to the amount of energy required to recharge the system in the same amount of time. The roundtrip efficiency is a useful metric that has very practical and financial implications in a project. It shows an immediate and intuitive measure of the capacity of a storage system to successfully retrieve the energy that is put into it, and whether or not it makes sense to build such a system. At the level of the stack, the roundtrip efficiency can be defined in the form of Equation 4.31:

$$\eta_{RT,Stack} = \frac{DC\ power\ produced\ in\ SOFC\ mode}{DC\ power\ consumed\ in\ SOEC\ mode}$$

$$\eta_{RT,Stack} = \frac{P_{e,SOFC}^{DC}}{P_{e,SOEC}^{DC}} \qquad 4.31$$

For this study, the SORC system was operated in both modes for equal amounts of time, therefore Equation 4.31 can be written in terms of electric power instead of energy. This definition considers the electric DC power directly produced in SOFC mode and consumed in SOEC mode, thus the effect of inverters or rectifiers is not taken into account.

Equation 4.31 is useful for evaluating the conditions that directly affect the performance of the stack, which in general include pressure, temperature, fuel utilization, current density, and other parameters presented in Chapter 2 and Sections 4.1-4.2. However, the addition of the BOP components requires expanding this definition to account for elements that consume work (mainly compressors, pumps and blowers) and elements that produce or recover work (namely turbines) as well as the final AC power produced and consumed by the interaction of the SORC system

and the power grid through electric heaters, generators, inverters and rectifiers. The system total roundtrip efficiency is defined as Equation 4.32:

$$\eta_{RT,System} = \frac{Net\ AC\ power\ produced\ in\ SOFC\ mode}{Net\ AC\ power\ consumed\ in\ SOEC\ mode}$$

$$= \frac{(P^{DC}_{e,SOFC} - P^{DC}_{e,comp,SOFC} + P^{DC}_{e,turb,SOFC}) \cdot \eta_{inv} - \dot{Q}_{in.SOFC}}{\frac{(P^{DC}_{e,SOEC} + P^{DC}_{e,comp,SOEC})}{\eta_{inv}} - (P^{DC}_{e,turb,SOEC} \cdot \eta_{inv}) + \dot{Q}_{in.SOEC}} \qquad 4.32$$

where $P^{DC}_{e,comp}\ [W]$ is the total power consumed by pumps, compressors and blowers, and $P^{DC}_{e,turb}\ [W]$ is the total power recovered by turbines. In the definition of Equation 4.32, it is assumed that the pumps, compressors and blowers are run with DC power, while turbines generate electric work through AC generators that have the same efficiency of the inverters and rectifiers in the system, η_{inv}. The term $\dot{Q}_{in}\ [W]$ represents the external heating utilities required to warm up material streams where needed. In the case of the Base System, these heat requirements are assumed to be provided with AC electric power from the grid.

It must be noted that the stack and system roundtrip efficiencies just defined may overestimate the final roundtrip efficiency, as these do not include the effects of losses encountered during startup and shutdown sequences like gas purges, or the effects of leakages, cells degradation, stacking of cells, water management or ancillary equipment [38].

4.5.2. Exergy Analysis

While the roundtrip efficiency is a concept that derives from the First Law of Thermodynamics – conservation of energy – the exergy efficiency is a concept that derives from the Second Law – the increase of entropy. The exergy efficiency gives insight into how energy is used within a system, and how its quality is reduced after each process that takes place inside it. Therefore, this metric has a more fundamental value as it makes it possible to see how much real systems deviate from a thermodynamically reversible system, and where are the areas of improvement regarding energy transfer and conversion.

This work will not make a detailed explanation of the thermodynamic principles behind the concept of exergy and exergy analysis as these can be found in academic texts like that of Çengel and Boles [20] or Moran et al. [39]; nonetheless, the different types of exergy and exergy losses considered for the systems designed are explained.

Types of exergy considered

Exergy is defined as the maximum amount of useful work that can be obtained from a certain amount of energy, during a (reversible) process that brings a system into equilibrium using the environment as the only reservoir of heat and matter, which is referred as the "dead state". There are several ways to classify exergy; Figure 4.5 shows a useful schematic for this purpose based on the work of Gundersen [40]. Physical exergy relates to the ability of a system to perform work because of its differences in kinetic energy, potential energy, temperature and pressure with respect to the dead state, while keeping its chemical composition constant. On the other hand, **chemical exergy** is the work that a system can perform by changing its chemical composition through mixing or separation processes, and chemical reactions where the final products are found in the composition of the environment.

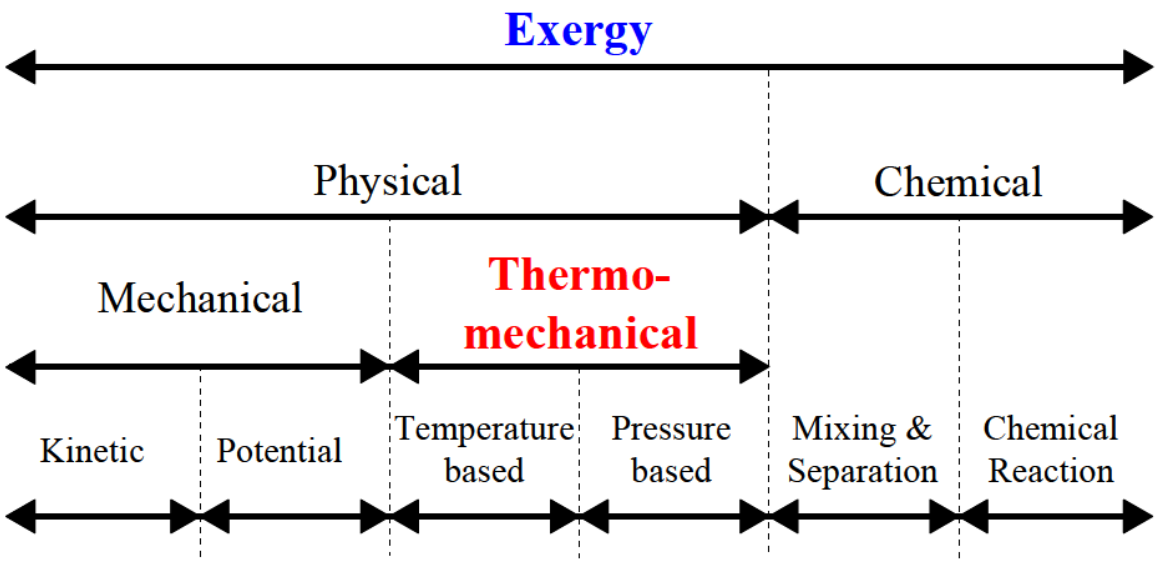

Figure 4.5. Classification of exergy.

In the systems studied here, mechanical exergy due to kinetic and potential energy is not considered, as changes in these quantities are not very large. However, changes in thermo-mechanical and chemical exergies are significant and are therefore considered. The total exergy rate in a flow of matter, $Ex_{stream}\,[W]$, can be described by Equations 4.33-4.35 [39] [40]:

$$Ex_{stream} = Ex_{TM} + Ex_{chem} \tag{4.33}$$

$$Ex_{TM} = \dot{N} \cdot [(h - h^o) - T_o(s - s^o)] \tag{4.34}$$

$$Ex_{chem} = \sum \dot{N}_k \cdot \left[R\ T_o\ ln\left(\frac{p_k}{p_o}\right) + \Delta g_k^o + R\ T_o\ ln\left(\frac{p_o}{p_{k,env}}\right)\right] \tag{4.35}$$

where $Ex_{TM}\,[W]$ and $Ex_{chem}\,[W]$ are the thermo-mechanical and chemical components of the total exergy flow. The **thermo-mechanical exergy**, or TM exergy, is the maximum work available from the system due to its temperature and pressure difference to the dead state. Aspen Plus offered property sets that could determine the TM exergy rates of the material streams through the system, using as the dead state a standard temperature of $T_o = 25°C$ and a standard pressure of $p_o = 1.01325\ [bar]$.

Unfortunately, Aspen Plus does not calculate chemical exergies for the different material or energy streams. These then had to be determined within calculator blocks and added to the values of TM exergy from Aspen, according to Equation 4.33. This calculation was not necessary for every stream within the system, but only for those that underwent a process where the chemical exergy changed. These processes included the mixing of streams with different compositions, and chemical reactions like those within the SORC stack. The chemical exergy of the syngas mixtures entering and leaving the system through the storage tanks was also calculated in order to define the exergy efficiency of the system.

As can be seen within the brackets of Equation 4.35, the total chemical exergy is composed of three main terms, which from left to right consider the:

1. Decomposition of the gas mixture into individual components and compression of each component k from its partial pressure, p_k $[bar]$, to standard pressure, p_o $[bar]$.

2. Reversible conversion at standard conditions of each component k into species found in the environment, Δg_k^o $[J/mol]$.

3. Expansion of the reaction products from standard pressure to their partial pressures in the environment, $p_{k,env}$ $[bar]$.

In order to calculate Step 3 of this sequence, the Baehr environmental composition was used [25]. Said composition and the corresponding partial pressure of each component is shown in Table 4.5 below.

Table 4.5. Baehr environmental composition and environmental partial pressures.

Component	Mole fraction	$p_{k,env}$ $[bar]$
$H_2O_{(g)}$	0.0312	0.0316
$H_2O_{(l)}$	0.0000	0.0000
CO_2	0.0003	0.0003
N_2	0.7565	0.7665
O_2	0.2030	0.2057
Ar	0.0090	0.0091

Step 2 and Step 3 could be combined for each component into a single molar chemical exergy at standard conditions. For this, the standard Gibbs free energy of formation of each component in the syngas mixture was needed; these are shown in Table 4.6.

Table 4.6. Standard Gibbs free energy of formation.

Component	$\Delta g^{o}_{f,k}\ [J/mol]$
$H_2O_{(g)}$	−228,610
CO_2	−394,390
H_2	0.0
CO	−137,160
CH_4	−50,800
N_2	0.0
O_2	0.0

The molar chemical exergy at standard conditions, $ex^{o}_{chem,k}\ [J/mol]$, was then obtained with Equation 4.36 [40] for each of the components found in the SORC system, finally resulting in Table 4.7.

$$ex^{o}_{chem,k} = \Delta g^{o}_{k} + RT \cdot ln\left(\frac{p_o}{p_{k,env}}\right) = \left(\Delta g^{o}_{f,products} - \Delta g^{o}_{f,reactants}\right) + RT \cdot ln\left(\frac{p_o}{p_{k,env}}\right) \quad 4.36$$

Table 4.7. Molar chemical exergy at standard conditions.

Component	$ex^{o}_{chem,k}\ [J/mol]$
$H_2O_{(g)}$	8,595
$H_2O_{(l)}$	0.0
CO_2	20,108
H_2	235,229
CO	275,361
CH_4	830,202
N_2	692
O_2	3,953

Equation 4.35 for the total chemical exergy of a flow of matter can be combined with Equation 4.36 to rewrite it into the more compact Equation 4.37:

$$Ex_{chem} = \sum \dot{N}_k \cdot \left[R\, T_o\, ln\left(\frac{p_k}{p_o}\right) + ex^o_{chem,k} \right] \qquad 4.37$$

Internal and external exergy losses

Unlike energy, exergy is not conserved but is destroyed within the system due to irreversibilities in the different processes taking place inside it. There are many sources of exergy destruction, however the most relevant in this study included [20]:

- Heat transfer through a finite temperature gradient.
- Unrestrained expansion of material streams through valves.
- Mixing of fluids at different temperatures and with different compositions.
- Friction inside turbines, compressors and pumps.
- Chemical reactions.

Exergy destruction losses are also referred as **internal exergy losses**, since they occur within the system or at its boundaries. On the other hand, **external exergy losses** are those that relate to the exergy that leaves the boundaries of the system inside material and energy streams that are not products of the system but waste streams or energy losses [20]. External exergy losses include, for example:

- Waste heat flows that leave the plant, like exhaust air, hot water flows, cooling air, or cooling water.
- Losses through radiation and convection.

- Waste flows that still have chemical exergy content.

- Material losses.

Mass and energy flows that cause external exergy losses are sometimes unavoidable, such as heat losses through radiation, but they are also sometimes the result of the system not having any use for the available exergy or not having the equipment to recover it. For example, there is little use for a cooling water stream that leaves at $40°C$, therefore this water is usually only treated and disposed.

Exergy flows in the SORC system

Figure 4.6 shows the different flows of exergy that can be considered for the SORC system. The boundaries of the system are represented by the boundaries of the rectangle; therefore, the system is treated as a black box, and inside it all the processes that cause internal exergy losses are added together.

In Figure 4.6, the term $Ex_{Q,in}\ [J/sec]$ represents the exergy of the external heating utilities required to warm up material streams where needed. As explained before, for the Base System these heat requirements were assumed to be provided with electric heaters. Since electric energy is pure work, then $Ex_{Q,in} = \dot{Q}_{in}$, meaning that all the electric energy used is equal to the exergy transferred and is turned completely into heat for the cold streams. The term $P_{e,gross}^{AC}\ [J/sec]$, is the gross AC power produced in SOFC mode and consumed in SOEC mode after considering the energy required to operate all the BOP components aside from the electric heaters.

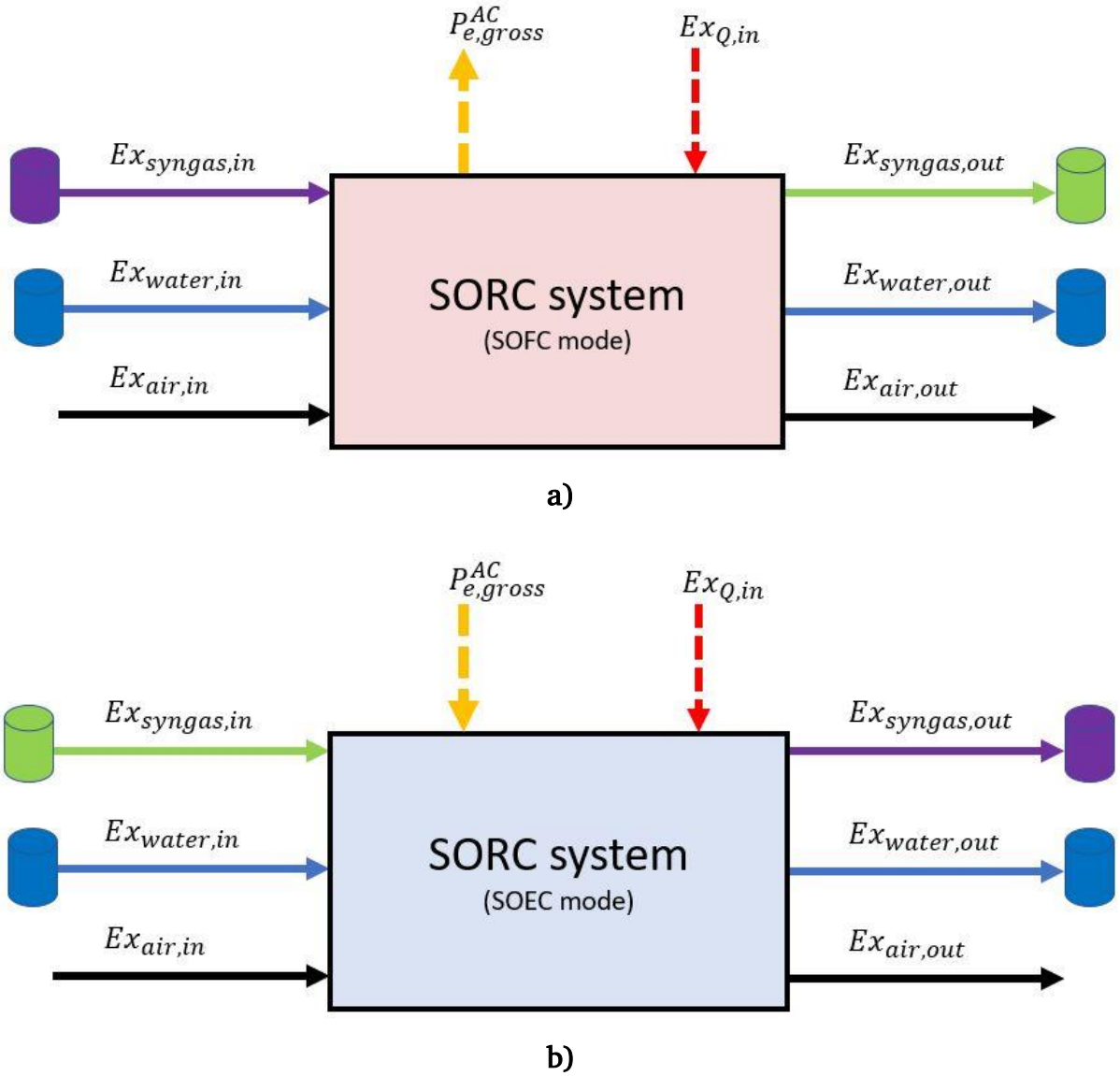

Figure 4.6. Exergy flows in the SORC system for a) SOFC mode and b) SOEC mode. Solid lines represent material streams of rich syngas (purple), spent syngas (green), water (blue) and air (black). Dashed lines represent exergy flows of electricity.

For this work, it was assumed that the storage tanks were not insulated and enough time always passed after storage that every component in the vessels finally reached the temperature of the dead state. Therefore, streams sent to storage lost all their available temperature-based TM exergy to the environment and when they came from storage they were always at the temperature of the dead state ($25°C$), as can be observed in Table 4.2. This was done in order to represent a worst-case scenario where it was not possible to take advantage of the thermal energy and exergy still contained

in the hot outlet streams when the system was operated again after switching the mode of operation. Water and air were also assumed to enter and leave the system at the pressure of the environment, therefore these streams had negligible total thermo-mechanical exergy.

Due to the difference between the average composition of air (79% nitrogen and 21% oxygen) and the composition of Baehr state (Table 4.5), the inlet and outlet air streams have a chemical exergy content. Nevertheless, changes in this chemical exergy inside the system are very low, especially compared to changes in the thermo-mechanical exergy, therefore the calculation of chemical exergy of the inlet and outlet air could be neglected.

All these temperature, pressure and chemical exergy assumptions just presented imply that the terms $Ex_{water,in}\ [J/sec]$ and $Ex_{air,in}\ [J/sec]$ in Figure 4.6 are equal to zero, and the terms $Ex_{water,out}\ [J/sec]$ and $Ex_{air,out}\ [J/sec]$ are always external exergy losses since this exergy is finally lost to the environment. However, this is not the case for the terms $Ex_{syngas,in}\ [J/sec]$ and $Ex_{syngas,out}\ [J/sec]$, which still have a high chemical and pressure-based TM exergy even after losing their temperature-based TM exergy to the environment.

Exergy efficiency

Unlike the roundtrip efficiency, the exergy efficiency is not normally defined considering both modes of operation at the same time. Instead, it is calculated for each mode of operation. It is possible to formulate the exergy efficiency in two different ways: Equation 4.38 is known as the **universal exergy efficiency**, $\eta_{Ex,Univ}$, while Equation 4.39 is known as the **functional exergy efficiency**, $\eta_{Ex,Func}$.

$$\eta_{Ex,Univ} = \frac{Exergy\ out}{Exergy\ in} \qquad 4.38$$

$$\eta_{Ex,Func} = \frac{Exergy\ recovered}{Exergy\ expended} \qquad 4.39$$

The universal exergy efficiency is defined as the ratio of the total sum of the exergy leaving the system to the total sum of the exergy entering the system and gives an intuitive measure of the overall thermodynamic performance of the entire system. This definition, however, doesn't have as much engineering value as the functional exergy efficiency. Unlike the universal efficiency, the functional efficiency gives information on the ability of the system to transform an exergy input into another form of exergy with useful value, taking into consideration the specific function of the system. Therefore, the functional exergy efficiency is more apt to show the thermodynamic performance of the storage system on the basis of its purpose and as a result is the exergy efficiency examined in this work.

In SOFC mode, the purpose of the system is to produce electric power when there is not enough of it in the grid to supply the demand. Therefore, the system must transform the exergy of the stored syngas into electricity. The exergy expended is the difference between the exergy of the inlet and outlet syngas mixtures. The exergy gained from the system is the net power produced and transferred to the grid, which is given by the gross AC power produced in SOFC mode after considering the energy required to operate all the BOP components, minus the electric power consumed to heat up material streams. As a result, the functional exergy efficiency for operation in SOFC mode is given by Equation 4.40:

$$\eta_{Ex,Func,SOFC} = \frac{P_{e,gross}^{AC} - Ex_{Q,in}}{Ex_{syngas,in} - Ex_{syngas,out}}$$

$$= \frac{\left(P_{e,SOFC}^{DC} - P_{e,comp,SOFC}^{DC} + P_{e,turb,SOFC}^{DC}\right) \cdot \eta_{inv} - Ex_{Q,in}}{Ex_{syngas,in} - Ex_{syngas,out}} \qquad 4.40$$

In SOEC mode, the purpose of the system is to store excess electric energy from the grid in the form of chemical bonds of syngas. Therefore, the system must transform electricity into syngas. Here, the energy expended is given by the net AC power consumed in SOEC mode after considering the gross energy required to operate all the BOP components, plus the electric power consumed to heat up material streams. The exergy gained is the difference between the exergy of the outlet and inlet syngas mixtures, which is mostly dictated by their difference in chemical exergy and

pressure-based TM exergy since the gases cool down to the temperature of the dead state after storage. Therefore, the functional exergy efficiency for operation in SOEC mode is given by Equation 4.41:

$$\eta_{Ex,Func,SOEC} = \frac{Ex_{syngas,out} - Ex_{syngas,in}}{P^{DC}_{e,gross} + Ex_{Q,in}}$$

$$= \frac{Ex_{syngas,out} - Ex_{syngas,in}}{\frac{\left(P^{DC}_{e,SOEC} + P^{DC}_{e,comp,SOEC}\right)}{\eta_{inv}} - \left(P^{DC}_{e,turb,SOEC} \cdot \eta_{inv}\right) + Ex_{Q,in}} \qquad 4.41$$

4.6. Solution Methodology

This section gives an explanation of how the SORC model developed was executed in Aspen Plus to obtain all the relevant results presented in the next chapter. It must be noted that one convergence of Aspen Plus calculated the results for SOFC mode and SOEC mode at the same time, as both models with their respective BOP were developed in the same Aspen flowsheet (Appendix D); a simulation methodology based on the work by Hauck et al. [10].

4.6.1. Input Parameters

Since the purpose of the BOP was primarily to bring all the components and material streams to and from the conditions needed for the electrochemical reactions in the stack, the operation of the whole system was mainly a function of the operating parameters of the solid oxide cells during SOFC and SOEC operation. Therefore, the initial step of the simulation process was to input the operating parameters of the SORC stack, which included the:

- Hydrogen-to-carbon ratio.
- Fuel utilization.
- Operating temperature of the stack in SOFC mode.
- Operating pressure of the stack in SOFC mode.
- Operating temperature of the stack in SOEC mode.
- Operating pressure of the stack in SOEC mode.
- Current density.
- Storage pressure of components (rich syngas, spent syngas, water).

The last element in this list is not of a stack parameter, but it was needed to define the operating pressure of the BOP components according to the pressure drops shown in Table 4.4. An Aspen calculator block was used to input all these operating conditions and was also used to calculate and assign the necessary oxygen flow through the electrolyte for both modes of operation, according to the input fuel utilization and the current density.

4.6.2. Equilibrium Compositions

As explained in Section 2.3, it is important to select a syngas composition that is outside of the carbon deposition boundary for the temperatures and pressures used in the stack. Choosing a H/C ratio that fulfills this requirement can be done through *C-H-O* ternary diagrams like the one of Figure 2.5. However, the H/C ratio gives the general elemental composition for the chemical system, but not the equilibrium mole fractions of each component that is achieved as a function of the temperature and pressure of the stack. Since this final composition could have strong influences on the performance of the full SORC system, it was important to be able to input a desired

H/C ratio and let Aspen automatically determine the equilibrium molar composition of the rich and spent syngas mixtures, even if the temperature and pressure of operation in SOFC mode were different to those in SOEC mode.

The solution found in this project was to tie together the SOFC stack model to the SOEC stack model within an Aspen Hierarchy block named EQUIL in the way shown in Appendix F; a simulation tool referred as the **Equilibrium Arrangement**. In this tool the outlet syngas stream of the SOFC stack was connected to the inlet stream of the SOEC stack, with an intermediate Heater block (COOLER) that brought the SOFC outlet to the inlet conditions of the SOEC model. It was possible to do this since it was assumed that the gases were kinetically frozen outside of the stack models, so the composition that entered the SOEC stack would always be the same that left the SOFC stack, and vice versa.

The desired H/C ratio for the SORC system was then established by assigning to the inlet stream FCFUEL a hydrogen and carbon dioxide mixture. Table 4.8 shows examples of possible input compositions for H/C ratio values that are below the carbon deposition boundary [2]. This mixture went through all the fuel electrode blocks of the SOFC stack and left the block FSHIFTOU as the spent syngas mixture for SOEC mode. This mixture then entered the SOEC stack where it reacted in the fuel electrode blocks and left as the rich fuel mixture for SOFC mode. Since the blocks ESHIFTOU and FSHIFTOU were both RGibbs reactor models, the molar compositions coming out of them were already in chemical equilibrium.

Table 4.8. H/C ratio input compositions by mole fraction.

H/C ratio	H_2	CO_2
2	0.500	0.500
4	0.667	0.333
6	0.750	0.250
10	0.833	0.167
∞	1.000	0.000

In addition to determining the equilibrium compositions of the rich and spent syngas, the Equilibrium Arrangement also made it possible to automate the calculation of these compositions for different stack temperatures and pressures. Therefore, it became possible to perform quick sensitivity analyses of the SORC system for these parameters within the Aspen Plus simulation environment.

4.6.3. Assignment of Parameters and Calculation of Results.

Other calculator blocks were used to assign any parameters required by each block in the Aspen flowsheet, according to the defined input to the SORC stack. The difference between storage pressures and stack pressure was used to assign the pressure drop for each component, and estimate the overpressures needed at the outlet of compressors, blowers, pumps, turbines and valves. After every block input value had been assigned, the simulation run until it converged. Calculator blocks then took the results and performed energy and exergy calculations to determine the performance metrics introduced in Section 4.5 and other key values to examine the system, including exergy destruction per process and BOP component. Figure 4.7 shows a visual representation of the general solution methodology followed by the computer model.

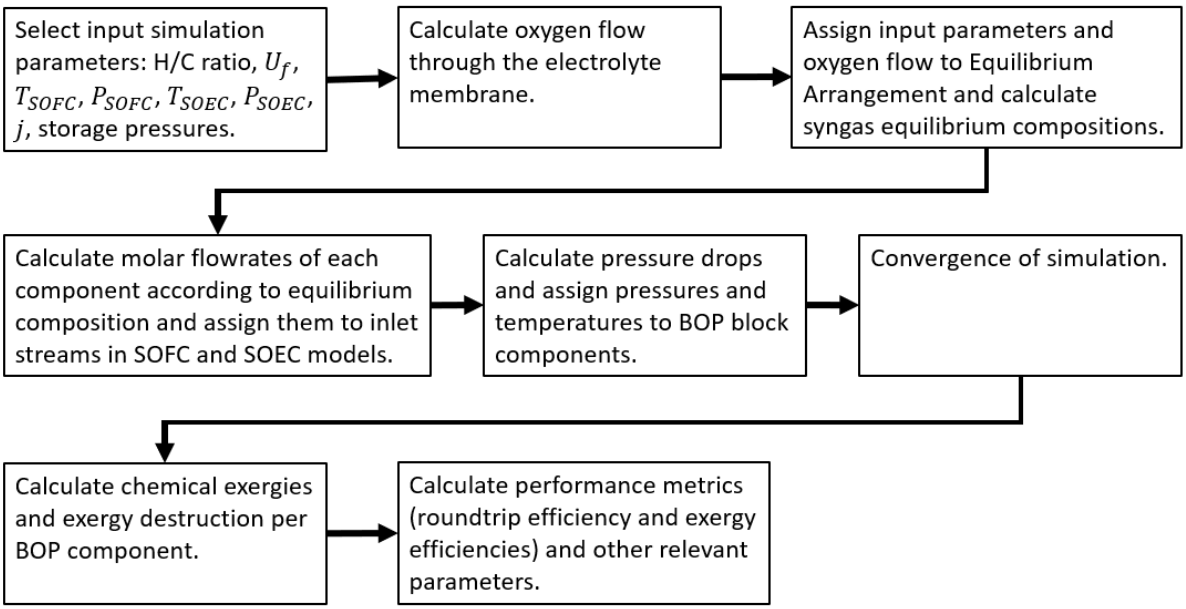

Figure 4.7. Model solution methodology.

5. RESULTS

This chapter introduces the results of the different tests and sensitivity analyses made on the Aspen Plus models developed in this project. First, the stack model was studied to understand the effects of the stack temperature, the stack pressure, current density and H/C ratio on the syngas composition and voltages, and the limitations that these impose to the whole system. The constraints found were incorporated into the analysis of the whole SORC system.

The second part of this chapter starts by showing the results of the Base System in order to set the minimum performance that the syngas-based SORC system developed can deliver. After this, a process of progressive improvement of the system was followed, culminating in a final configuration and operating strategy. Factors like heat integration, stack pressure and temperature, air recirculation and efforts for SOEC exothermic operation were examined.

5.1. Stack Results

Prior to adding any BOP component to create the SORC systems in Figure 4.4, the SOFC and SOEC stack models introduced in Section 4.3 were examined to understand the effects of temperature, pressure, current density and H/C ratio on the equilibrium compositions produced by each mode of operation and on the voltage that the SOCs demand or deliver. This section summarizes the results obtained and the constraints they imposed to the overall system design.

5.1.1. Effects on Syngas Composition

The main purpose of the composition analysis was to identify which conditions promote the formation of methane within the system. This project aimed at examining the performance and feasibility of an SORC storage system working exclusively with

syngas without the extra steps usually taken in other SORC models to promote methanation for heat integration. Therefore, methane was an undesired component within the gas mixture.

The syngas mixtures that came out of the stack after SOFC or SOEC operation could be affected by any parameter that can change the equilibrium of the system. The temperature and pressure of the system were easily identifiable variables and their effects usually correlate to the Le Chatelier's principle. However, the base elemental composition defined by the H/C ratio and the amount of oxygen added or taken from the system by the oxygen ionic current in the cells' electrolyte could also play an important role. The Equilibrium Arrangement introduced in Section 4.6.2 was a useful tool to quickly analyze in Aspen the interplay between these parameters.

Figure 5.1 and Figure 5.2 show the equilibrium composition of all the components of the rich and spent syngas mixtures as a function of the H/C ratio. It can be observed that the content of methane in the spent syngas mixture was negligible because during SOFC operation all the CH_4 was internally reformed and consumed. This behavior was found for the whole range of temperatures, pressures and current densities tested, which implied that SOFC operation didn't impose any methane content constraint. As a result, the focus was placed on the rich syngas mixture, since the electrolysis conditions are the only ones that allow the formation of methane inside the system.

As observed in Figure 5.1, an increase in H/C ratio brought the equilibrium towards hydrogen gas as the amount of carbon available for the formation of methane, carbon dioxide or carbon monoxide decreased. It would have been an advantage to use a high H/C ratio to avoid the formation of methane inside the system, however, this would produce too much hydrogen gas, which would increase compression power requirements given the low heat capacity and density of this gas [6]. Nevertheless, it can be seen that a combination of low temperatures and high pressures promoted methanation in SOEC mode. Decreasing the pressure of the stack in SOEC mode was a much more effective way to control the formation of methane than increasing the H/C ratio, which would also have advantages like decreasing the compression power for water and air streams and allowing to build a more mechanically stable stack.

Figure 5.1 also shows that an H/C ratio of 2 could also be used to reduce hydrogen gas formation, however, in practice a high excess of hydrogen is preferred to ensure no onset of carbon deposition. Given all these results, a compromise could be made at an H/C ratio = 4, where the chemical equilibrium (Figure 2.5) is enough to avoid carbon deposition but doesn't promote too much hydrogen gas formation.

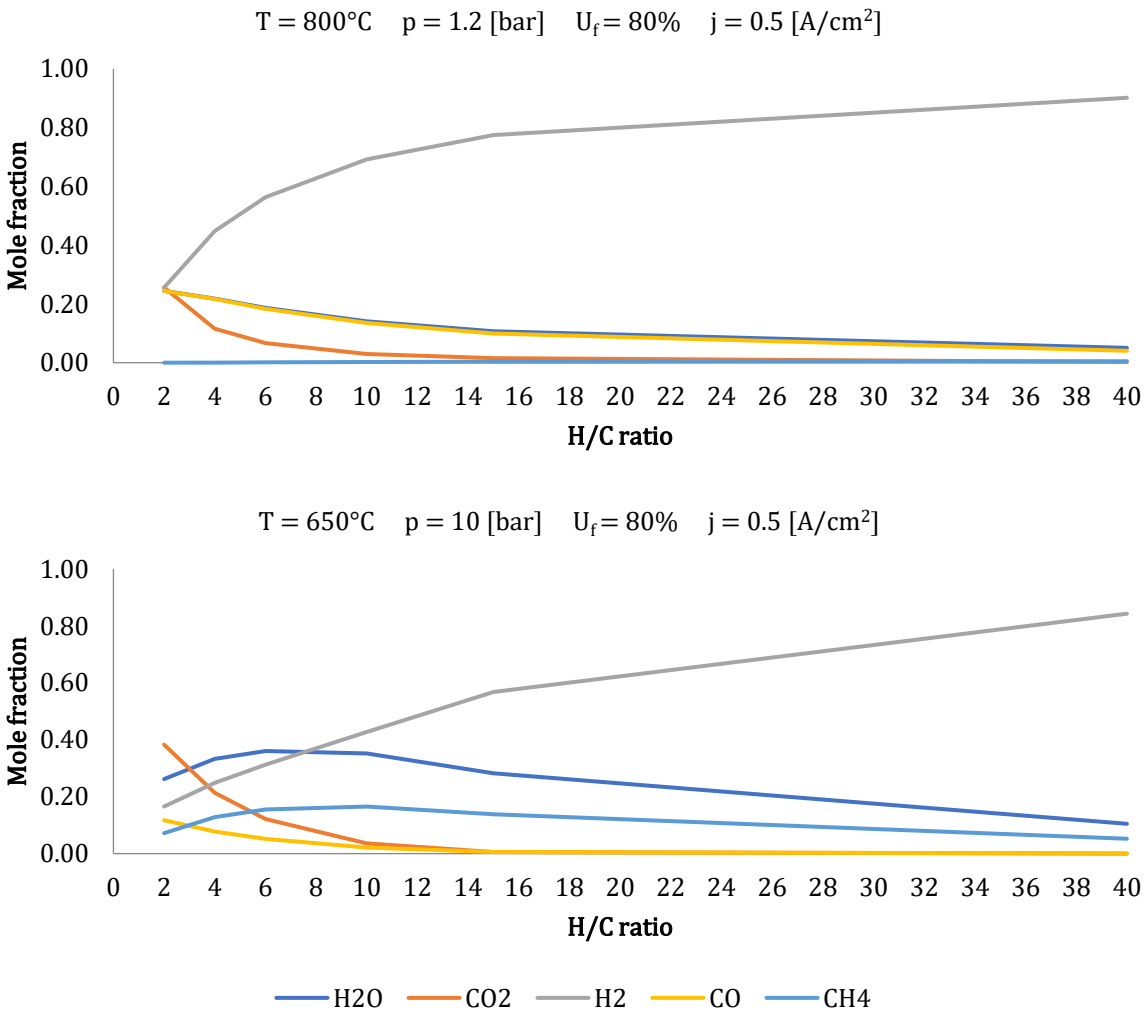

Figure 5.1. Rich syngas composition as a function of the H/C ratio. The amount of oxygen in the system is fixed by the current density, area of the cells and fuel utilization.

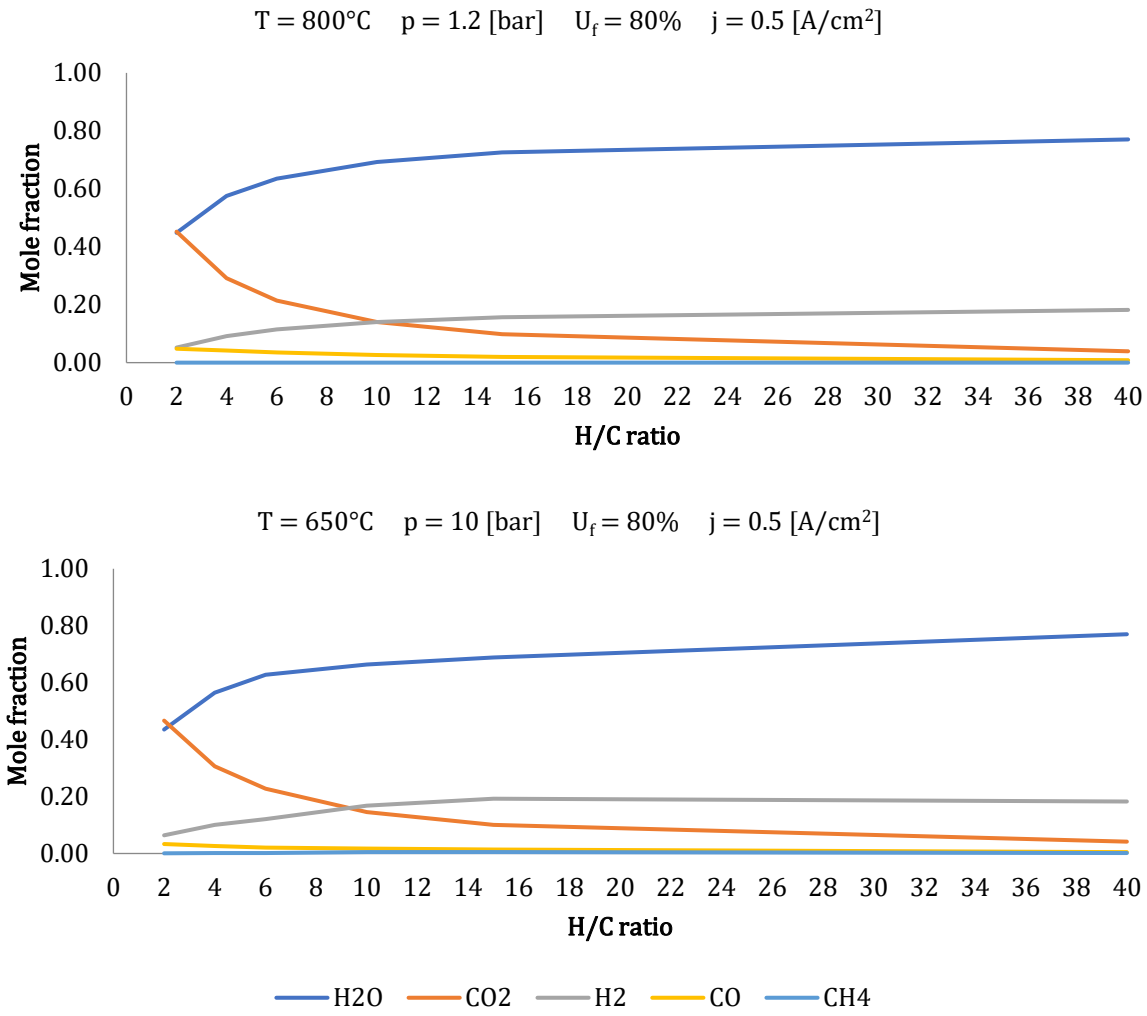

Figure 5.2. Spent syngas composition as a function of the H/C ratio. The amount of oxygen in the system is fixed by the current density, area of the cells and fuel utilization.

5.1.2. Effects on Voltage

The Aspen model was configured in such a way that changes in current do not affect the equilibrium composition of the rich and spent syngas. This is because the flow rate of these components is directly proportional to the oxygen flow rate through the electrolyte calculated for a specified current density and fuel utilization (Equations 4.22, 4.23 and 4.28). If, for example, the specified current doubles, then the oxygen flow rate doubles, and consequently the rich/spent syngas flow rate also doubles. This

was done following the logic that if the fuel utilization is fixed, then a larger current can't pass through the cells if there is not a larger flow rate of species to supply the number of molecules required for the electrochemical reactions to occur at such a charge transfer rate. Nevertheless, the current density did affect the operating voltage of the solid oxide cells through the polarization resistance on the cells.

Of more interest in this study of the stack was the effect of temperature and pressure on the cells' voltage, and the stack roundtrip efficiency of the SORC stack. Figure 5.3 shows the thermoneutral cell voltage, SOEC cell voltage, SOFC cell voltage and stack roundtrip efficiency as a function of temperature for two different pressures. A key feature of these curves is the point where the thermoneutral voltage and SOEC voltage cross each other ($V_{cell,SOEC} = U_{tn}$), revealing the exact temperature in which the SOEC operation changes from exothermic (red area) to endothermic mode (blue area). Decreasing temperature increased the Ohmic overpotential on the cells, thus generating more heat in the process. At the crossing of the curves, the heat generation was equal to the heat requirements of the reactions in the solid oxide cells, and the stack operated isothermally and adiabatically.

It is usually wanted to be able to operate in exothermic mode for the SOEC mode, since that way the outlets of the stack can be used to fully preheat the inlets. However, it can be seen in Figure 5.3 that a low temperature decreased the stack roundtrip efficiency since a lot of energy was lost overcoming the polarization resistances of the cells, especially the Ohmic overpotentials that increased exponentially as a result of the temperature drop. Therefore, if the types of electrolyte membranes used are not capable of having high ionic conductivity at low temperatures, then it would be prudent to operate at the highest possible temperature. Pressure, on the other hand, had an almost insignificant effect on the roundtrip efficiency, since it only affected concentration overpotentials, which in this case were only about 2% of the total polarization resistances given the low thickness of the electrodes used.

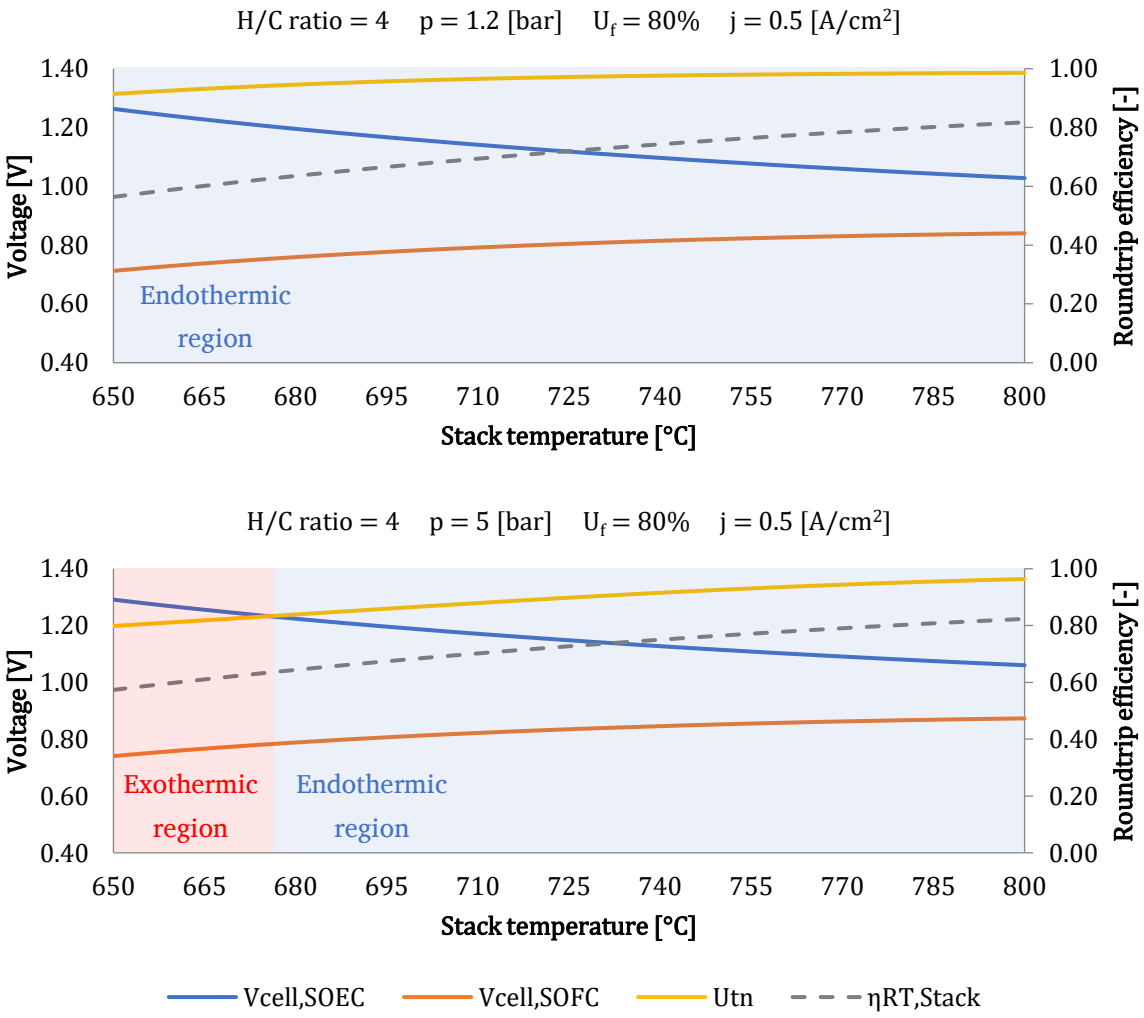

Figure 5.3. Representative voltages and stack roundtrip efficiency as a function of temperature and pressure: Thermoneutral cell voltage (yellow), SOEC cell voltage (blue), SOFC cell voltage (orange) and stack roundtrip efficiency (grey).

Figure 5.4 is a design map that effectively summarizes the most important results from the stack analysis; it shows the dry mole fraction of methane in the rich syngas mixture as a function of temperature and pressure for two current densities. As can be observed, increasing the current from 0.5 $[A/cm^2]$ to 1.0 $[A/cm^2]$ didn't change the methane content since the flow rates were proportional to the current density as explained before. It can also be seen from the figure that the methane content in the syngas increased with decreasing temperature and increasing pressure. The black horizontal line shows the maximum 1% content of methane allowed within the SORC system, therefore any combination of temperature and pressure above this line was

not possible within the system in SOEC mode. The diamonds on the methane lines represent the temperature at which $V_{cell,SOEC} = U_{tn}$. Therefore, temperatures to the left of these points represent exothermic operation (rea area), and to the right of these points represent endothermic operation (blue area). Putting all these factors together, it could be evident that in order to keep the methane content below 1% dry mole basis, pressures could not be higher than 4 $[bar]$ and the SORC would always operate endothermically in SOEC mode.

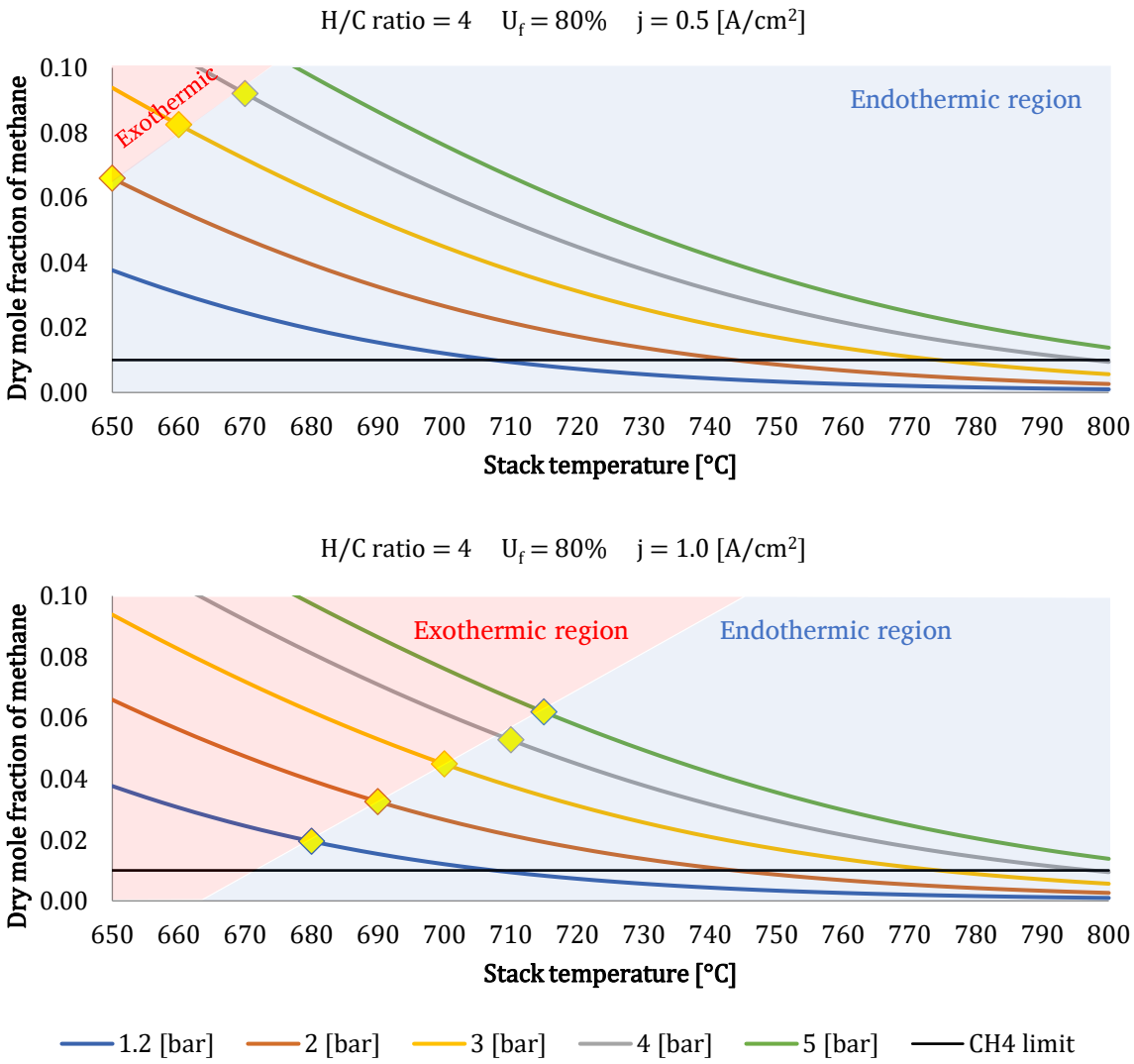

Figure 5.4. Dry mole fraction of methane in rich syngas mixture as a function of temperature and pressure. Diamonds show the temperature where $V_{cell,SOEC} = U_{tn}$.

According to the result seen in Figure 5.4, Table 5.1 indicates the temperature range in which the SORC system could operate for a specified pressure during SOEC mode in order to keep the methane content below 1% on a dry mole basis.

Table 5.1. Permitted temperature ranges and pressures in SOEC mode of operation.

Pressure $[bar]$	**Temperature range** $[°C]$
1.2	$705 - 800$
2	$745 - 800$
3	$775 - 800$
4	800

5.2. System Results

The results from the stack analysis made it possible to define operational constraints for the entire SORC system that narrowed the configuration possibilities for the BOP components as well as the operation strategies. Based on the works on solid oxide reversible cells of Wendel [2], Mottaghizadeh et al. [3], Sebastiani [24] and Mor [25], it was possible to arrive to the configuration of the Base System in Figure 4.4.

5.2.1. Base System Analysis

The analysis in Section 5.1 concluded that the stack should be operated at the highest possible temperature to obtain the highest possible stack roundtrip efficiency. However, the implementation of BOP components does not necessarily mean that the system roundtrip efficiency should follow this trend. A sensitivity analysis for the Base System was carried out in order to see the effect of stack temperature on the whole SORC system in a range between $705 - 800°C$. Figure 5.5 summarizes the results.

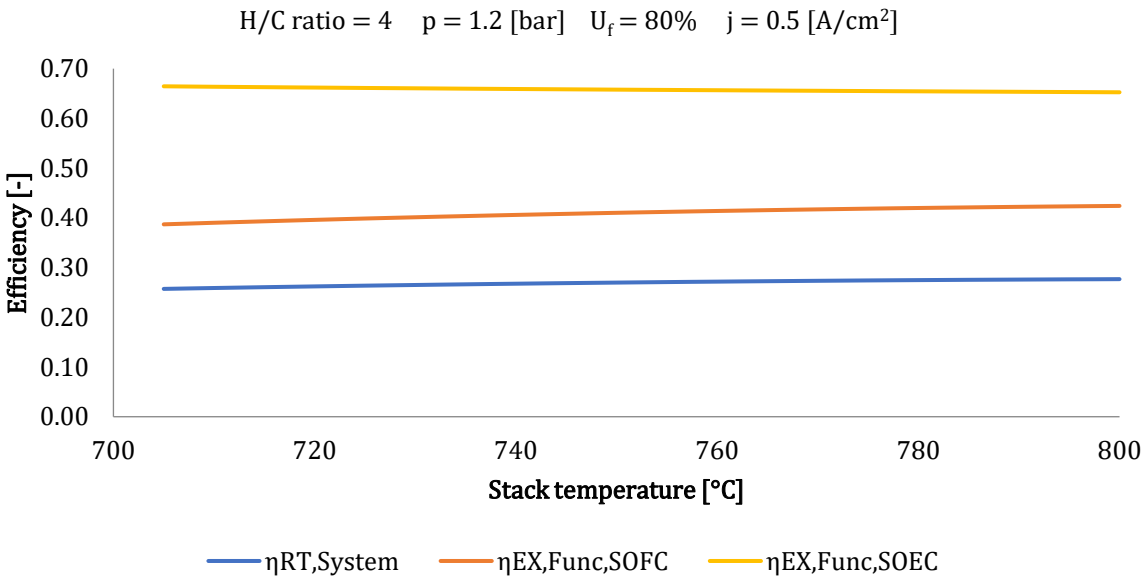

Figure 5.5. Performance metrics for Base System as a function of temperature: system roundtrip efficiency (blue), SOFC exergy efficiency (orange), SOEC exergy efficiency (yellow).

From the sensitivity analysis it can be observed that all performance metrics of the system remained relatively constant as a function of temperature. In the case of the roundtrip efficiency, as temperature decreased the overpotentials on the cells increased, reducing the performance. This was exacerbated by a slight increase in energy requirements in the air blower at lower temperature. In general, roundtrip efficiency and SOFC exergy efficiency improved at higher temperatures, showing that the stack conditions (mostly overpotentials) tend to dominate the performance of the system in SOFC mode. In SOEC mode, exergy efficiency declined at higher temperatures since more electric energy had to be used to evaporate water and warm up air above the temperature of the stack, overpowering the reduction of overpotentials at higher temperatures.

The system roundtrip efficiency might have a much larger weight when deciding what efficiencies should be promoted, since this metric has a more direct impact in the economics of the plant [2]. Therefore, a stack temperature of $800°C$ continued to be used for the analysis of the SORC system, since it resulted in the highest roundtrip efficiency.

Table 5.2 summarizes the most important values and performance metrics for the Base System under the base conditions shown in Table 4.2. In Table 5.2, and the subsequent tables in this chapter of similar style, the categories shown include:

- **Net power produced in SOFC mode:** net sum of the electric power produced by the stack in SOFC mode, power produced and consumed by the BOP, and power used for heating purposes.

- **Net power consumed in SOEC mode:** net sum of the electric power consumed by the stack in SOEC mode, power produced and consumed by the BOP, and power used for heating purposes.

- **Exergy lost/destroyed:**
    - **Stack:** exergy destroyed in the stack by the electrochemical and equilibrium reactions, plus heat transfer between material flows.

    - **Expansion:** exergy destroyed by thermodynamic irreversibilities inside turbines and expansion valves.

    - **Compression:** exergy destroyed by thermodynamic irreversibilities inside compressors or blowers.

    - **Heat transfer:** exergy destroyed in heat transfer processes inside heat exchangers and in electric heaters.

    - **Mixing:** exergy destroyed by the mixing of material streams at different temperatures, different pressures or with different molar compositions.

    - **Environment:** external exergy losses in material and energy streams that leave the system with exergy content above the dead state.

Table 5.2. Results for Base System.

Parameter	**Units**	**Base System**	
Stack temperature	$°C$	800	
Stack pressure	bar	1.2	
Current density	A/cm^2	0.5	
Net power produced in SOFC mode	kW	85	
Net power consumed in SOEC mode	kW	295	
Stack roundtrip efficiency	%	84	
System roundtrip efficiency	%	29	
SOFC exergy efficiency	%	44	
SOEC exergy efficiency	%	66	
Exergy lost/destroyed	**kW**	SOFC	SOEC
Stack		0.90	10
Expansion		1.6	0.80
Compression		2.4	2.6
Heat transfer		57	64
Mixing		3.8	4.9
Environment		35	16

From Table 5.2 it can be observed that although the stack conditions made it possible to have a large stack roundtrip efficiency, the system roundtrip efficiency decreased considerably with respect to the previous value because of the large difference between the net power produced in SOFC mode and the power consumed in SOEC mode. The main cause of this loss is the large amount of electric energy that was required to heat up streams within the system, which can also be evidenced in the high exergy destruction in heat transfer for both modes of operation. Exergy flows through the Base System can be appreciated in the exergy flow diagrams presented in Appendix G and Appendix H for SOFC and SOEC operation, respectively.

The exergy efficiency during SOFC operation also showed a rather low performance. The reason was that the exothermic nature of the reactions in this mode produced a lot of heat that was removed with the air stream, which had to be almost 15 times larger than the flow of rich syngas to keep the temperature of the stack constant. However, it was not possible to recover the exergy in this high-temperature air since no heat exchanger network was in place for this initial configuration (Section 4.4), therefore the air was vented to the atmosphere at a temperature of around $144°C$ and losses of exergy to the environment were very high.

On the other hand, the endothermic nature of the reactions in SOEC mode required a lower air flow rate about 12 times larger than that of the spent syngas, thus the heat transfer in the air preheater could cool down the outlet stream to a temperature of around $77°C$. This considerably reduced the exergy losses to the environment and resulted in a much larger exergy efficiency in SOEC mode. Nevertheless, the water flow rate through the water boiler was much larger in SOEC mode than in SOFC mode, therefore a lot of electric energy was invested in the production of steam, which increased the exergy losses in heat transfer compared to SOFC mode.

The analysis of the Base System showed how important is the heat management in an SORC system. Heat integration is necessary not only to save energy and increase roundtrip efficiency, but also for exergetic performance, since a lot of thermo-mechanical exergy was lost in the outlet flows and high-value electric energy was inefficiently used to produced heat to generate stream. It could then be concluded that the first improvement over the Base System had to be the addition of a heat transfer network.

5.2.2. Effect of Heat Integration

The heat transfer configuration engineered in this project for the Base System can be observed in Figure 5.6. It is the result of a trial-and-error exercise that aimed at using only the heat generated within the system to fulfill all heating requirements without the need of external heating utilities like the power grid. It was validated for several temperatures and pressures and worked within the ranges defined for these parameters in Section 4.4.

It must be noted that the heat exchanger network in SOFC mode changes from that in SOEC mode due to the differences in the energy flows in both processes. In total, 6 heat transfer processes were introduced in SOFC mode while 5 were introduced for SOEC mode. Only three of these exchangers were common for both modes of operation, therefore the remaining exchangers do not necessarily share the same bodies and more devices than needed might be present. It could be possible to achieve a simpler design with a heat optimization exercise or by redirecting flows with a good implementation of manifolds; however, this was outside of the scope of this project.

In SOFC mode all heating requirements could be supplied with the available heat within the system. On the other hand, in SOEC mode no flow was found with the right thermal characteristics to supply the heat required for water evaporation and for heating up the air stream above the temperature of the stack. In the case of the air stream, no flow in the system would be hotter than the inlet air to the stack during endothermic operation. In the case of the steam generation, no flow could provide enough heat to evaporate the large amounts of water needed for co-electrolysis.

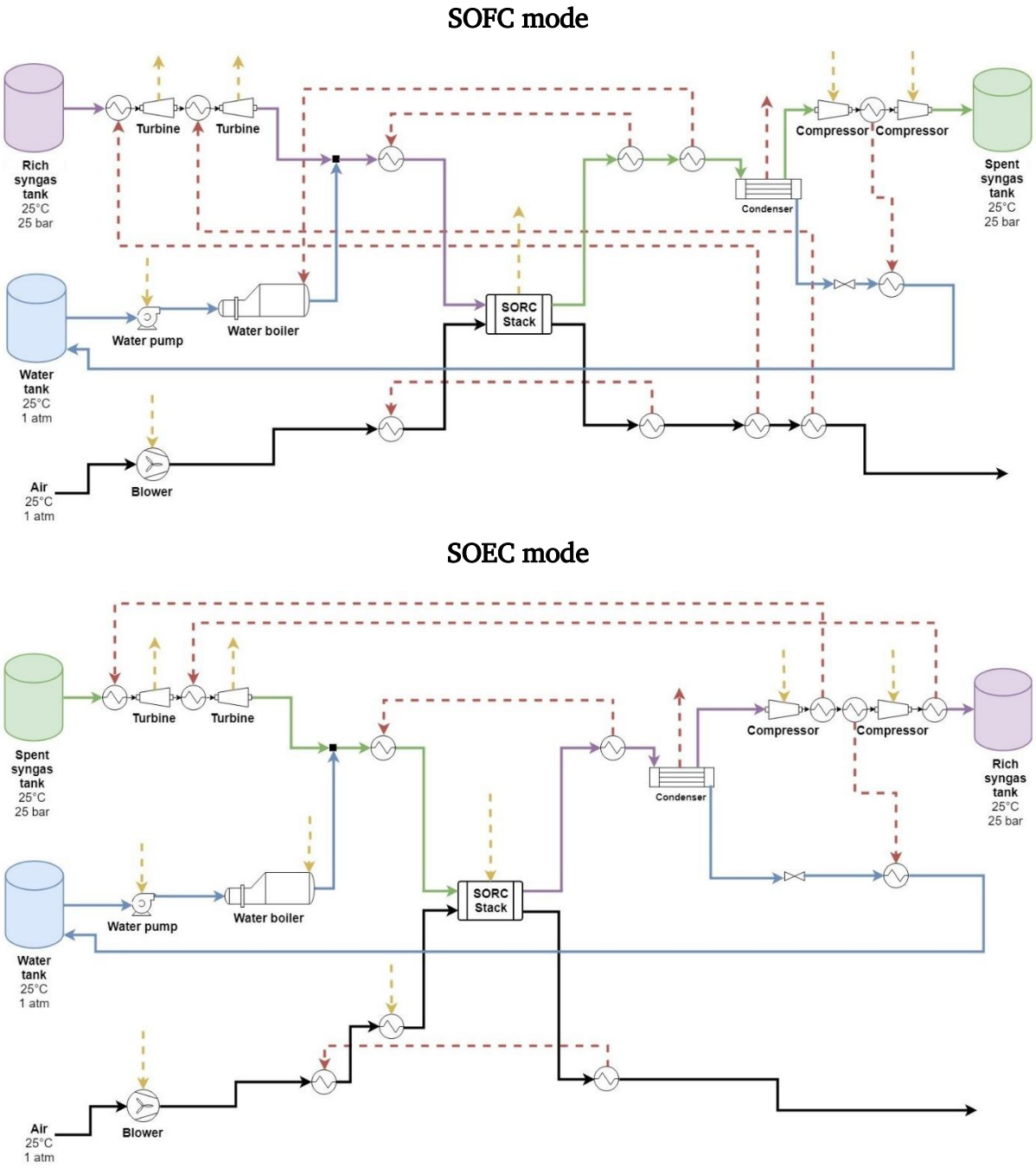

Figure 5.6. SORC Base System with heat integration. Solid lines represent material flows of rich syngas (purple), spent syngas (green), water (blue) and air (black). Dashed lines represent energy flows of heat (red) and electricity (yellow).

Figure 5.7 shows the comparison of performance metrics as a function of temperature between the Base System with no heat integration (dashed lines) and with heat integration (solid lines). Heat integration clearly improved the operation of the SORC system at any temperature, especially for the exergy efficiency in SOFC mode, where all heating requirements were fulfilled internally and any dependency on electric energy was removed, showing the importance of heat integration for better exergy utilization.

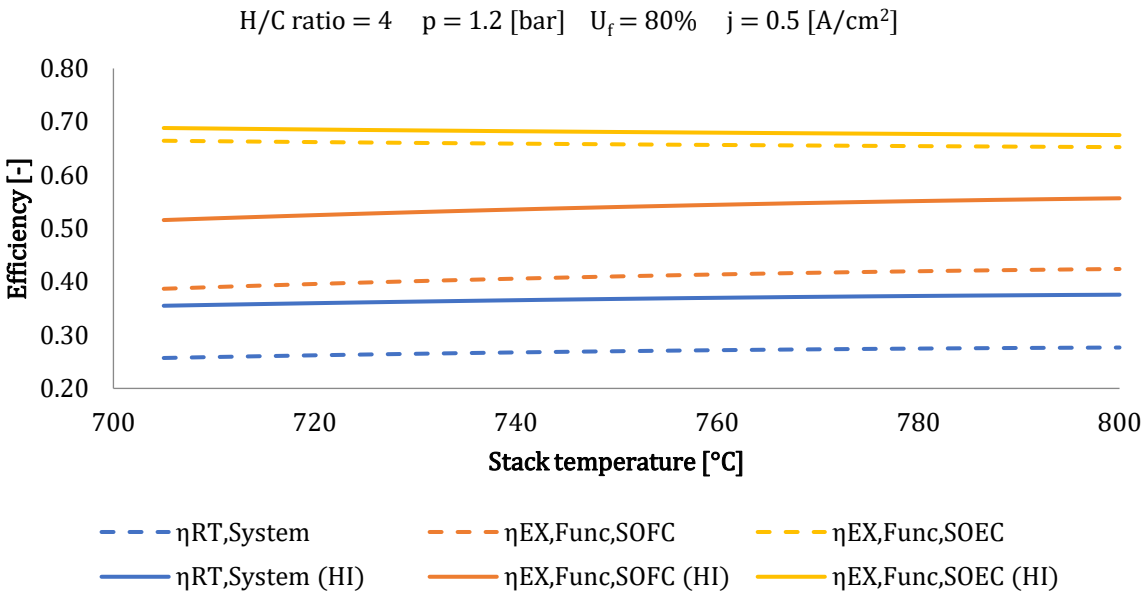

Figure 5.7. Performance metrics for the Base System (dashed lines) and improved system with heat integration (solid lines) as a function of temperature.

Table 5.3 shows a comparison between the performance metrics of the Base System and the performance metrics of the improved case with heat integration. High stack temperatures still showed the best roundtrip efficiency results in Figure 5.7 thus this comparison was made at a temperature of $800°C$. Heat integration was able to increase performance in all metrics. The roundtrip efficiency was improved by 9% since no electricity had to be used to heat up some of the streams; in SOFC mode no electric power was used at all anymore for this process, therefore the net power output drastically increased. The gains in SOEC mode power consumption were not as high since steam generation and heating of the air above the temperature of the stack were the most energy consuming processes besides the power consumption of the SORC stack, and electric power consumption in these operations could not be avoided.

Table 5.3. Effect of heat integration on system performance.

Parameter	**Units**	**Base System**		**With heat integration**	
Stack temperature	$°C$	800		800	
Stack pressure	bar	1.2		1.2	
Current density	A/cm^2	0.5		0.5	
Net power produced in SOFC mode	kW	85		108	
Net power consumed in SOEC mode	kW	295		288	
Stack roundtrip efficiency	%	84		84	
System roundtrip efficiency	%	29		38	
SOFC exergy efficiency	%	44		56	
SOEC exergy efficiency	%	66		68	
Exergy lost/destroyed	***kW***	SOFC	SOEC	SOFC	SOEC
Stack		0.90	10	0.90	10
Expansion		1.6	0.80	1.6	0.80
Compression		2.4	2.6	2.4	2.6
Heat transfer		57	64	41	59
Mixing		3.8	4.9	4.0	4.3
Environment		35	16	26	13

Exergy efficiency in SOFC mode saw the largest improvement between all efficiency metrics. The reasons behind this were that first of all no electric power had to be used to generate heat, which by itself was a very inefficient use of high-quality energy, but also that the heat transfer between streams in the system had the advantage that the temperature differences between primary and secondary steams were not too high, therefore exergy destruction through finite temperature differences were reduced. These two effects also improved the exergy efficiency in SOEC mode, however the gains were much lower since not all heating requirements could be fulfilled internally.

The heat transfer processes made it possible to keep energy inside the system by exchanging it between hot outlet flows and cold inlet flows. As a result, the streams that leave the system could be cooled down much more than in the absence of a heat transfer network, and the exergy losses to the environment were reduced, improving the exergy efficiencies of the system, particularly in SOFC mode where a lot of heat was produced as a result of the exothermic reactions in the stack.

A particularity of the system in Figure 5.6 was the use of the water separated in the condenser for the intercooling between the compression steps of the syngas sent to storage. Since the water was depressurized in an adiabatic expansion valve, its temperature dropped low enough to use it for this purpose. This made it possible to remove a water-cooling system, thus reducing the overall complexity of the system, its energy consumption and associated exergy losses.

Heat integration could effectively reduce the exergy destruction in heat transfer processes and should be implemented when possible. Nevertheless, the system up to this point still lacked a way to recover some of the energy expended to move the large amounts of air that were needed in both modes of operation, which with heat integration still remains around 15 times the mole flow of rich syngas in SOFC mode and around 12 times the mole flow of spent syngas in SOEC mode. In order to recover some of this energy it was necessary to pressurize the system to a point where the pressure ratios were above 2 to justify the use of air turbines [37].

5.2.3. Effect of System Pressurization

Above compression pressure ratios of 2 the density of air could not be considered constant anymore, therefore the blower in the SORC system was changed to a compressor. Figure 5.8 shows the Base System with heat integration and the addition of a compressor and a turbine in the air stream. Because the air was needed as hot as possible after compression, this process was done in one step without intercooling. Additionally, the expansion in the turbine was also done in one step and without preheating in order to cool down the outlet air to a temperature low enough to avoid excessive exergy losses to the environment.

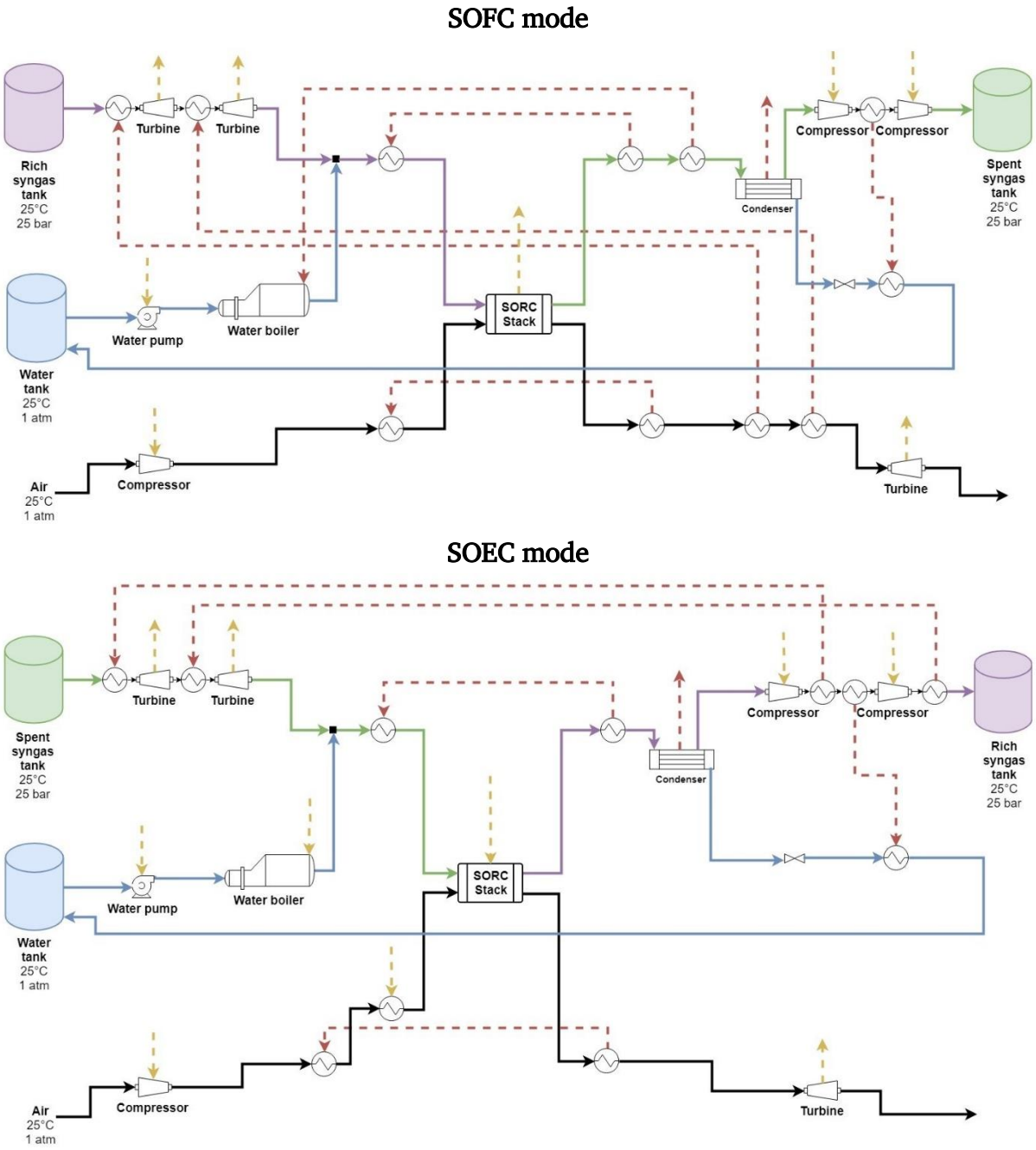

Figure 5.8. Pressurized SORC Base System with heat integration. Solid lines represent material flows of rich syngas (purple), spent syngas (green), water (blue) and air (black). Dashed lines represent energy flows of heat (red) and electricity (yellow).

Changing the pressure inside the system can have many consequences on the different BOP components that can change the temperature-based behaviors previously examined. For this reason, another sensitivity analysis was made for the SORC system with heat integration as a function of stack pressure and stack temperature. As it was found in the stack analysis of Section 5.1, the maximum pressure for SOEC operation allowed was 4 $[bar]$ in order to keep the methane content below 1%. This constraint also limited the full range of temperatures of operation for the stack according to Table 5.1. However, the full range of $705 - 800°C$ was analyzed in order to be able to find tendencies in the results.

Figure 5.9 shows the results for the SORC system roundtrip efficiency, SOFC exergy efficiency and SOEC exergy efficiency. As can be observed, the initial pressurization from 1.2 $[bar]$ to 2 $[bar]$ provoked a significant increase in the first two performance metrics as the energy recovered by the air turbine helped offset some of the energy that had to be used to run the air compressor. The result was a final increase in the electric power output in SOFC mode and a reduction in the energy consumed in SOEC mode. The exergy efficiency of the latter, however, did not show a large improvement since exergy losses in the water boiler and in the electric air heater were still the dominant sources of inefficiency.

It can be observed in Figure 5.9 that the benefits of higher pressures start decreasing with further increases in pressure beyond 2 $[bar]$, except for temperatures at the low end of the range. Nevertheless, the system could not be operated at such low temperature because the excessive formation of methane at these higher pressures would violate the 1% methane constraint. It was likely that the presence of methane was responsible for part of the improvement at low temperatures, since the compression, expansion and heating characteristics of the syngas changed.

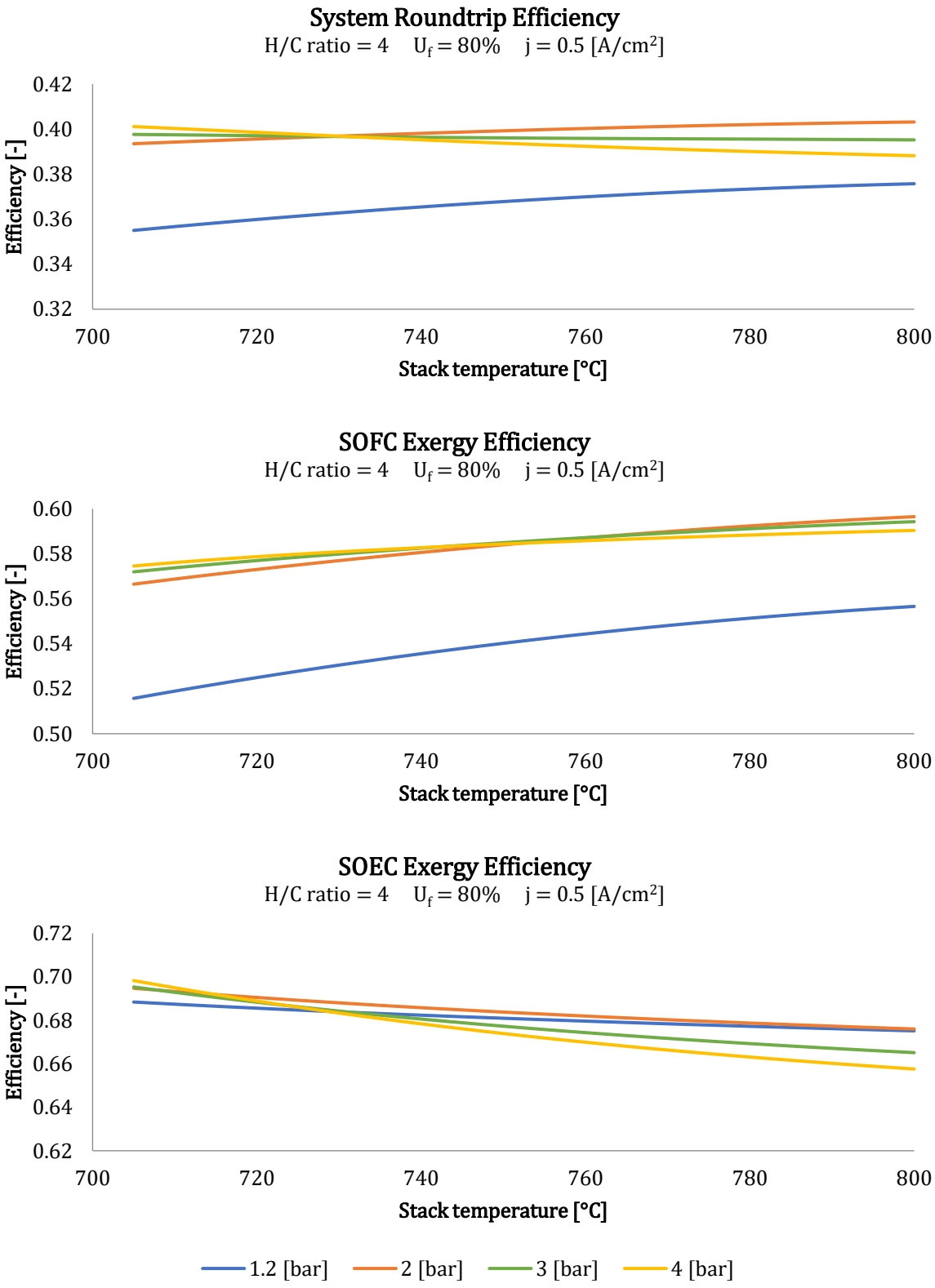

Figure 5.9. Performance metrics for Base System with heat integration as a function of temperature and pressure.

At high temperatures, the decrease in efficiency for higher pressures was mostly the result of the difference between the power consumed by the air compressor and the power recovered by the air turbine. Figure 5.10 shows for both modes of operation the power consumed and recovered by the different compression and expansion processes in the system for the air and syngas streams, along with the power of the SORC stack. The turbines in the syngas stream had the capacity to cover the compression requirements of the same stream after the stack for SOFC mode, and in both modes the compression power reduced with increasing stack pressure since the pressure ratio between the storage tanks and the stack decreased. However, none of these was the case for the air stream, where the compression power always exceeded the energy recovered with the air turbine, and the difference between the two increased as the pressure of the stack was increased. Since the power produced in SOFC mode and the power consumed in SOEC mode remained relatively constant at all pressures, there was always a net increase in power consumption after the pressure was increased above 2 [bar] that brought down the efficiency of the whole system.

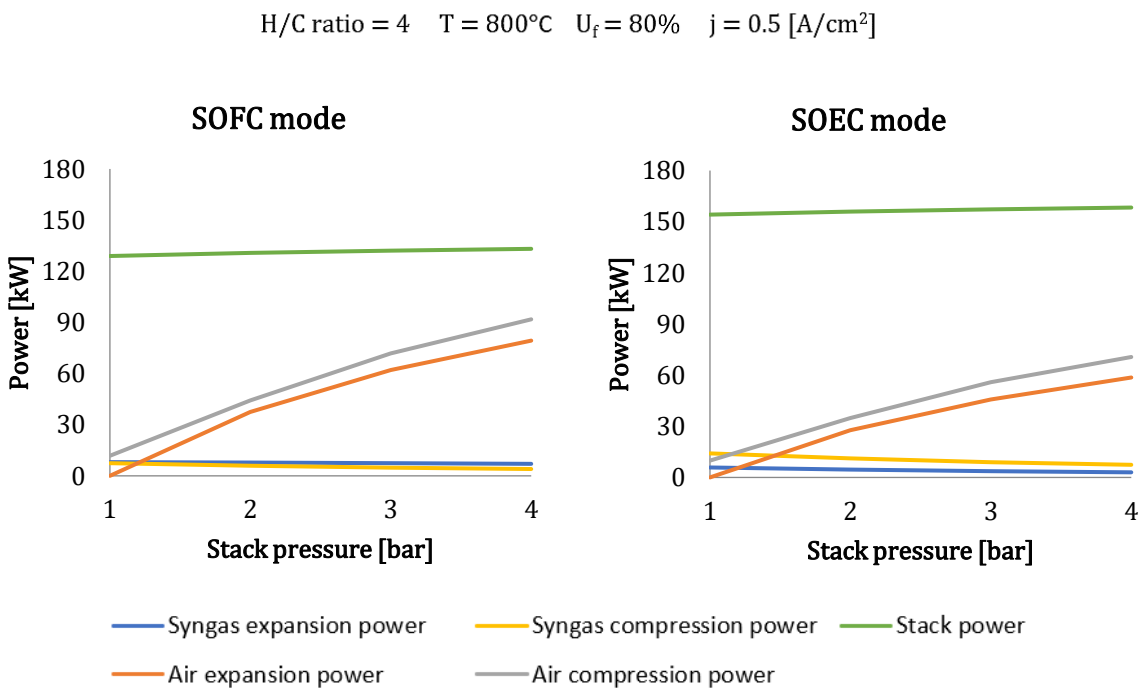

Figure 5.10. Power production and consumption in the SORC system as a function of the stack pressure.

In a regular open gas cycle, fuel would be combusted with the air to increase its temperature to very high levels before a gas turbine, thus the expansion would create enough work to offset the compression requirements of the working fluid. In the SORC system it was not possible to reheat the outlet oxidant stream to the needed temperatures before expansion since no internal stream was found that had the right thermal characteristics. Nevertheless, Mor [25] explored the use of a recirculation loop in the air stream to reduce the compression power for the air stream; a strategy that was implemented and whose results are shown in the following section.

Without the implementation of recirculation, a pressure of 2 [bar] brought the largest benefits for the SORC system at high temperature. Table 5.4 shows a comparison between the Base System with heat integration at 1.2 [bar] and at 2 [bar]. It can be observed that at 2 [bar] the addition of the turbine in the oxidant stream increases the net power output of the system in SOFC mode while no appreciable change can be seen in the power consumed in SOEC mode. This had the final effect of increasing the roundtrip efficiency of the system by 2%.

The increase in pressure had the disadvantage of increasing exergy destruction in expansion and compression processes because of the additional turbine in the system and because more energy had to be invested in the compression of the air. However, large exergetic improvements could be achieved in heat transfer and environmental losses. In the former case, the higher pressure of the stack reduced the pressure ratio per expansion step of the syngas from storage, which meant that the syngas left each turbine at a higher temperature than with the stack at atmospheric pressure. As a result, the temperature difference between the material flows in the reheating process was decreased and exergy losses because of heat transfer through a finite temperature difference were reduced. More pressure inside the system in general also reduced the amount of heat transferred between all heat exchangers.

Environmental losses decreased because the pressure ratio between compression steps of the syngas stream was also reduced and the gas left at a lower temperature of 145°C compared to the Base System at 206°C. The turbine in the air stream was capable of cooling down the outlet oxidant to a temperature of 172°C, which was not lower than the outlet temperature achieved at atmospheric pressure (144°C). However, the turbine recovered a large portion of the TM exergy available in the air stream, which

finally left the system with less total exergy than the same stream at atmospheric pressure, thus effectively reducing environmental losses.

Table 5.4. Effect of pressurization on system performance.

Parameter	**Units**	**With heat integration at 1.2 [bar]**		**With heat integration at 2 [bar]**	
Stack temperature	$°C$	800		800	
Stack pressure	bar	1.2		2	
Current density	A/cm^2	0.5		0.5	
Net power produced in SOFC mode	kW	108		116	
Net power consumed in SOEC mode	kW	288		288	
Stack roundtrip efficiency	%	84		84	
System roundtrip efficiency	%	38		40	
SOFC exergy efficiency	%	56		60	
SOEC exergy efficiency	%	68		68	
Exergy lost/destroyed	**kW**	SOFC	SOEC	SOFC	SOEC
Stack		0.90	10	0.80	9.2
Expansion		1.6	0.80	6.2	4.7
Compression		2.4	2.6	6.2	5.5
Heat transfer		41	59	32	54
Mixing		4.0	4.3	3.7	4.3
Environment		26	13	19	5.8

5.2.4. Effect of Air Recirculation

Figure 5.11 shows the implementation of an air recirculation loop in the SORC system. The principle behind it is that a fraction of the hot and pressurized outlet oxidant stream is separated and mixed with the colder inlet air coming from the compression step. This looped mass of air then reduces the amount of fresh air that needs to be added to the system to fulfill heating purposes in SOEC mode and cooling purposes in SOFC mode, and acts as a preheating step for the fresh air. As a result, a lower mass of air goes through compression and less power is needed for this step.

On the negative side, the recirculation of the outlet oxidant stream from the stack decreases the partial pressure of oxygen at the inlet for SOFC mode, while it increases its partial pressure in SOEC mode, both of which reduce the performance of the SORC by reducing the reversible voltage in SOFC mode and increasing it in SOEC mode (Equation 2.17). This as well would increase the concentration overpotentials in SOFC mode by decreasing the oxygen concentration in the flow channels of the cells that allow the diffusion of these molecules from the bulk gas to the TPBs; and by increasing the oxygen concentration at the bulk in SOEC mode reducing the concentration difference between the TPBs and the bulk gas, making oxygen diffusion outside of the oxygen electrode harder [2] [24] [25]. Because of these effects, a tradeoff between reduced compression power and less performance in the stack must be made.

The results of the sensitivity analysis of performance parameters for recirculation ratios of 0.20 and 0.50 are shown in Figures 5.12-5.14. It can be seen in these that for the case with no air recirculation, stack pressures above $2\,[bar]$ lead to a loss in efficiency at higher temperatures. However, the decrease in compression requirements by increasing the amount of recirculated air gradually changed this tendency, improving the efficiency of high stack pressures at higher temperatures. At a recirculation ratio of 0.50 all performance metrics for pressures above $2\,[bar]$ became larger or almost equal to the performance at $2\,[bar]$ (between the range of $2-4\,[bar]$). The general increase of all performance metrics and the improvement of the efficiency of the system at higher pressures showed that air recirculation should always be used for both modes of operation.

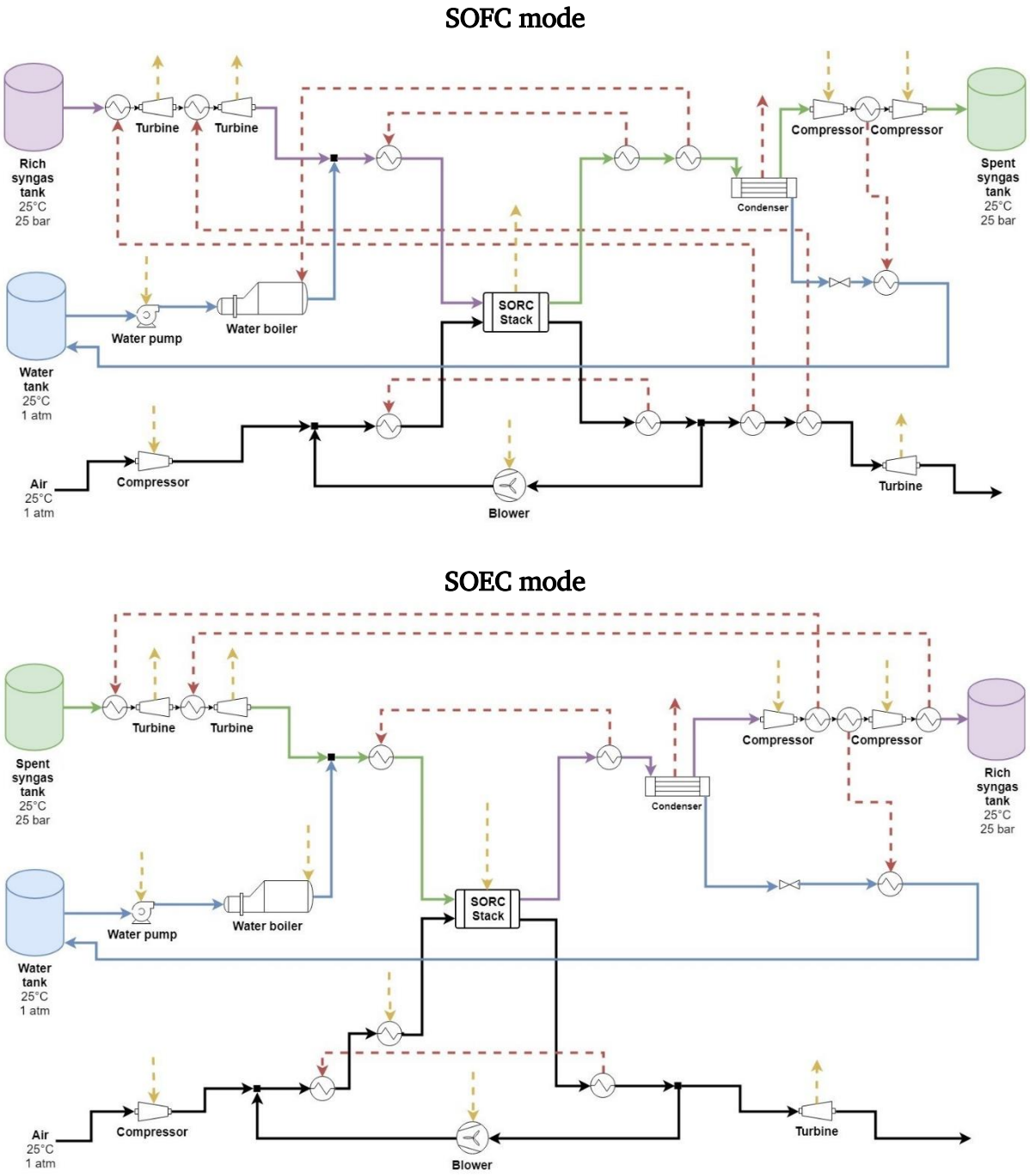

Figure 5.11. Pressurized SORC Base System with heat integration and air recirculation. Solid lines represent material flows of rich syngas (purple), spent syngas (green), water (blue) and air (black). Dashed lines represent energy flows of heat (red) and electricity (yellow).

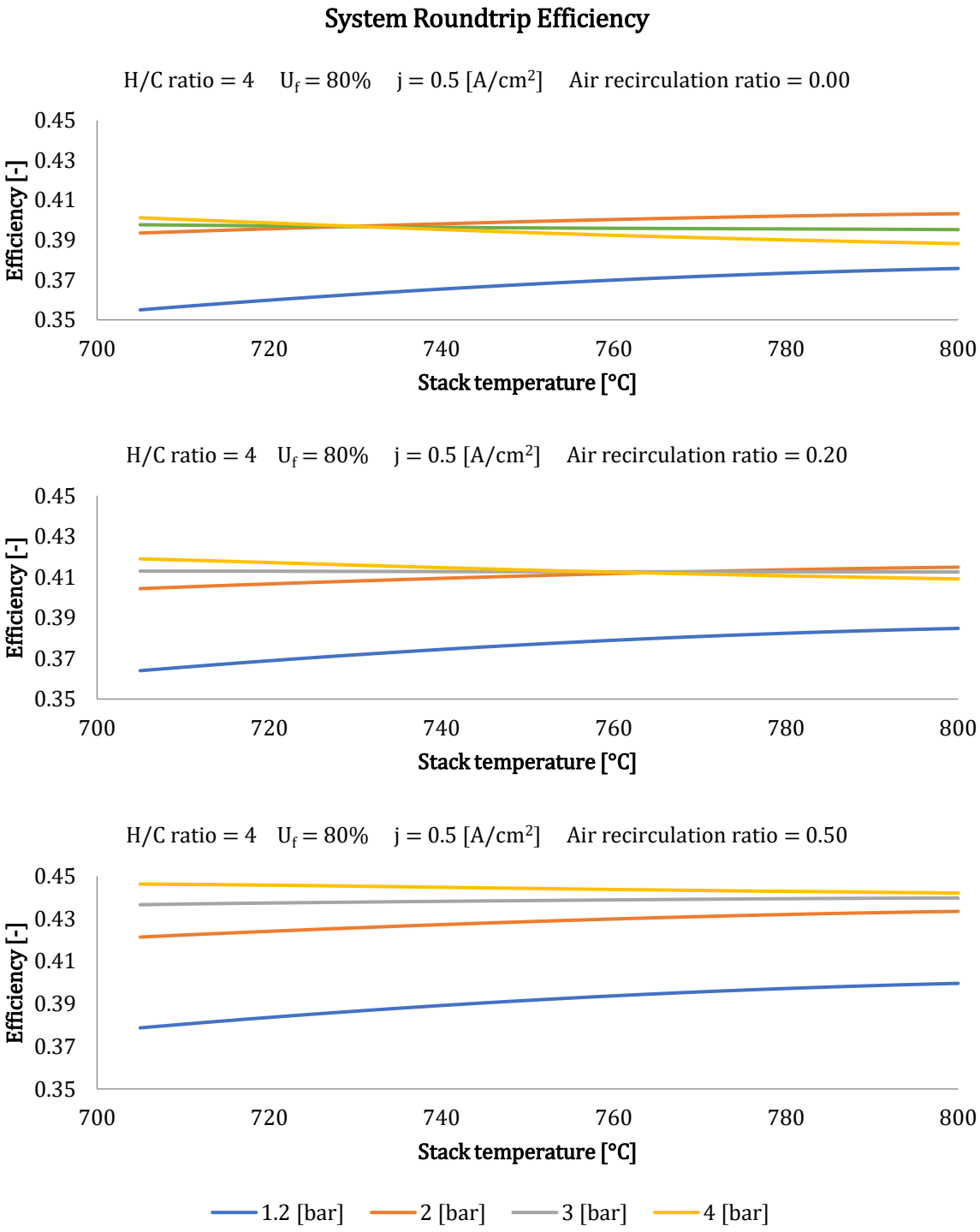

Figure 5.12. System roundtrip efficiency as a function of pressure, temperature and air recirculation ratio for the SORC Base System with heat integration and air recirculation.

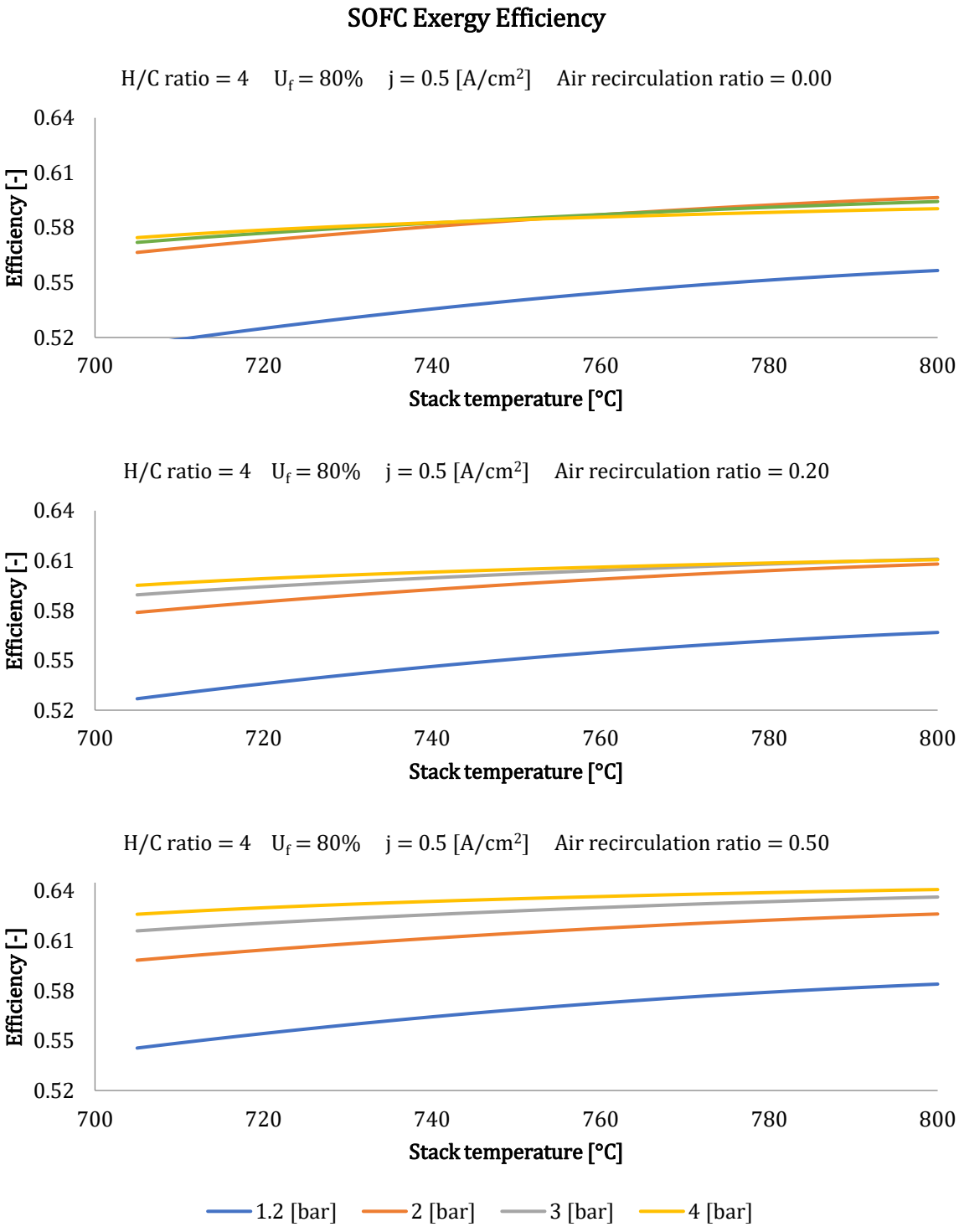

Figure 5.13. System SOFC exergy efficiency as a function of pressure, temperature and air recirculation ratio for the SORC Base System with heat integration and air recirculation.

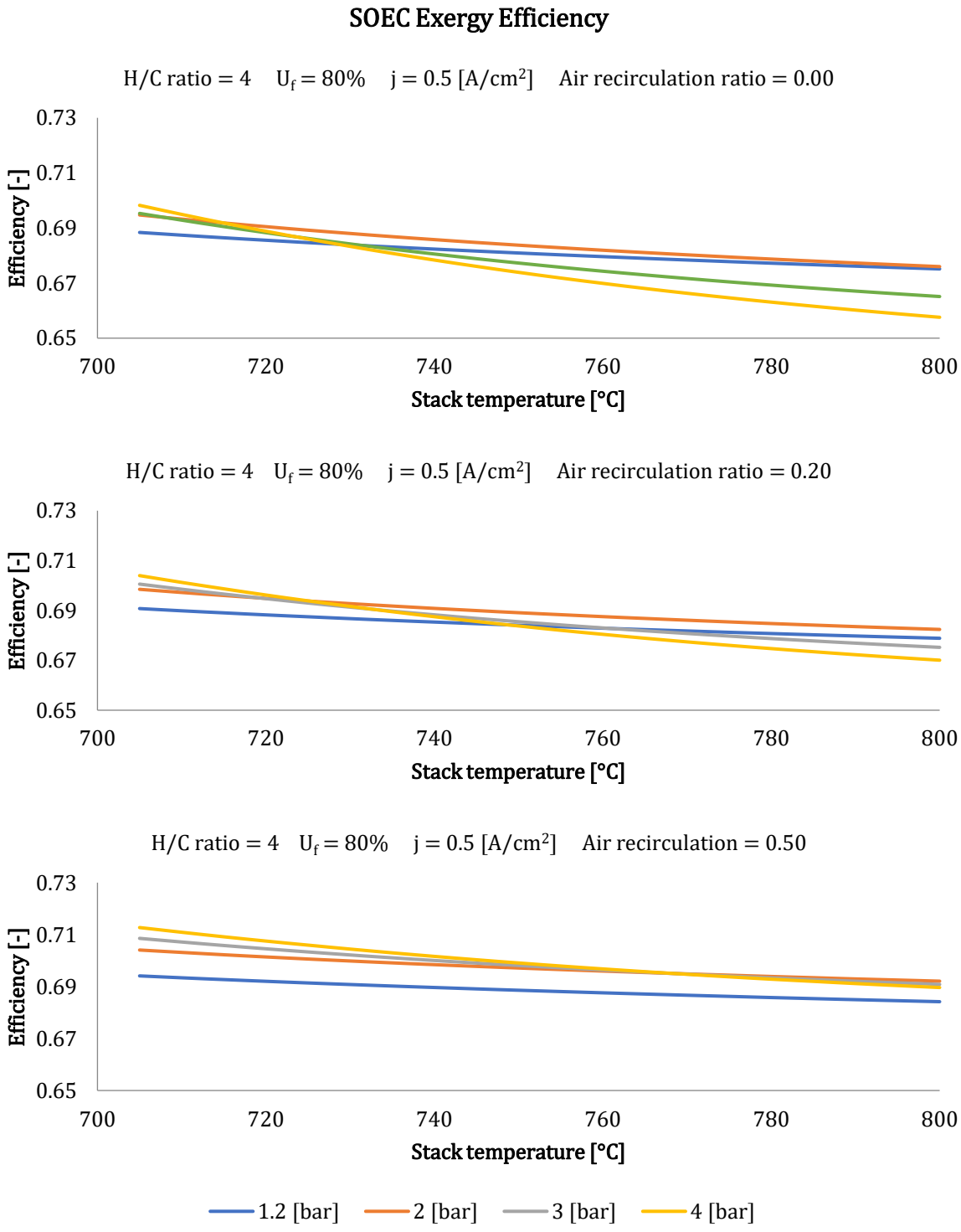

Figure 5.14. System SOEC exergy efficiency as a function of pressure, temperature and air recirculation ratio for the SORC Base System with heat integration and air recirculation.

The results of this project showed that a high recirculation ratio make it possible to work effectively at high pressures as long as concentration overpotentials are not a limiting loss inside the SORC stack. Since the maximum operating pressure allowed in SOEC mode was 4 [bar], the recirculation ratio was limited to 0.50. Table 5.5 shows a comparison between the Base System with heat integration at 2 [bar] and without recirculation, and at 4 [bar] with 0.50 air recirculation.

Table 5.5. Effect of pressurization and air recirculation on system performance.

Parameter	**Units**	**With heat integration at 2 [bar]**		**With heat integration at 4 [bar] and recirculation**	
Stack temperature	$°C$	800		800	
Stack pressure	bar	2		4	
Current density	A/cm^2	0.5		0.5	
Air recirculation ratio	–	0.00		0.50	
Net power produced in SOFC mode	kW	116		124	
Net power consumed in SOEC mode	kW	288		282	
Stack roundtrip efficiency	%	84		84	
System roundtrip efficiency	%	40		44	
SOFC exergy efficiency	%	60		64	
SOEC exergy efficiency	%	68		68	
Exergy lost/destroyed	**kW**	SOFC	SOEC	SOFC	SOEC
Stack		0.80	9.2	0.70	8.1
Expansion		6.2	4.7	5.8	4.5
Compression		6.2	5.5	5.5	4.5
Heat transfer		32	54	19	50
Mixing		3.7	4.3	6.1	4.9
Environment		19	5.8	21	7.3

In Table 5.5, the net power produced in SOFC mode was increased because of much lower requirements in compression power due to the lower inlet of fresh air. Although the power produced by the air turbine diminished almost proportionately, the higher operating pressure in the system at 4 [bar] made it possible for the outlet air to leave at a higher temperature after the air preheater than at 2 [bar], thus it became possible to reheat the rich syngas with this stream (Figure 5.11) to much higher temperatures during its expansion from storage pressure, therefore more power could be recovered.

Exergy losses to the environment slightly increased since the oxidant outlet stream left at a higher temperature after expansion than at 2 [bar] pressurization without recirculation. Losses in heat transfer were reduced because the air recirculation acted as a preheating step before the preheating heat exchanger, therefore less energy was transferred in the latter; however, in exchange exergy losses in mixing increased.

In SOEC mode the exergy efficiency was basically unchanged by the use of recirculation. Exergy destruction in compression and heat exchanging were reduced, but this was offset by an increase in exergy losses to the environment and exergy destruction in mixing. Net power consumption was slightly decreased by the reduction in the compression ratio of the rich syngas sent to storage and the decrease in compression power of the air.

The system configuration shown in Figure 5.11 and Appendix E (in Aspen Plus) is the best system that could be achieved in this work on the basis of roundtrip and exergy efficiencies for a syngas-operated SORC, working under the constraints given in Section 4.4. This final configuration working under the operating conditions in the last column of Table 5.5 is referred as the Advanced System. Exergy flows through this system can be appreciated in the exergy flow diagrams presented in Appendix I and Appendix J for SOFC and SOEC modes, respectively.

The Advanced System was compared to the Base System in Table 5.6: in general, a lot of energetic and exergetic improvements could be obtained when the SORC system was able to depend less on external energy sources like the power grid. The greatest overall improvement was obtained with the implementation of heat integration. Pressurization of the system and air recirculation had benefits on the exergy side, but these mostly had an effect of the roundtrip efficiency of the system. Heat integration

was therefore the greatest contributor to the exergy efficiency and further improvements of this metric could be achieved mostly by achieving an optimized use of internal energy streams.

Table 5.6. Comparison between Base System and Advanced System.

Parameter	**Units**	**Base System**		**Advanced System**	
Stack temperature	$°C$	800		800	
Stack pressure	bar	1.2		4	
Current density	A/cm^2	0.5		0.5	
Air recirculation ratio	$-$	0.00		0.50	
Net power produced in SOFC mode	kW	85		124	
Net power consumed in SOEC mode	kW	295		282	
Stack roundtrip efficiency	%	84		84	
System roundtrip efficiency	%	29		44	
SOFC exergy efficiency	%	44		64	
SOEC exergy efficiency	%	66		68	
Exergy lost/destroyed	**kW**	SOFC	SOEC	SOFC	SOEC
Stack		0.90	10	0.70	8.1
Expansion		1.6	0.80	5.8	4.5
Compression		2.4	2.6	5.5	4.5
Heat transfer		57	64	19	50
Mixing		3.8	4.9	6.1	4.9
Environment		35	16	21	7.3

6. CONCLUSIONS

The purpose of this master thesis was to design and improve an energy storage system that uses solid oxide reversible cells and syngas as fuel. These cells transform electric energy into chemical energy by performing the co-electrolysis of water and carbon dioxide to produce syngas, which is later consumed by the same cells to produce electric energy when this is required in a power grid. This design of this system was implemented in Aspen Plus in order to test it under different operating conditions and improve it from a simple configuration on the basis of roundtrip and exergy efficiencies. Each iteration of the system was compared to its former state in order to formulate a strategy to increase performance. Answering the research questions stated in the introduction of this report, the main conclusions from this work are:

- SORC stacks based on YSZ cells should work at the highest possible temperatures that the system can withstand, since Ohmic overpotentials limit drastically their stack roundtrip efficiency at lower temperatures, and by extension the entire system roundtrip efficiency is also compromised. High temperatures also helped reduce the formation of methane in the system along with low pressures, making it possible to operate exclusively with syngas ($H_2 + CO$). Operation at high temperatures, however, implied that the system will always work under endothermic co-electrolysis conditions that strongly affect the overall heat integration of the system.

- The main sources of exergy losses during SOFC and SOEC operation include heat transfer processes and environmental losses. The first can be reduced by replacing electric heaters with heat exchangers, and by using with the latter material streams that have a smaller temperature difference. Environmental losses can be reduced by decreasing the temperature of outlet flows through heat integration with another internal stream, or by expansion in turbines if pressures are high enough to use them.

- Heat integration gives the largest improvements in exergy efficiency. It helped to avoid using electric power for heating purposes, thus avoiding the conversion of high-value energy into heat. It was also possible to decrease temperature differences between primary and secondary streams in heat exchangers thus reducing exergy destruction in heat transfer processes. However, full heat integration was not possible for SOEC operation in this project, since no internal heat sources with proper characteristics could be found for steam generation. From a system that uses only electric power for heating purposes, to a system with full heat integration in SOFC mode and partial heat integration in SOEC mode, system roundtrip efficiency was improved from 29% to 38%; SOFC exergy efficiency improved from 44% to 56%; and SOEC exergy efficiency improved from 66% to 68%.

- The endothermic/exothermic behavior of the stack requires large flow rates of air to add/remove the heat necessary for isothermal operation of this component. As a result, a lot of energy is needed to provide air to the system especially at high pressures. In order to reduce these flow rates and increase energetic performance, a combination of system pressurization, air recirculation and outlet air expansion in a turbine can be used that has the final effect of reducing energy-intensive compression requirements. In combination with heat integration, this overall advanced configuration can achieve improvements in system roundtrip efficiency from 29% to 44%; in SOFC exergy efficiency from 44% to 64%; and in SOEC exergy efficiency from 66% to 68%.

Moderate to high exergy efficiencies can be achieved in syngas-based SORC systems like the one developed in this study. However, some analyzes argue that the energy storage systems required to help implement intermittent renewable energy technologies should be able to achieve roundtrip efficiencies higher than 60% [41]. As a result, the syngas-operated SORC system developed here is questionable candidates for balancing power grids by itself, therefore it should be coupled with other processes that can help increase the roundtrip efficiency.

7. RECOMMENDATIONS AND FUTURE WORK

This project had a total duration of 8 months. Because of the low amount of time only some of the BOP components in the system could be observed, therefore some optimization strategies were not explored and several simplifications had to be introduced. Some recommendations and opportunities for future work include:

- **Optimization of heat integration:** the trial-and-error exercise used in this project to establish a preliminary heat transfer network worked to be able to measure its effect on system performance. However, this methodology doesn't guarantee the best possible configuration of exchangers and doesn't include a detailed dimensioning. As shown in this project, heat integration is critical for high energy and exergy efficiency, thus this aspect of the system should be more carefully designed.

- **Condenser and cooling cycles:** simple cooling water cycles were used where needed, which mostly consisted of a water pump and a heat exchanger. More complex cooling or refrigeration cycles were not explored which can potentially increase the performance of the system.

- **Heat storage and insulation of storage tanks:** heat storage within dedicated media like phase-change materials could be incorporated in the system along temperature management strategies like the ones shown by Mottaghizadeh et al. [3]. Additionally, the insulation of the storage tanks of water and syngas can be considered in order to reduce environmental energy and exergy losses. In this project a worst-case scenario was assumed where stored compounds always cooled to the temperature of the environment, but this might not always be the case. This, however, requires defining how long the system will be operated in each mode, and how long the system may remain idle, which at the ends depends on the storage application.

- **Higher methane content:** in this project the methane content was kept below 1% on a dry mole basis in order to be able to develop a system working exclusively with synthesis gas to provide a point of reference for more complex configuration. However, as it was said before higher methane contents are not necessarily detrimental to performance, therefore other studies can attempt strategies to improve the system developed here without worrying about the amount of methane produced and compare the results to this work and improve our knowledge about the feasibility of certain process chains.

- **Integration of liquid fuels synthesis:** if the system is reconsidered as a production plant for synthesis of fuels from electricity of the gird, the incorporation of a process like Fischer-Tropsch may improve the performance of the system in SOEC mode, given the high exothermic nature of the reactions involved that could be used to supply the heat needed. SOFC operation would then be used to supply electric power to the grid during times of insufficient renewable energy production (when SOEC operation is not possible), however for short periods of time in order to not consume too much syngas feedstock. The use of SOFC mode could then help avoid long periods of inactivity and improve the economics of the system.

- **Techno-economic analysis:** only efficiency metrics of technical nature where considered in this project. However, economic indicators like the levelized cost of energy or the capital cost can also impact the final decision-making process for this type of systems, especially when the system is used for comparisons with more complex designs of the same or different nature. Additionally, the techno-economic analysis can help determine if the system developed here is more suited for short or long-term storage applications.

References

[1] Z. Schiffer and K. Manthiram, "Electrification and Decarbonization of the Chemical Industry," *Joule,* vol. 1, no. 1, pp. 10-14, 2017.

[2] C. Wendel, "Design and Analysis of Reversible Solid Oxide Cell Systems for Electrical Energy Storage," Colorado School of Mines, Golden, 2015.

[3] P. Mottaghizadeh, S. Santhanam, M. Heddrich, A. Friedrich and F. Rinaldi, "Process modeling of a reversible solid oxide cell (r-SOC) energy storage system utilizing commercially available SOC reactor," *Energy Conversion and Management,* vol. 142, pp. 477-493, 2017.

[4] University of Cambridge, "Solid oxide fuel cells (SOFCs)," University of Cambridge, 2004. [Online]. Available: https://www.doitpoms.ac.uk/tlplib/fuel-cells/high_temp_sofc.php. [Accessed 1 August 2018].

[5] Y. Redissi and C. Bouallou, "Valorization of carbon dioxide by co-electrolysis of CO2/H2O at high temperature for syngas production," *Energy Procedia,* vol. 37, pp. 6667-6678, 2013.

[6] EG&G Technical Services, Fuel Cell Handbook, Morgantown: U.S. Department of Energy, 2004.

[7] J. Larminie and A. Dicks, Fuel Cell Systems Explained, Chichester, England: John Wiley & Sons, 2003.

[8] S. van Nielen, "Techno-economic Assessment of Solid Oxide Fuel Cells and Fuel-assisted Electrolysis Cells in Future Energy Systems," Delft University of Technology, Delft, 2016.

[9] W. Li, Y. Shi, Y. Luo and N. Cai, "Elementary reaction modeling of solid oxide electrolysis cells: Main zones for heterogeneous chemical/electrochemical reactions," *Journal of Power Sources,* vol. 273, pp. 1-13, 2015.

[10] M. Hauck, S. Herrmann and H. Spliethoff, "Simulation of a reversible SOFC with Aspen Plus," *International Journal of Hydrogen Energy,* vol. 42, no. 15, pp. 10329-10340, 2017.

[11] C. Stoots, J. O'Brien, S. Herring and J. Hartvigsen, "Syngas Production via High-Temperature Coelectrolysis of Steam and Carbon Dioxide," *Journal of Fuel Cell Science and Technology,* vol. 6, pp. 1-12, 2009.

[12] C. Wendel, P. Kazempoor and R. Braun, "A thermodynamic approach for selecting operating conditions in the design of reversible solid oxide cell energy systems," *Journal of Power Sources,* vol. 301, no. 93-104, 2016.

[13] C. Wendel, P. Kazempoor and R. Braun, "Novel electrical energy storage system based on reversible solid oxide cells: System design and operating conditions," *Journal of Power Sources,* vol. 276, pp. 133-144, 2015.

[14] Department of Energy of the United States, "FUEL CELL TECHNOLOGIES OFFICE: Hydrogen Storage," Department of Energy of the United States,

[Online]. Available: https://www.energy.gov/eere/fuelcells/hydrogen-storage. [Accessed 17 August 2018].

[15] National Energy Technology Laboratory, "An Engineering-Economic Analysis of Syngas Storage," National Energy Technology Laboratory, 2008.

[16] V. Nguyen and L. Blum, "Syngas and Synfuels from H2O and CO2: Current Status," *Chemie Ingenieur Technik,* vol. 87, no. 4, pp. 354-375, 2015.

[17] C. Graves, S. Ebbesen and M. Mogensen, "Co-electrolysis of CO2 and H2O in solid oxide cells: Performance and durability," *Solid State Ionics,* vol. 192, no. 1, pp. 398-403, 2011.

[18] C. Callaghan, "Kinetics and Catalysis of the Water-Gas-Shift Reaction: A Microkinetic and Graph Theoretic Approach," Worcester Polytechnic Institute, Massachusetts, 2006.

[19] L. Barelli and A. Ottaviano, "Solid oxide fuel cell technology coupled with methane dry reforming: A viable option for high efficiency plant with reduced CO2 emissions," *Energy,* vol. 71, pp. 118-129, 2014.

[20] Y. Çengel and M. Boles, Thermodynamics: An Engineering Approach, New York: McGraw-Hill Education, 2014.

[21] J. Stempien, Q. Sun and C. S., "Solid Oxide Electrolyzer Cell Modelling: A Review," *Journal of Power Technologies,* vol. 93, no. 4, pp. 216-246, 2013.

[22] W. Doherty, A. Reynolds and D. Kennedy, "Computer simulation of a biomass gasification-solid oxide fuel cell power system using Aspen Plus," *Energy,* vol. 35, no. 12, pp. 4545-4555, 2010.

[23] Z. He, H. Li and E. Birgersson, Reduced Modelling of Planar Fuel Cells, Springer International Publishing, 2017.

[24] F. Sebastiani, "Thermodynamic and exergy analysis of reversible solid oxide cell systems," Delft University of Technology, Delft, the Netherlands, 2014.

[25] R. Mor, "Energy, exergy and cumulative exergy losses analysis of bidirectional solid oxide cell system," Delft University of Technology, Delft, the Netherlands, 2015.

[26] M. Ni, M. Leung and D. Leung, "Parametric study of solid oxide steam electrolyzer for hydrogen production," *International Journal of Hydrogen Energy,* vol. 32, no. 13, pp. 2305-2313, 2007.

[27] E. Hernández-Pacheco, D. Singh, P. Hutton, N. Patel and M. Mann, "A macro-level model for determining the performance characteristics of solid oxide fuel cells," *Journal of Power Sources,* vol. 138, no. 1-2, pp. 174-186, 2004.

[28] A. Buttler, R. Koltun, R. Wolf and H. Spliethoff, "A detailed techno-economic analysis of heat integration in high temperature electrolysis for efficient hydrogen production," *International Journal of Hydrogen Energy,* vol. 40, no. 1, pp. 38-50, 2015.

[29] S. Ebbesen, C. Graves and M. Mogensen, "Production of Synthetic Fuels by Co-Electrolysis of Steam and Carbon Dioxide," *International Journal of Green Energy,* vol. 6, no. 6, pp. 646-660, 2009.

[30] P. Kazempoor and R. Braun, "Model validation and performance analysis of regenerative solid oxide cells for energy storage applications: Reversible operation," *International Journal of Hydrogen Energy,* vol. 39, no. 11, p. 5955–5971, 2014.

[31] B. Tjaden, M. Gandiglio, A. Lanzini, M. Santarelli and M. Järvinen, "Small-scale biogas-SOFC plant: Technical analysis and assessment of different fuel reforming options," *Energy and Fuels,* vol. 28, no. 6, pp. 4216-4232, 2014.

[32] A. Amiri, P. Vijay, M. Tadé, K. Ahmed, G. Ingram, V. Pareek and R. Utikar, "Planar SOFC system modelling and simulation including a 3D stack module," *International Journal of Hydrogen Energy,* vol. 41, no. 4, pp. 2919-2930, 2016.

[33] L. Barelli, G. Bidini and A. Ottaviano, "Hydromethane generation through SOE (solid oxide electrolyser): Advantages of H2O-CO2 co-electrolysis," *Energy,* vol. 90, pp. 1180-1191, 2015.

[34] W. Zhang, E. Croiset, P. Douglas, M. Fowler and E. Entchev, "Simulation of a tubular solid oxide fuel cell stack using AspenPlus unit operation models," *Energy Conversion and Management,* vol. 46, no. 2, pp. 181-196, 2005.

[35] P. Aravind, *Personal communication with PV Aravind, TU Delft,* Delft, 2018.

[36] S. Chan, K. Khor and Z. Xia, "A complete polarization model of a solid oxide fuel cell and its sensitivity to the change of cell component thickness," *Journal of Power Sources,* vol. 93, no. 1-2, pp. 130-140, 2001.

[37] T. Woudstra, *Personal communication with Theo Woudstra, TU Delft,* Delft, 2018.

[38] E. Bernier, J. Hamelin, K. Agbossou and T. Bose, "Electric round-trip efficiency of hydrogen and oxygen-based energy storage," *International Journal of Hydrogen Energy,* vol. 30, no. 2, pp. 105-111, 2005.

[39] M. Moran, H. Shapiro, D. Boettner and M. Bailey, Fundamentals of Engineering Thermodynamics, Chichester: John Wiley, 2010.

[40] T. Gundersen, An Introduction to The Concept Of Exergy And Energy Quality, Trondheim, Norway: Norwegian University of Science and Technology, 2009.

[41] U.S. Department of Energy, "Grid Energy Storage," U.S. Department of Energy, 2013.

Appendix A

jV-curve of the electrochemical computer model compared to experimental results by Kazempoor and Braun [30]

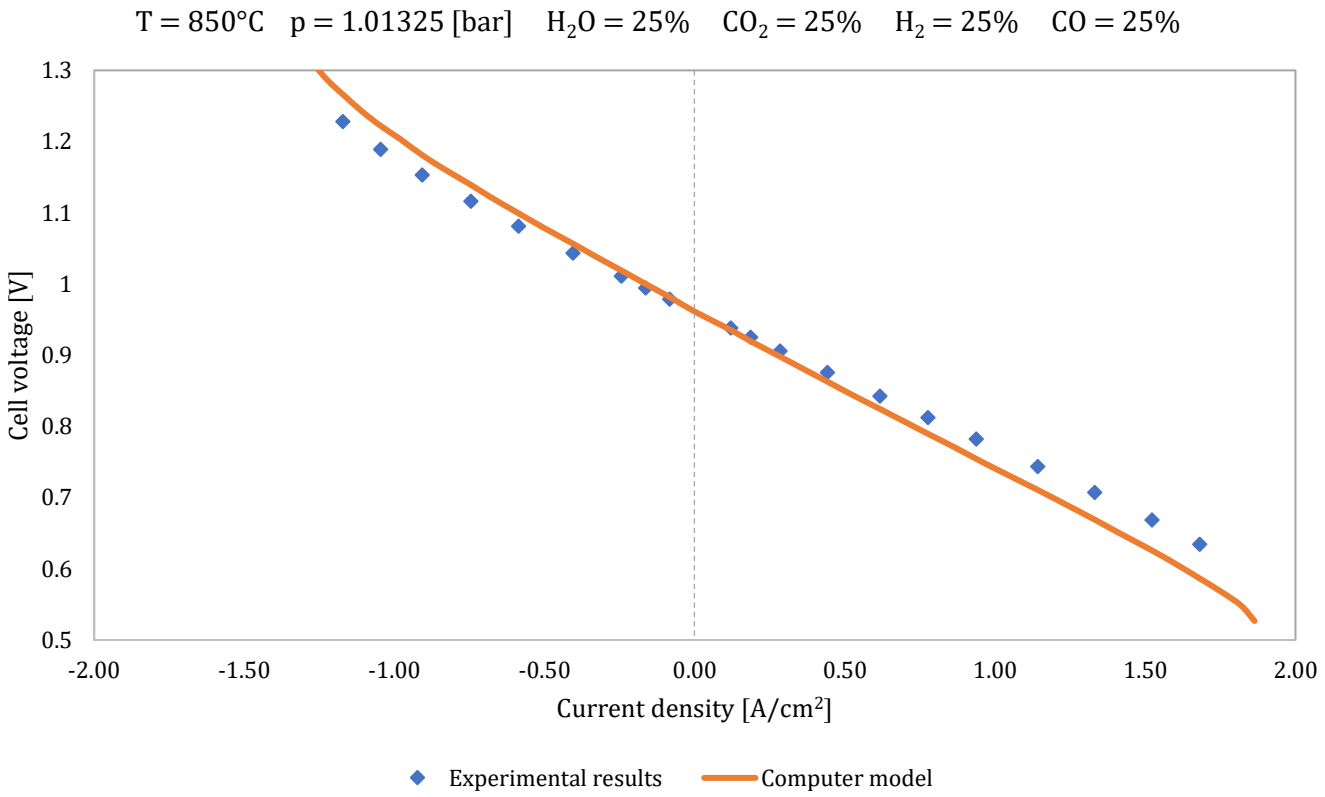

Appendix B

Aspen Plus model for the SORC Base System in SOFC mode

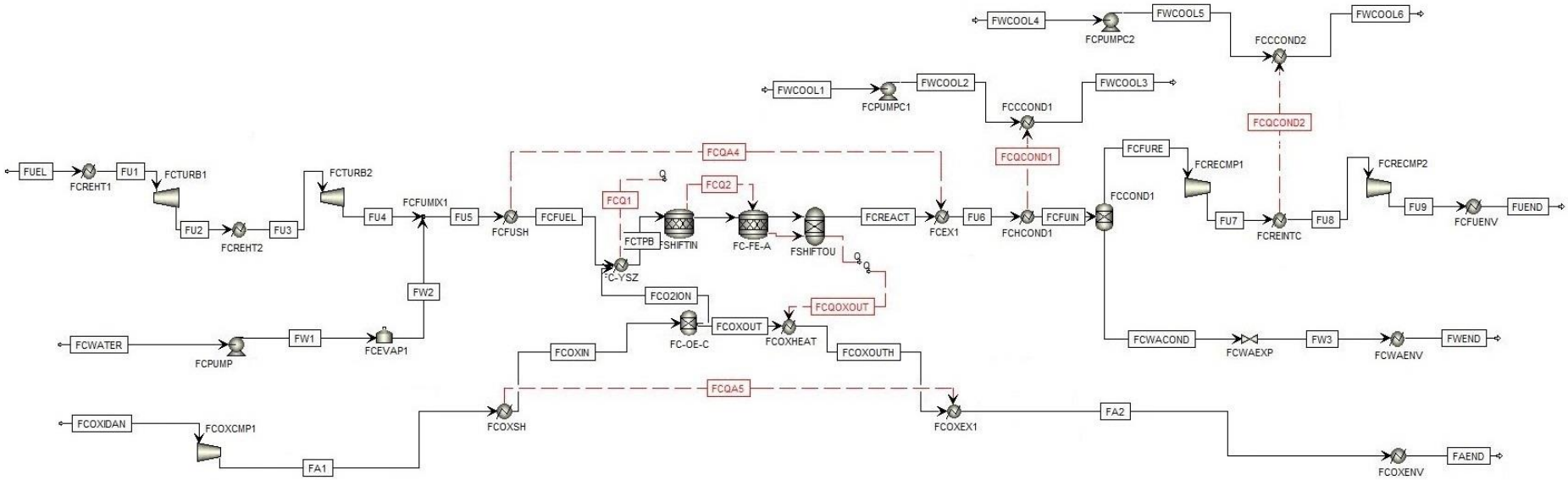

Appendix C

Aspen Plus model for the SORC Base System in SOEC mode

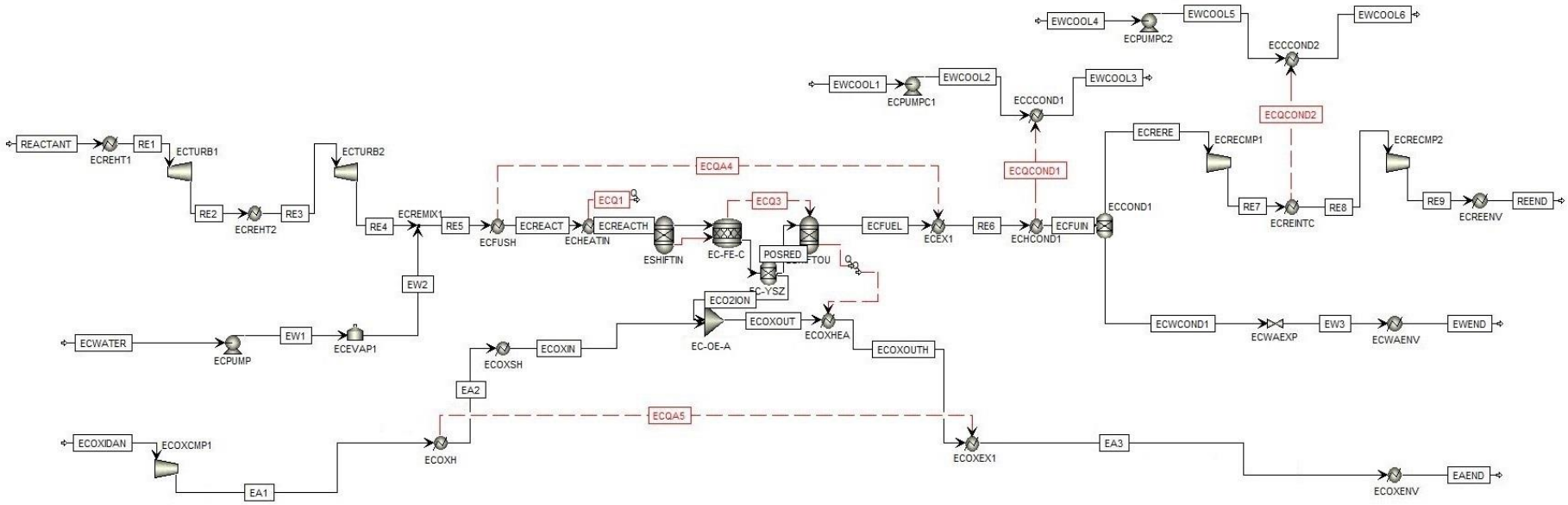

Appendix D

Full Aspen Plus model for the SORC Base System

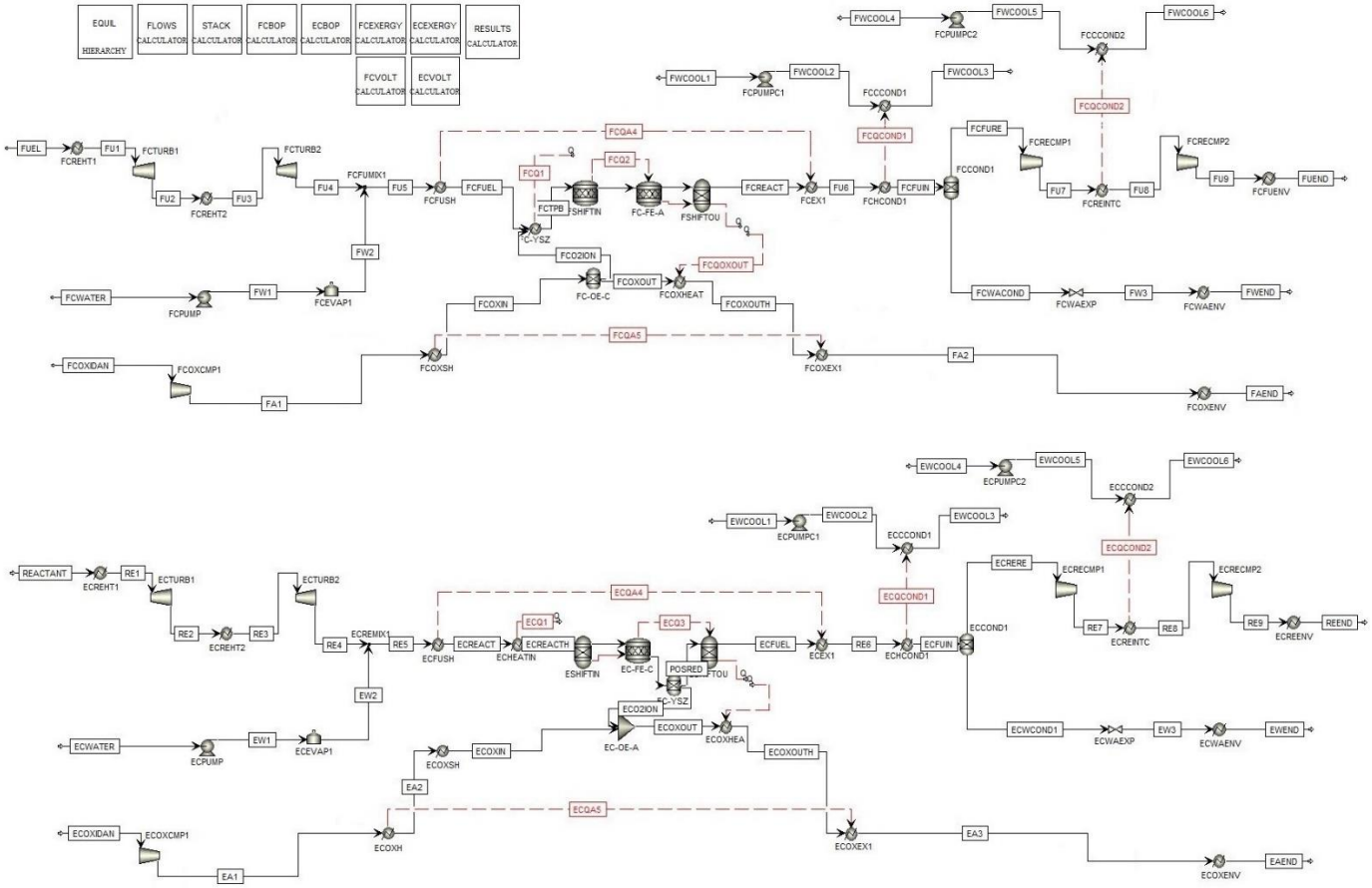

Appendix E

Full Aspen Plus model for the SORC Advanced System

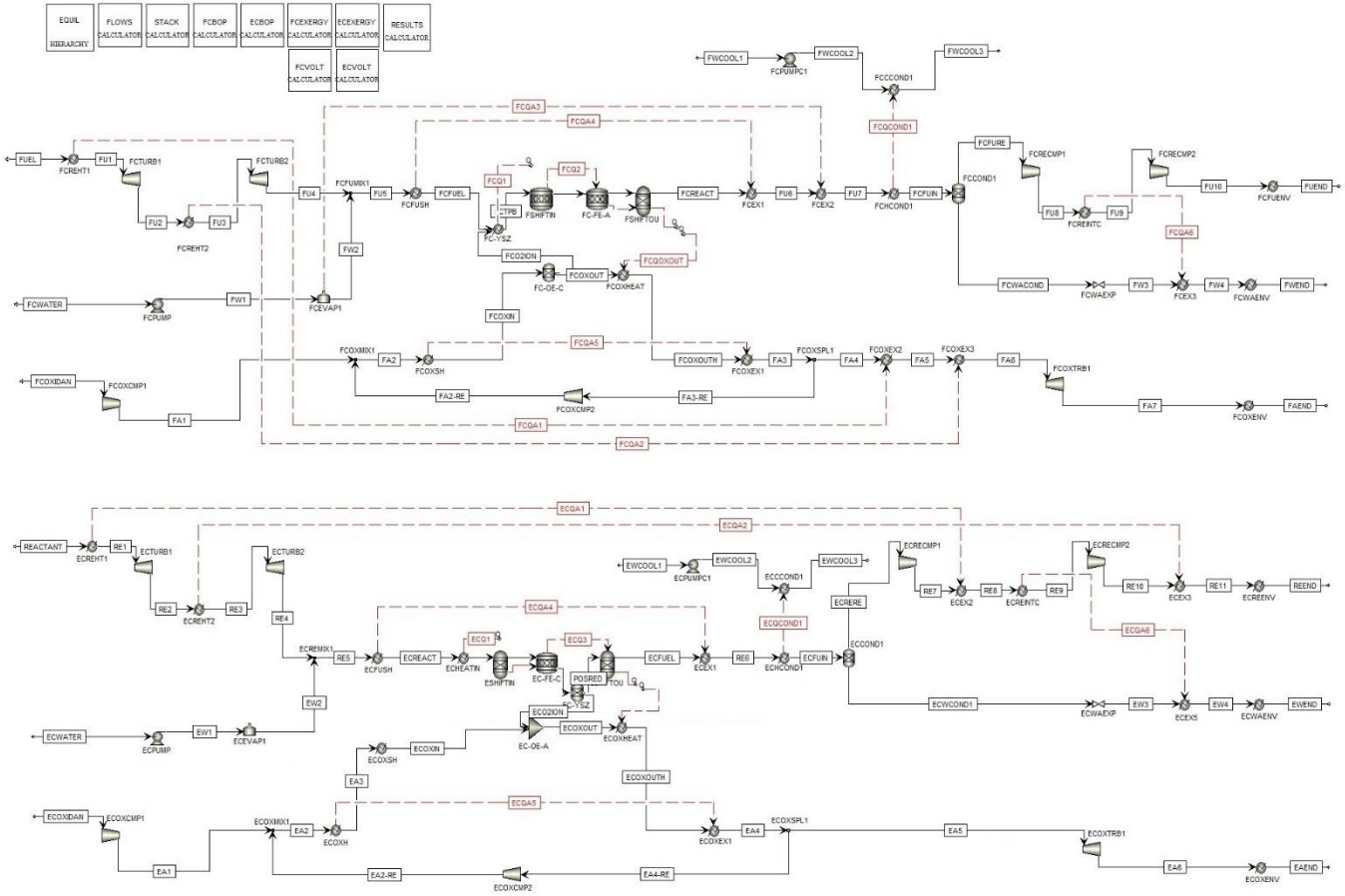

Appendix F

Equilibrium Arrangement in Aspen Plus

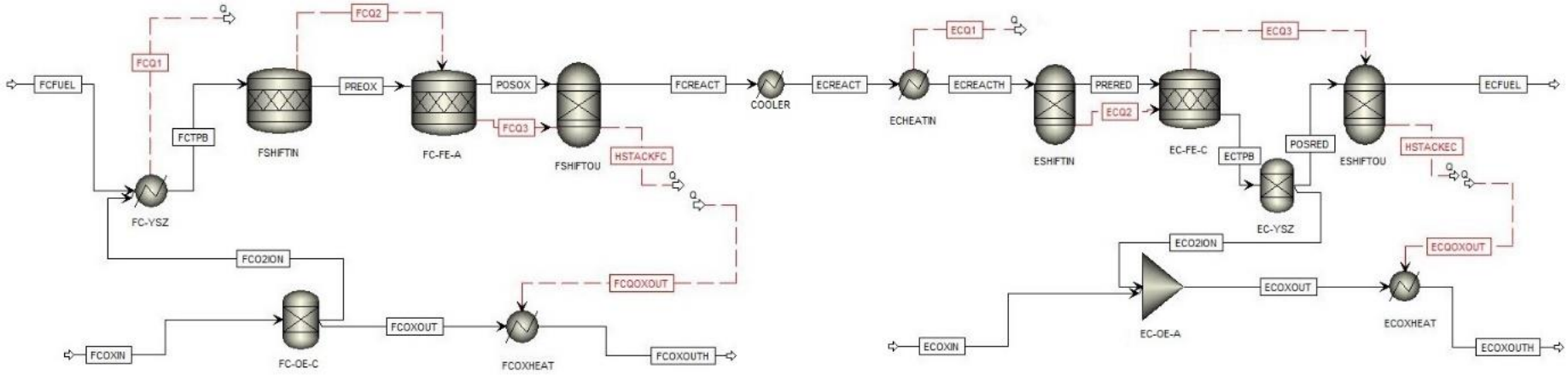

Appendix G

Exergy flow diagram for the SORC Base System in SOFC mode

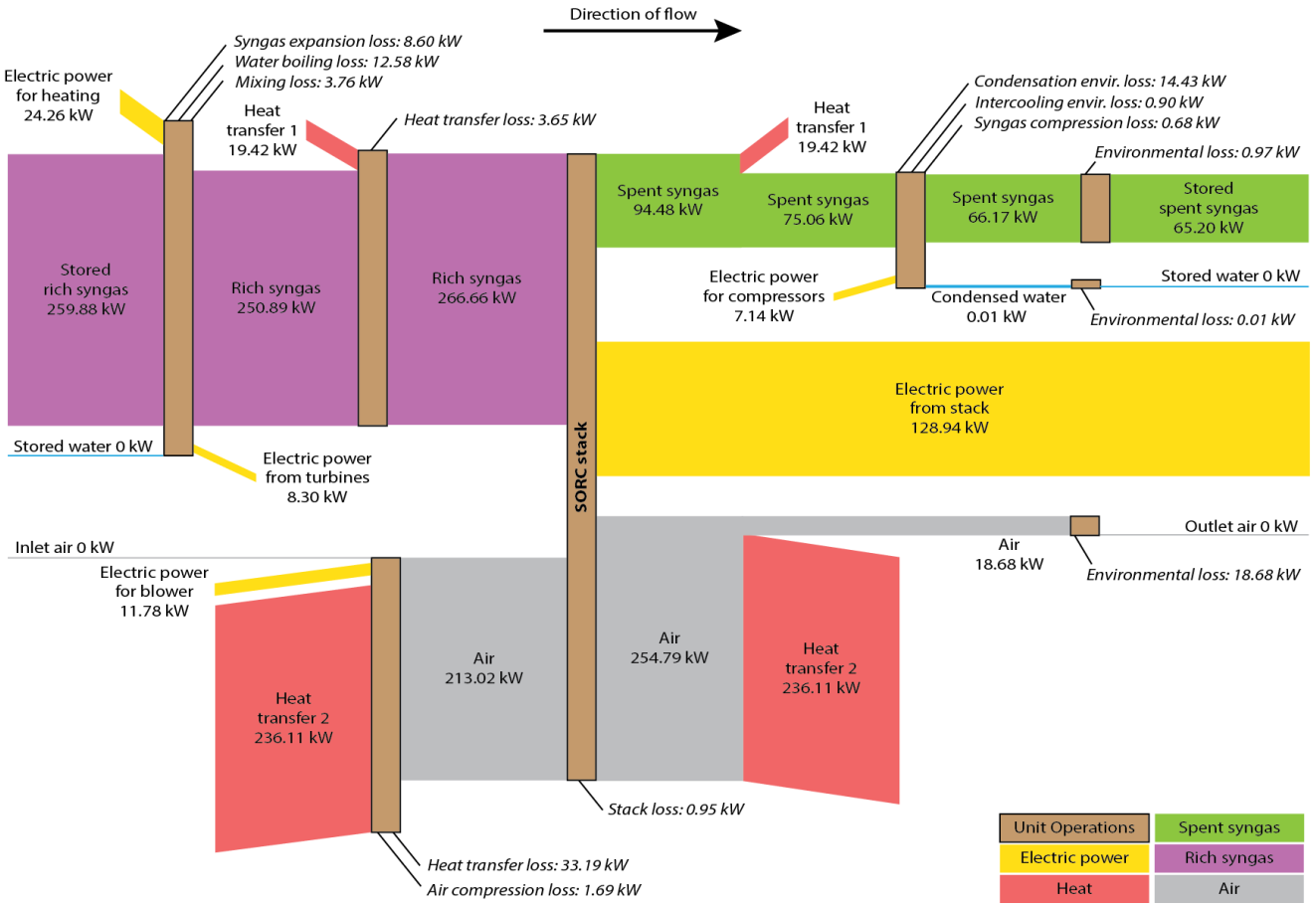

Appendix H

Exergy flow diagram for the SORC Base System in SOEC mode

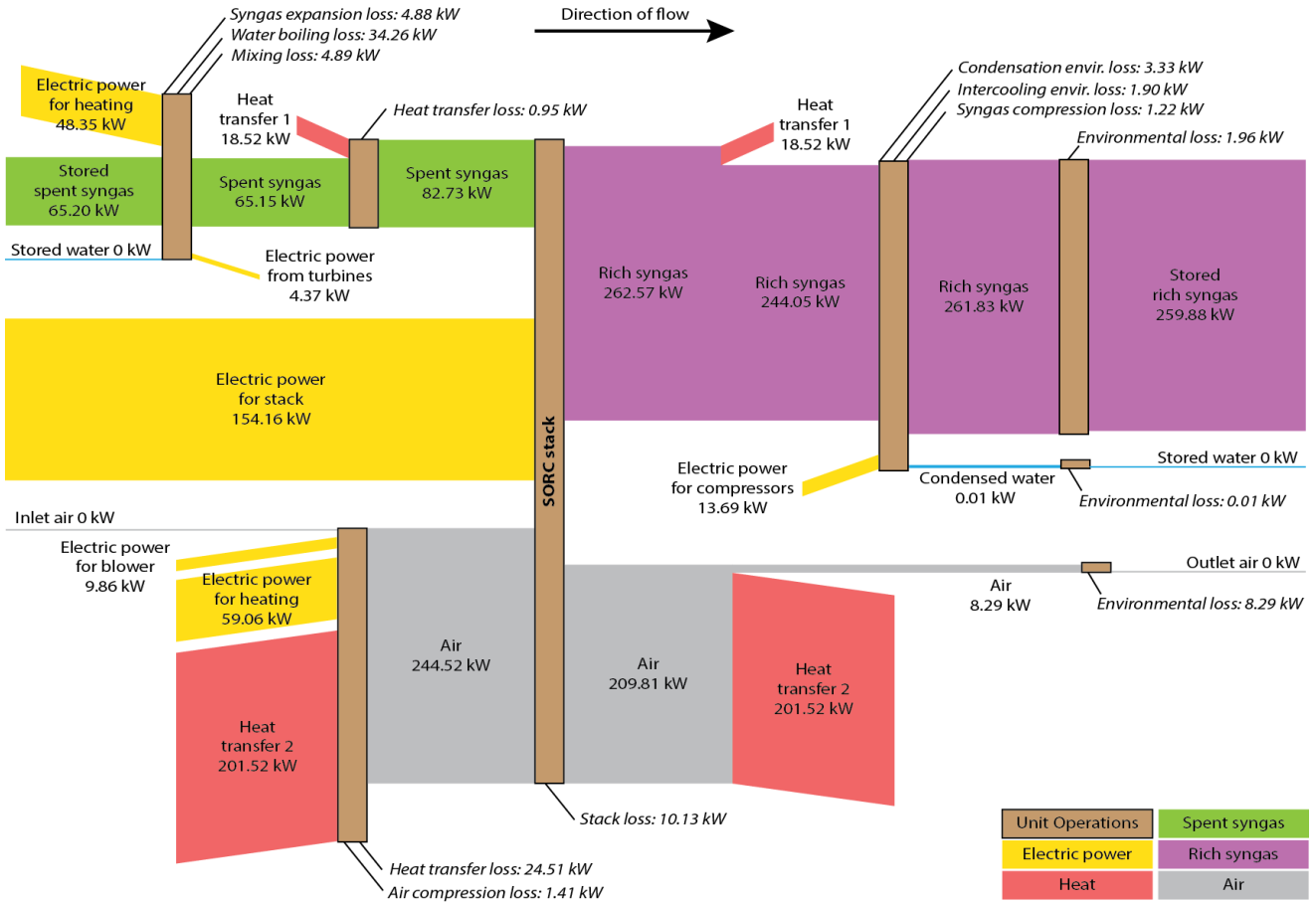

Appendix I

Exergy flow diagram for the SORC Advanced System in SOFC mode

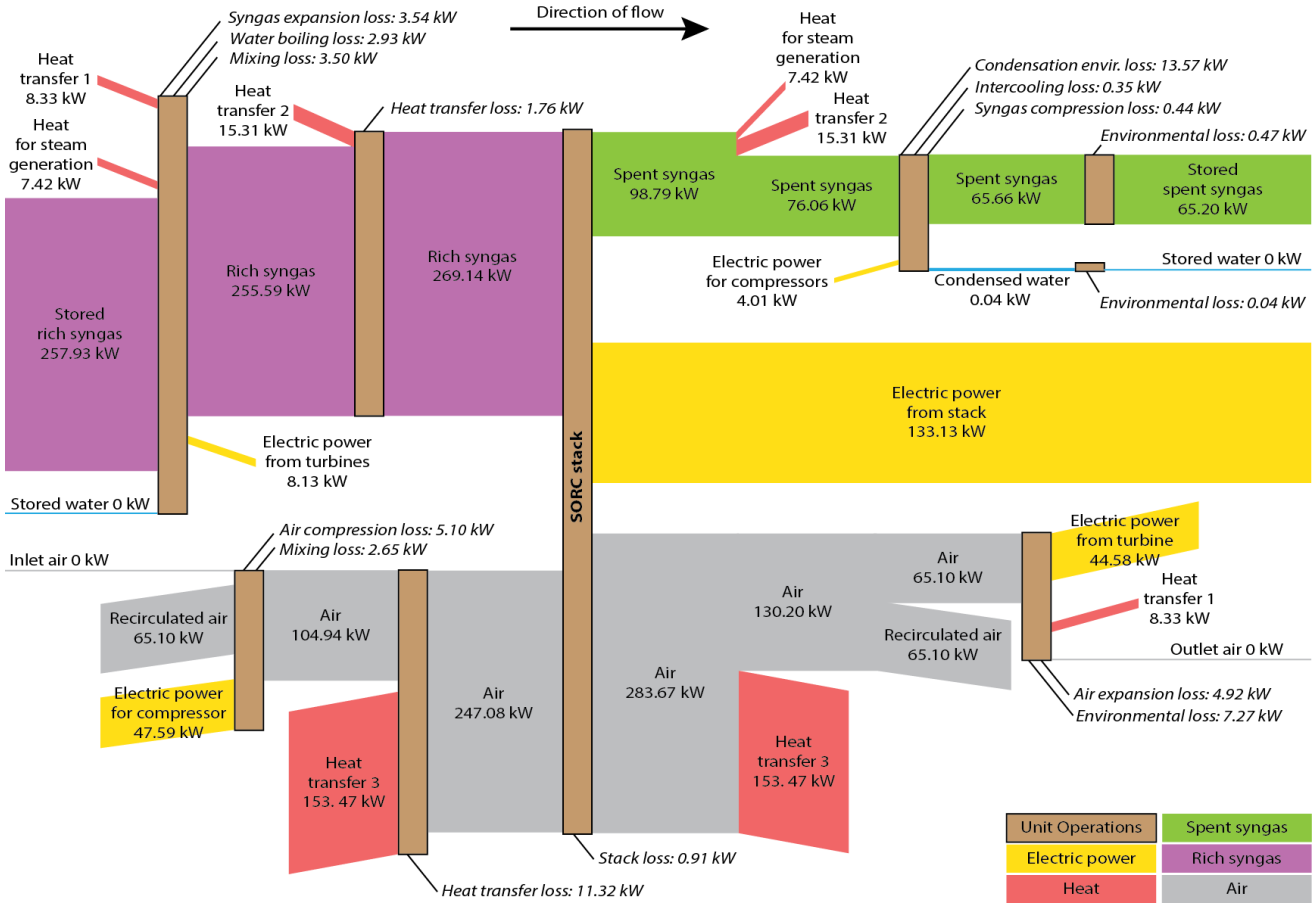

Appendix J

Exergy flow diagram for the SORC Advanced System in SOEC mode